81-07

INFLUENCE OF FIBER ORIENTATION DISTRIBUTION ON STRENGTH OF NOTCHED COMPOSITES

MICHAEL C. LINDELL

CENTER FOR COMPOSITE MATERIALS

College of Engineering
University of Delaware
Newark, Delaware

*MSG DI4 DROLS PROCESSING - LAST INPUT IGNORED

*MSG DI4 DROLS PROCESSING-LAST INPUT IGNORED

-- 1 OF 1
-- ***DTIC DOES NOT HAVE THIS ITEM***
-- 1 - AD NUMBER: D433441
-- 6 - UNCLASSIFIED TITLE: INFLUENCE OF FIBER ORIENTATION DISTRIBUTION
-- ON STRENGTH OF NOTCHED COMPOSITES,
--10 - PERSONAL AUTHORS: LINDELL,M. C. ;
--11 - REPORT DATE: MAY , 1981
--12 - PAGINATION: 127P
--14 - REPORT NUMBER: CCM-81-07
--20 - REPORT CLASSIFICATION: UNCLASSIFIED
--21 - SUPPLEMENTARY NOTE: THESIS SUBMITTED TO UNIVERSITY OF DELAWARE
-- IN PARTIAL FULFILLMENT OF REQUIREMENTS FOR BACHELOR'S DEGREE WITH
-- DISTINCTION IN MECHANICAL ENGINEERING.
--22 - LIMITATIONS (ALPHA): APPROVED FOR PUBLIC RELEASE; DISTRIBUTION
-- UNLIMITED. AVAILABILITY: CENTER FOR COMPOSITE MATERIALS, COLLEGE OF
-- ENGINEERING, UNIV. OF DELAWARE, NEWARK, DE. 19711
--33 - LIMITATION CODES: 1
--******
-- END OF DISPLAY LIST

-- ((ENTER NEXT COMMAND))

INFLUENCE OF FIBER ORIENTATION DISTRIBUTION ON STRENGTH OF NOTCHED COMPOSITES

By

Michael C. Lindell

R. Byron Pipes, Thesis Advisor

A thesis submitted to the Faculty of the University of Delaware in partial fulfillment of the requirements for a Bachelor's Degree with Distinction in Mechanical Engineering.

May 1981

ABSTRACT

A short fiber composite material containing a circular notch is analyzed to determine the effect of fiber orientation on material property and strength characteristics. Several models are presented, each assuming a different state of fiber orientation, and analyzed with a finite element structural analysis program to determine performance under axial load. Numerous contour plots are presented for each model which display the dependence of material characteristics on fiber orientation and show the stress and displacement distributions. A failure model is then developed which predicts strength reduction as a function of notch size. It was found that, relative to the isotropic or orthotropic condition, strength levels of the various models vary by no more than 10-11 percent for a given notch size. It is also shown that, given a notch size and corresponding strength reduction in an isotropic or orthotropic case, notch sizes up to 50 percent larger result in no greater strength reduction. Lastly, it is found that a particular model may be of greater strength than another for a certain notch size range and be of inferior strength in a different range. Thus, relative strength is found to be dependent on absolute notch size.

TABLE OF CONTENTS

LIST OF TABLES

LIST OF FIGURES

I. INTRODUCTION

When dealing with discontinuous fiber-reinforced composite materials it becomes a difficult task to accurately predict the performance of a part made of such material. This is due to the strong dependence of material strength on the local fiber orientation within the structure. For injection molded, short fiber composite materials this orientation state is determined by the flow conditions and molding geometry. In areas within a mold near walls or other obstructions the shearing forces within the flow and the sudden changes in flow direction cause the fibers to deviate from the random orientation, isotropic condition. This gives rise to a variation in material properties. Thus, isotropic elastic theory is rendered useless since it cannot account for material property variation. If the fiber orientation were non-random yet uniform throughout, orthotropic elastic theory could be used to predict performance since it can account for directional-dependence of material properties. However, flow condition typically yield wide variations in fiber orientation and hence material properties can vary from point to point throughout the structure. This local

material property variation can cause sharp variations in stress distribution and hence strength. In structures containing holes or notches of some sort, the fiber orientation in the notch region can lead to stress concentration of greater magnitude than under isotropic conditions. Since there is no analytical model which can account for pointwise material property variation it becomes necessary to develop experimental procedures and empirical models which can predict fiber orientation and corresponding material strength.

This paper investigates the variation of stress and strength with fiber orientation distribution in an injection molded, infinite plate containing a circular hole. The material is a resin-fiber-filler composite consisting of polyester, E-glass, and calcium carbonate, respectively. The material properties and other characteristics of this composite are shown in Table 1. The structural analysis is accomplished with the aid of a finite element structural analysis program. In the analysis the effect of fiber orientation is taken into account by allowing the material properties to vary from element to element throughout the finite element grid. In the models presented fiber orientation was prescribed. Once the fiber orientation is defined at various points in the grid, material property assignment becomes possible. This is

MATERIAL	YOUNG'S MODULUS (PSI)	SHEAR MODULUS (PSI)	POISSON'S RATIO	VOLUME FRACTION	ASPECT RATIO
POLYESTER (RESIN)	0.510×10^6	0.196×10^6	0.301	0.504	- - -
E-GLASS (FIBER)	0.105×10^8	0.394×10^7	0.333	0.179	500
CALCIUM CARBONATE (FILLER)	0.693×10^7	0.262×10^7	0.323	0.317	- - -

TABLE 1. MATERIAL CHARACTERISTICS

accomplished with the aid of a computer code developed at the University of Delaware by Jarzebski et al. [1] which, given the material composition and fiber orientation, can estimate the corresponding orthotropic material properties.

The entire finite element set-up was accomplished with a computer-aided design program written at the University of Delaware by Quigley [4]. This code interfaces the material property predictions given by Jarzebski [1] with the finite element grid by assigning each element material properties which reflect the local fiber orientation and distribution. Thus, the structure is viewed as consisting of as many different materials as there are number of elements. As the elements are made smaller the model approaches a system whose material properties vary from point to point. Quigley's program creates the mesh by user input and organizes all the information necessary in order to execute the SAPV finite element analysis code.

Finite element results are then analyzed and a failure model is developed. Stress concentrations arising at the hole are examined for various fiber orientations including the isotropic and orthotropic conditions for comparison. Contour plots are provided for Young's moduli, shear moduli, displacement, and stress to examine the effect of fiber orientation on each of these

parameters. The results are then extended to predict strength characteristics for structures containing hole sizes other than the one examined here. Lastly, conclusions are drawn regarding the results of this study.

II. THE MODEL

The performance of discontinuous short fiber composites depends upon the material properties determined by fiber orientation. In a structure whose fibers are non-randomly oriented, this dependence leads to a pointwise variation in material properties which makes it impossible to analyze the structure analytically. Finite element analysis lends itself to this type of analysis and has the ability to model complex geometries and material property distributions. With the aid of existing computer codes it is possible to create the model and assign element-dependent material properties, given the state of fiber orientation at various points throughout the finite element grid. Once the element material properties are assigned and the boundary conditions stated it becomes a simple matter of executing a finite element code to predict the stresses and deflections within the structure.

A. FINITE ELEMENT MODEL

The structure being modeled is a molded infinite plate containing a circular hole. Since the finite element analysis requires the structure to have finite boundaries

it will be assumed that a width-to-hole radius ratio of 8.0 will approximate the infinite plate conditions. Figure 2.1 shows the dimensions of the model used. The structure is loaded such that the nominal stress in the part is 1000 psi (6.89 MPa). In the finite element model symmetry is assumed about the hole transverse to the loading direction. This reduces the number of elements and nodal points required to define the structure, hence reducing solution time and cost. The finite element grid and applied boundary conditions are shown in Figure 2.2 and Figure 2.3 is an enlargement.

The stresses and fiber orientation in the part in areas away from the hole should be uniform since there are no flow changes in those areas. Hence, the grid was not made exceedingly fine there. However, significant variations in stress and fiber orientation should occur in the region near the hole. Therefore, the grid was finely divided in that region to allow for sharp stress and material property variation.

To create the finite element model the computer-aided design program written by Quigley [4] was employed. This is an interactive program which organizes an input data file compatible with the SAPV finite element analysis code. The program permits automatic and manual mesh

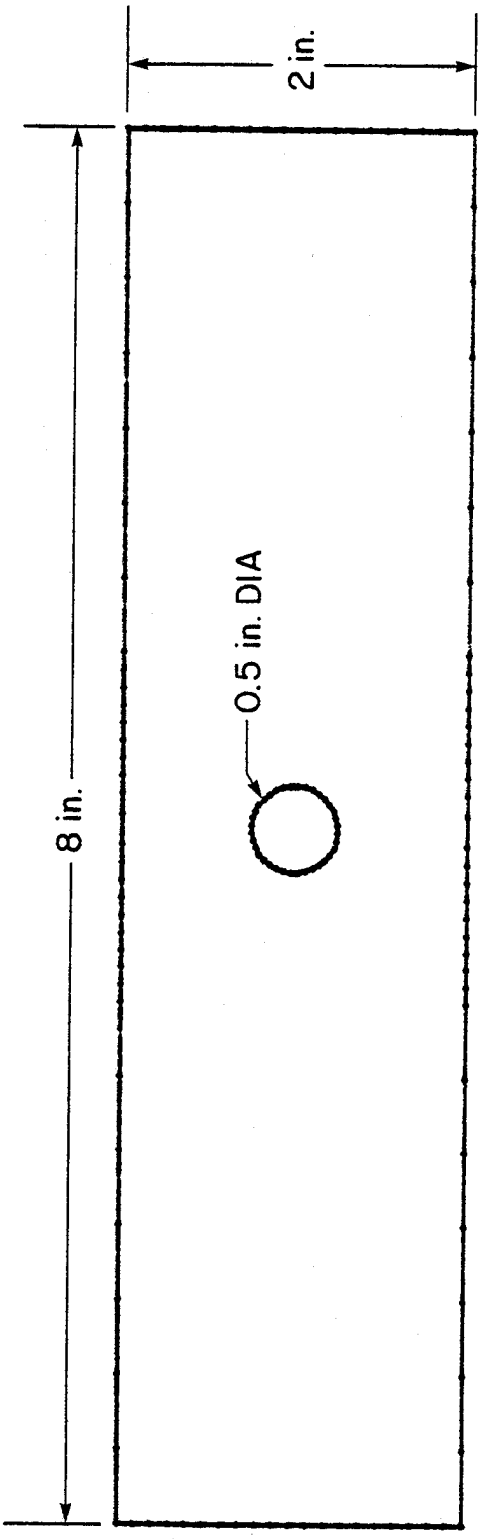

FIG. 2.1 DIMENSIONS OF THE MODEL

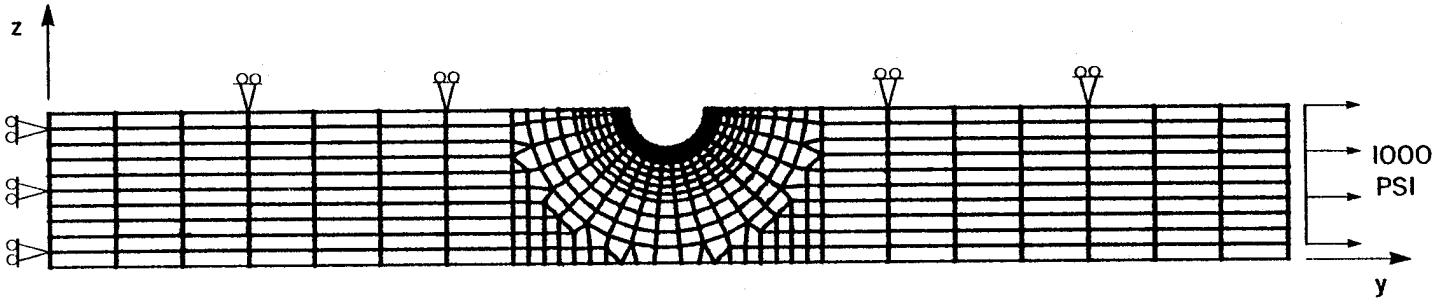

FIG. 2.2 FINITE ELEMENT GRID

Rollers represent the condition along the entire length of an edge.

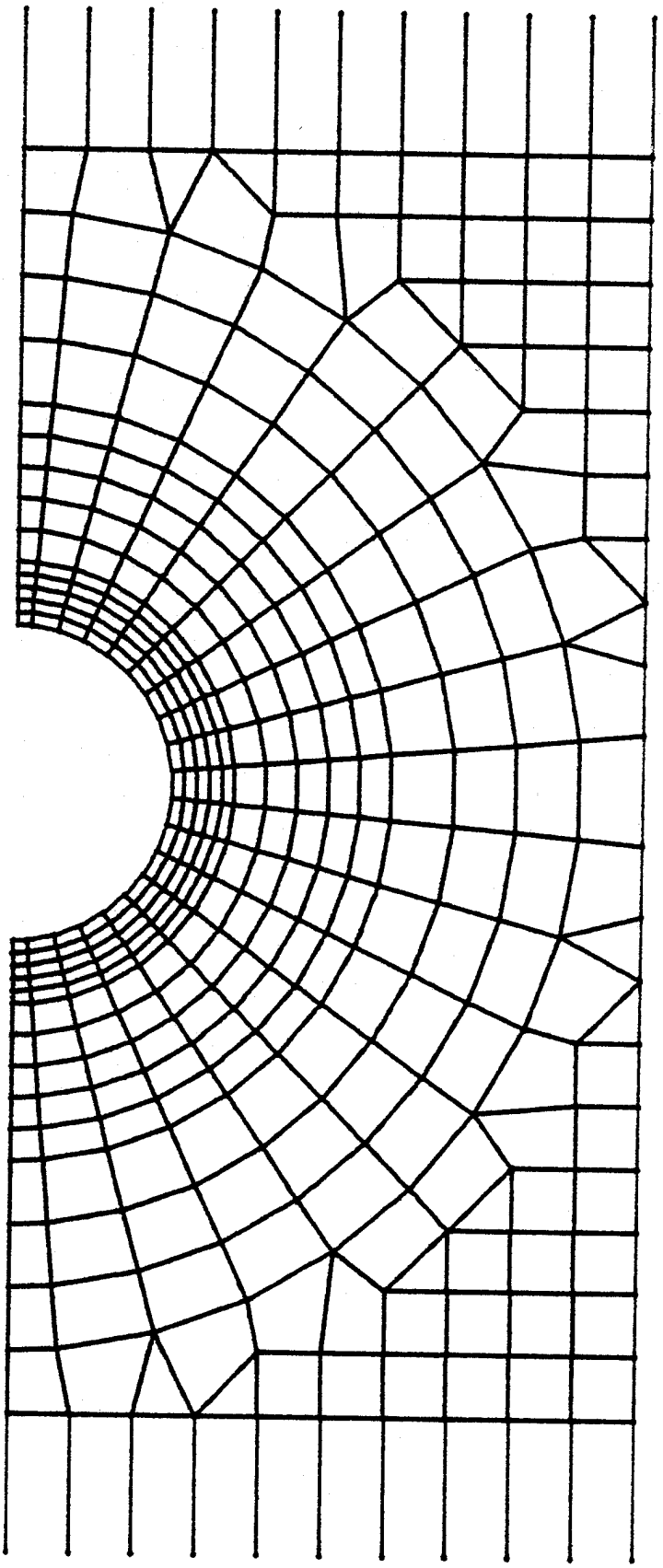

FIG. 2.3 ENLARGEMENT OF FINITE ELEMENT MESH NEAR THE HOLE

generation, nodal point boundary condition assignment, material property assignment, and organizes all the input information required for the finite element analysis. Another feature of this program pertinent to this work is its ability to make use of the finite element results for the purpose of plotting stress, deflection, fiber orientation, and material property contours. The program was key to the work and was used extensively.

B. FIBER ORIENTATION

Eight separate models are presented, each having a unique state of fiber orientation. It was stated that these fiber patterns were merely assumed, they are not necessarily accurate. This is due in part to a lack of information regarding the actual fiber orientation in such a molded part. Therefore, several models based on simplified fluid mechanics principles are presented. Before discussing these models the basic ideas concerning fiber orientation should be discussed.

Since the state of fiber orientation within a structure is the most important factor in determining the structure's strength, it becomes necessary to develop descriptors which quantitatively characterize the orientation state. For the cases considered in this study the fibers will be assumed to have orientations lying in the plane of

the plate, i.e., out of plane fiber tilting is not permitted. It is not the objective of this paper to present the theory of these orientation descriptors; the reader may consult Pipes et al. [7] for such a discussion. It will suffice to say that, for the planar orientation states considered here, there exists a parameter known as the Hermans Orientation Factor, f, which takes on the value of f=0.0 for a completely random, planar isotropic condition and assumes the value of f=1.0 for a completely columnated, planar orthotropic orientation state. All other orientation states between completely random and completely columnated will assume values between 0.0 and 1.0 depending upon the degree of randomness and columnation. It should be noted that this orientation factor applies to localized bundles of fibers and not to the structure as a whole. Such a bundle of fibers is shown in Figure 2.4 having a random orientation and a completely columnated orientation. Thus, the structure is assumed to be composed of many bundles of fibers dispersed throughout the resin-filler matrix, each bundle having its own unique Hermans Orientation Factor.

For the purposes of this study there exists another orientation descriptor which, in combination with the Hermans Orientation Factor, will uniquely define the state of orientation at a point within the structure. This parameter is an angle, which will be called β, which is a

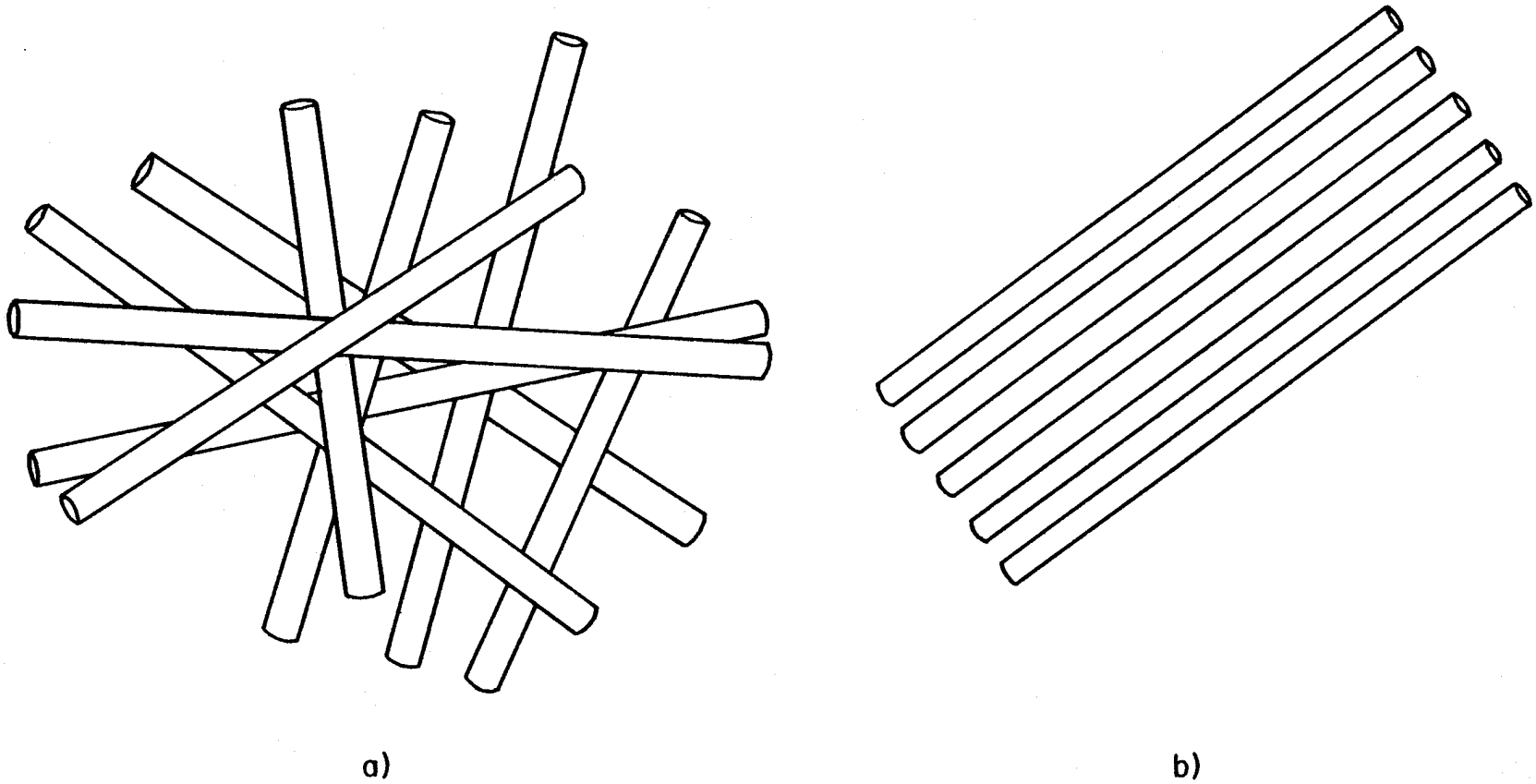

FIG. 2.4 TYPICAL FIBER BUNDLES: (a) RANDOM ORIENTATION
(b) COLUMNATED ORIENTATION

measure of the average angle from the horizontal of all fibers in a particular fiber bundle. For example, a fiber bundle with a Hermans Orientation Factor of f=0.8 might be situated in the global Y-Z plane as shown in Figure 2.5. The angle β is the average rotation from the horizontal of all of the fibers in the bundle. Thus, for the example shown the average rotation of the three fibers happens to coincide with the alignment of the center fiber. Specifying the Hermans Orientation Factor and the average rotation of the bundle at numerous points within the structure will then uniquely define the orientation state throughout that structure. From these two parameters the corresponding material properties can be computed.

A total of eight cases were studied in this work. The first three cases dealt with homogeneous materials. That is, the rotation of the fiber bundle, β, and the Hermans Orientation Factor, f, had constant values throughout the structure. Specifically, Case 1 models an in-plane isotropic material with f=0.0 and β=0.0 everywhere; Case 2 models an in-plane orthotropic material with f=1.0 and β=0.0 everywhere; and Case 3 also models an in-plane orthotropic material with f=0.5 and β=0.0 everywhere.

For the last five cases the rotation parameter, β, was assigned at points in the structure in such a way that

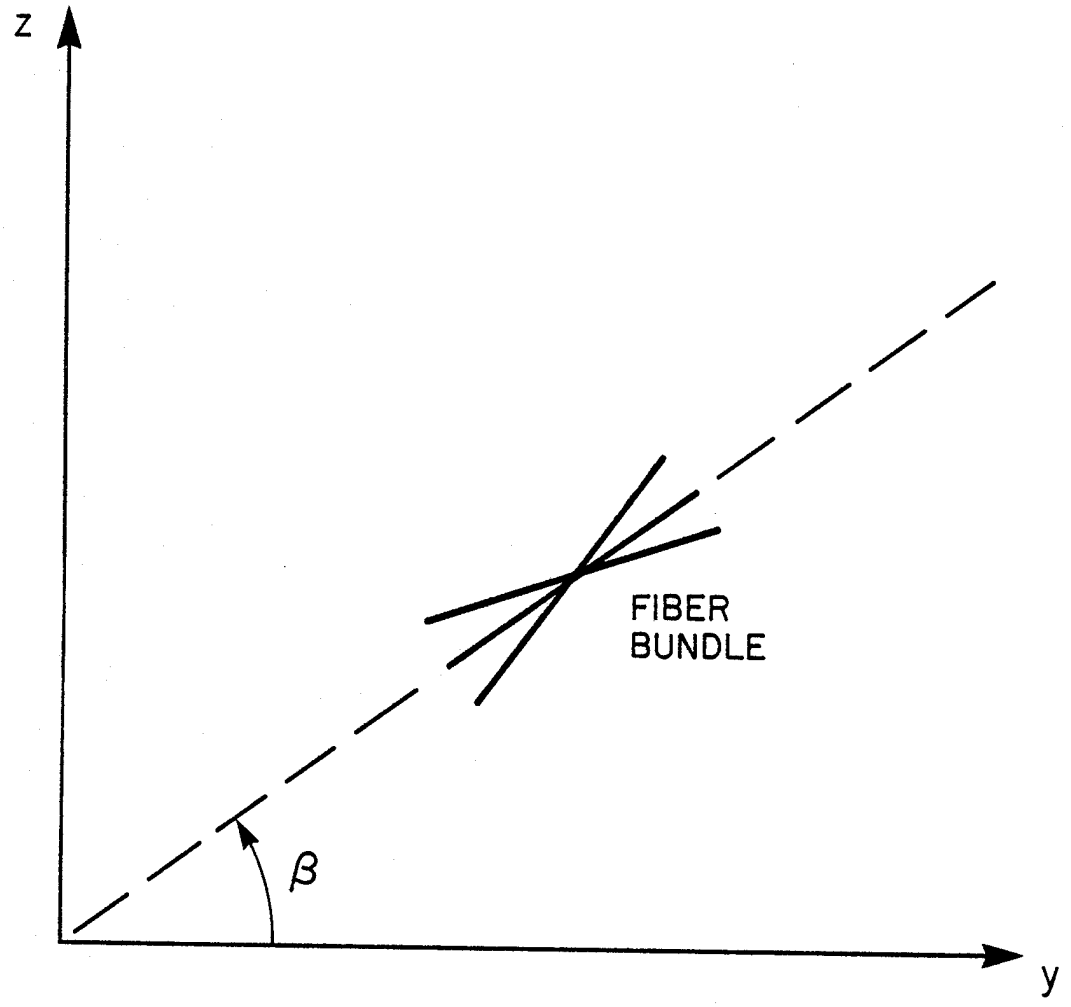

FIG. 2.5 AVERAGE ROTATION OF A FIBER BUNDLE, β

the value it assumed for a particular fiber bundle corresponded to the tangent angle of the streamline at that point for the case of an ideal flow field over a circular cylinder. The radius of the cylinder corresponds to the radius of the hole. In other words, the fiber bundles are situated such that they orient themselves along the streamlines of an ideal flow field over a circular cylinder. Figure 2.6 shows the streamlines for an ideal flow over a cylinder.

The equation for the streamlines in terms of the coordinates shown in Figure 2.6 is:

$$\psi(Y,Z) = V_\infty Z\left(1 - \frac{R^2}{Y^2+Z^2}\right) \qquad (1)$$

where:

V_∞ = Upstream velocity = constant

R = radius

When $\psi(Y,Z)$ is constant, equation (1) corresponds to a particular streamline. The equation can be written as:

$$\psi(Y,Z)/V_\infty = Z\left(1 - \frac{R^2}{Y^2+Z^2}\right) \qquad (2)$$

By setting $\psi(Y,Z)$ equal to some constant, ψ', whose value is determined by the choice of Y and Z, and taking the total differential of the resulting expression the slope of

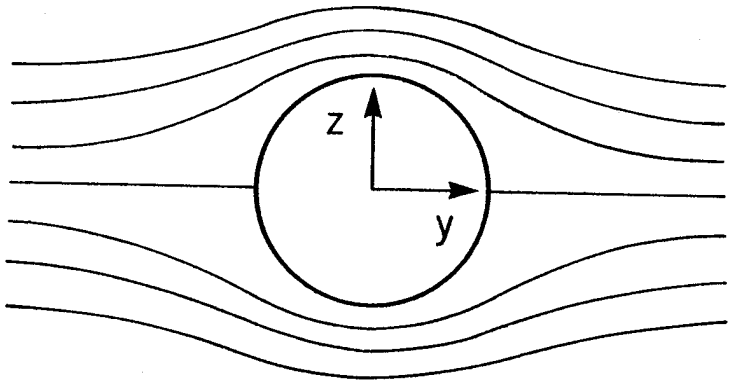

FIG. 2.6 STREAMLINES FOR IDEAL FLOW OVER A CIRCULAR CYLINDER

the streamlines, dZ/dY, can be expressed as a function of the corrdinates Y and Z. Since ψ'/V_∞ is a constant, then:

$$d(\psi'/V_\infty) = 0 \tag{3}$$

Hence:

$$d(\psi'/V_\infty) = 0 = \frac{\partial \psi}{\partial Y} dY + \frac{\partial \psi}{\partial Z} dZ \tag{4}$$

Then, from equation (4):

$$dZ/dY = - \frac{\partial \psi/\partial Y}{\partial \psi/\partial Z} \tag{5}$$

Since:

$$\frac{\partial \psi}{\partial Y} = \frac{2R^2 YZ}{(Y^2+Z^2)^2} \tag{6}$$

and:

$$\frac{\partial \psi}{\partial Z} = 1 - R^2 \frac{(Y^2-Z^2)}{(Y^2+Z^2)^2} \tag{7}$$

then:

$$\frac{dZ}{dY} = - \frac{\partial \psi/\partial Y}{\partial \psi/\partial Z} = \frac{2YZ}{(Y^2-Z^2) - (\frac{Y^2+Z^2}{R})^2} \tag{8}$$

Equation (8) gives the slope of the streamline at any point Y,Z in the flow field. By taking the arctangent of this expression the rotation of the streamline from the horizontal Y-axis is found. This rotation is the parameter defined as β.

$$\beta = \tan^{-1} \left(\frac{dZ}{dY}\right) \tag{9}$$

Hence, for cases (4) through (8) β values throughout the structure were calculated from equation (9). All β values for each model were calculated at the same points in the structure and hence each model has the same β profile. Figure 2.7 is a contour plot of constant values of β in the vicinity of the hole. The contours all pass through points A or B because the slope dZ/dY is undefined there. A particular contour will then intersect the circle at a point whose slope corresponds to the value of the contour intersecting. This is because the streamlines just next to the hole will be tangent to the hole.

With the exception of Case 4, the Hermans Orientation Factors for the cases with β following ideal streamlines are defined by various functions having radial and/or angular dependences in regions within three radii of the hole edge. Outside the three radii region the hole will be assumed to have no effect and the material will be

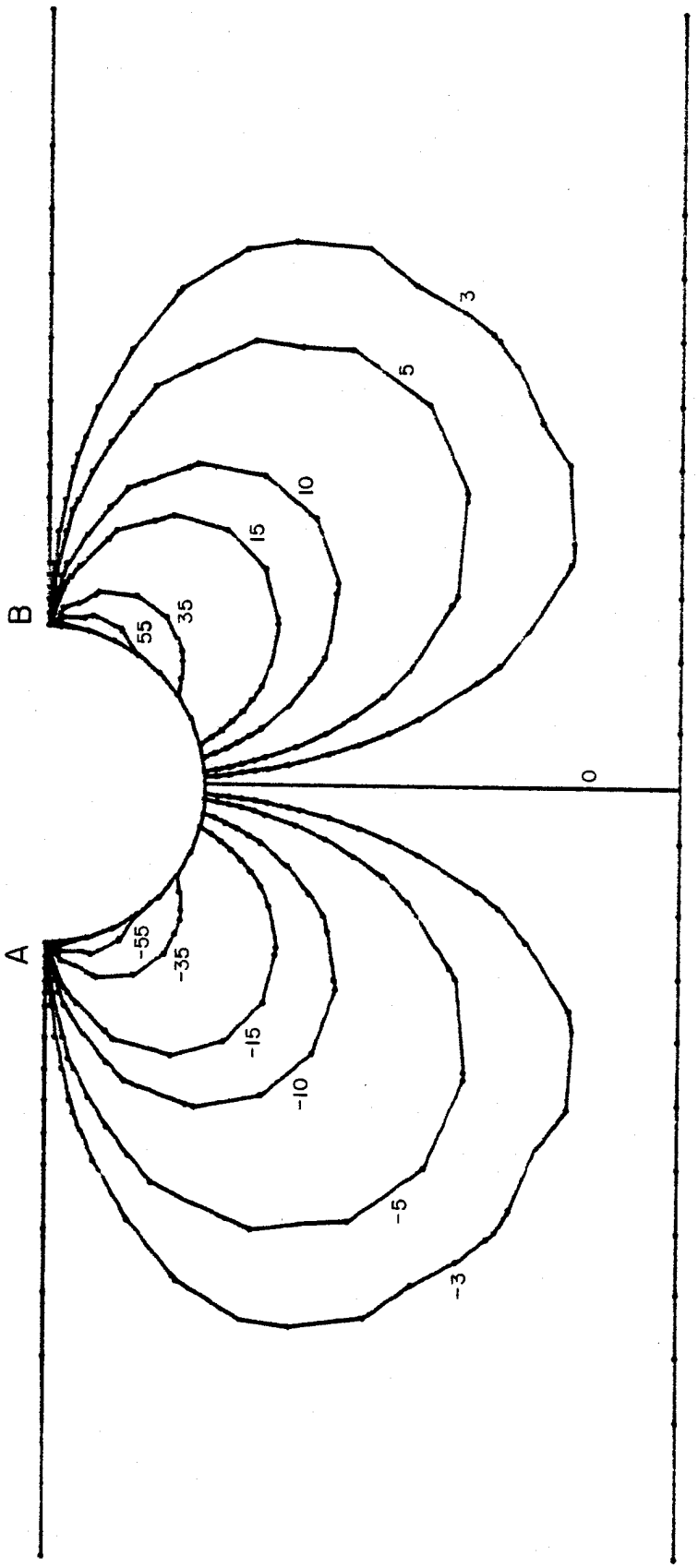

FIG. 2.7 CONTOURS OF CONSTANT FIBER BUNDLE ROTATION, β

β in degrees.

modeled as planar isotropic, i.e., f=0.0. For Case 4 the Hermans Orientation Factor will be f=1.0 everywhere.

C. SPECIFIC CASES INVESTIGATED

CASE 1:

This case is modeling the planar isotropic condition. This means that f=0.0 everywhere regardless of the presence of the hole. The rotation parameter β for this case does not matter since the local degree of columnation is completely random. This would be the model for a perfectly inviscid flow field.

CASE 2:

The in-plane orthotropic state is modeled in this case. The fibers are assumed to be perfectly columnated, f=1.0, and β=0.0 everywhere. Again, the presence of the hole is viewed as having no effect on the fiber orientation, the fibers are all perfectly columnated and are aligned in the direction of loading.

CASE 3:

This is another model of an in-plane orthotropic orientation. However, in this case the fibers are semi-random, semi-columnated, i.e., f=0.5, and have an average alignment in the loading direction, i.e., β=0.0. Once

again the hole is assumed to have no effect toward orienting the fibers. These first three cases are provided to to give an idea of the strength characteristics in parts with homogeneous fiber distributions.

CASE 4:

Case 4 deviates from the homogeneous condition. In this model the fibers are all perfectly columnated, f=1.0, but their average alignment is dependent upon the local slope of the streamlines in the flow field. In areas relatively far from the hole the fibers will be aligned in the loading direction but near the hole there will be a wide variation in fiber alignment and hence, a wide variation in material properties. Once again, the hole has no effect on fiber columnation, they have the same degree of columnation everywhere. This particular case is provided in order to judge the effect of fiber bundle alignment on strength by comparing this case with Case 2 ($f=1.0$, $\beta=0.0$).

CASE 5:

In this and the remaining cases an attempt is made to account for the shearing effects of the hole, in a simplified manner, by imposing radial and/or angular dependence on the Hermans Orientation Factor. This effect will be assumed to be confined to an area within three

radii of the hole edge. As stated earlier the average alignment of the fiber bundles, β, for the remaining cases depends on the local streamline slope. In this particular case the Hermans Orientation Factor is assumed to be a linear function of the radial position, independent of the angle α. These radial and angular coordinates are shown in Figure 2.8. The value assigned to f at the hole edge, r=0.25, is f=1.0 and decreases linearly for a distance of three radii to r=1.0 where it has the value f=0.0. The function for f is:

$$f(r) = \frac{4}{3}(1-r) \qquad .25 \leq r \leq 1.0 \tag{10}$$

A contour plot for constant values of f is shown in Figure 2.9.

CASE 6:

In the case of fluid flowing over a cylinder there are regions just before and just after the cylinder in which local mixing occurs due to abrupt flow changes and drag forces. It might be expected that the fibers in these regions would have a somewhat random orientation due to the mixing. In an attempt to account for this phenomenon this case, in addition to a radial orientation dependence, also imposes an angular dependence on the degree of

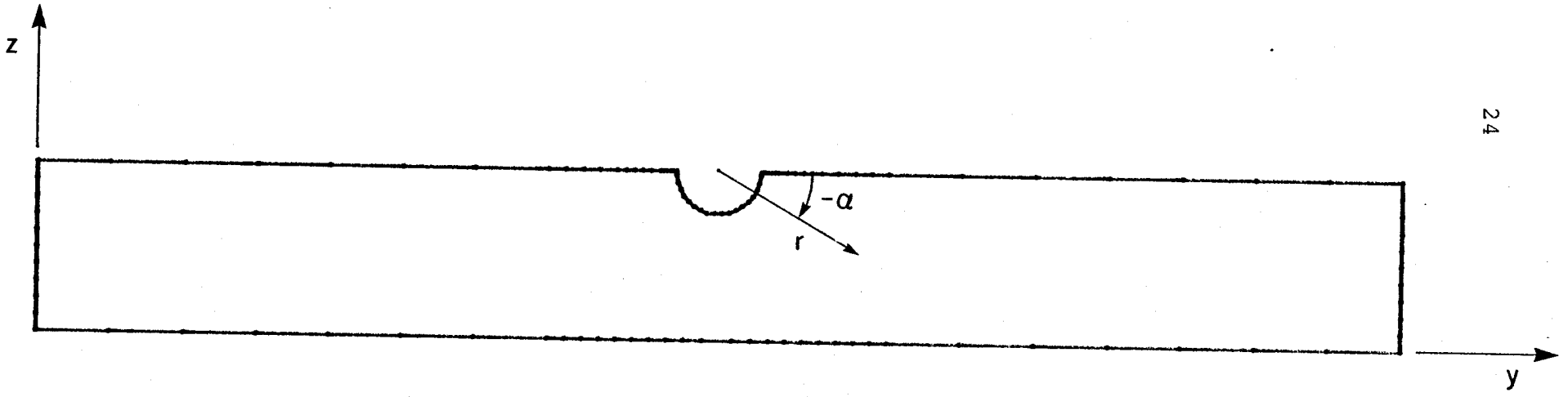

FIG. 2.8 RADIAL AND ANGULAR COORDINATES FOR THE HERMANS ORIENTATION FACTOR

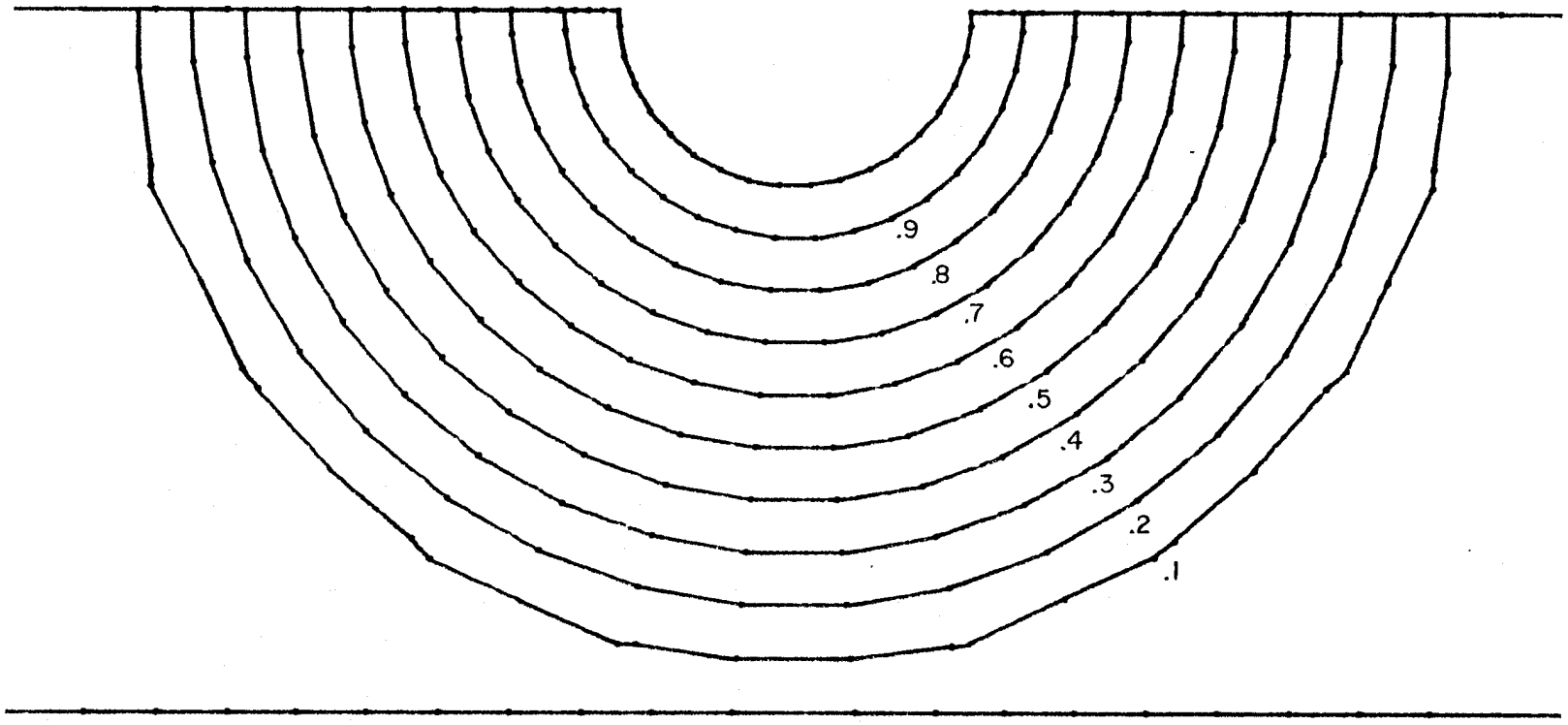

FIG. 2.9 CONTOURS OF CONSTANT f : CASE 5

orientation. This angular dependence is imposed by multiplying the function in Case 5 (equation (10)) by the sine of the position angle α. The sine function was chosen to suggest that the rate of change in degree of columnation is greater at values of α near 0° and -180° and smaller when α is in the vicinity of -90°. The function is given by equation (11) where the negative sign is included because α is negative.

$$f(r,\alpha) = -\frac{4}{3}(1-r)\sin\alpha \qquad \begin{matrix} 0.25 \leq r \leq 1.0 \\ -180° \leq \alpha \leq 0° \end{matrix} \qquad (11)$$

Thus when α is near 0° or -180° the Hermans Orientation Factor is small regardless of the radial value. Then for values of α approaching -90° f begins to assume the distribution given in Case 5. A contour plot for constant values of f is shown in Figure 2.10.

CASE 7:

In Cases 5 and 6 the relationship between f and the radial position was modeled as being linear. It may be the case that the Hermans Orientation Factor drops off sharply from a value near unity at the hole edge to a value near zero a short distance away. Taking this into account and still attempting to model the angular dependence with a sine relationship, an exponential decay is imposed on

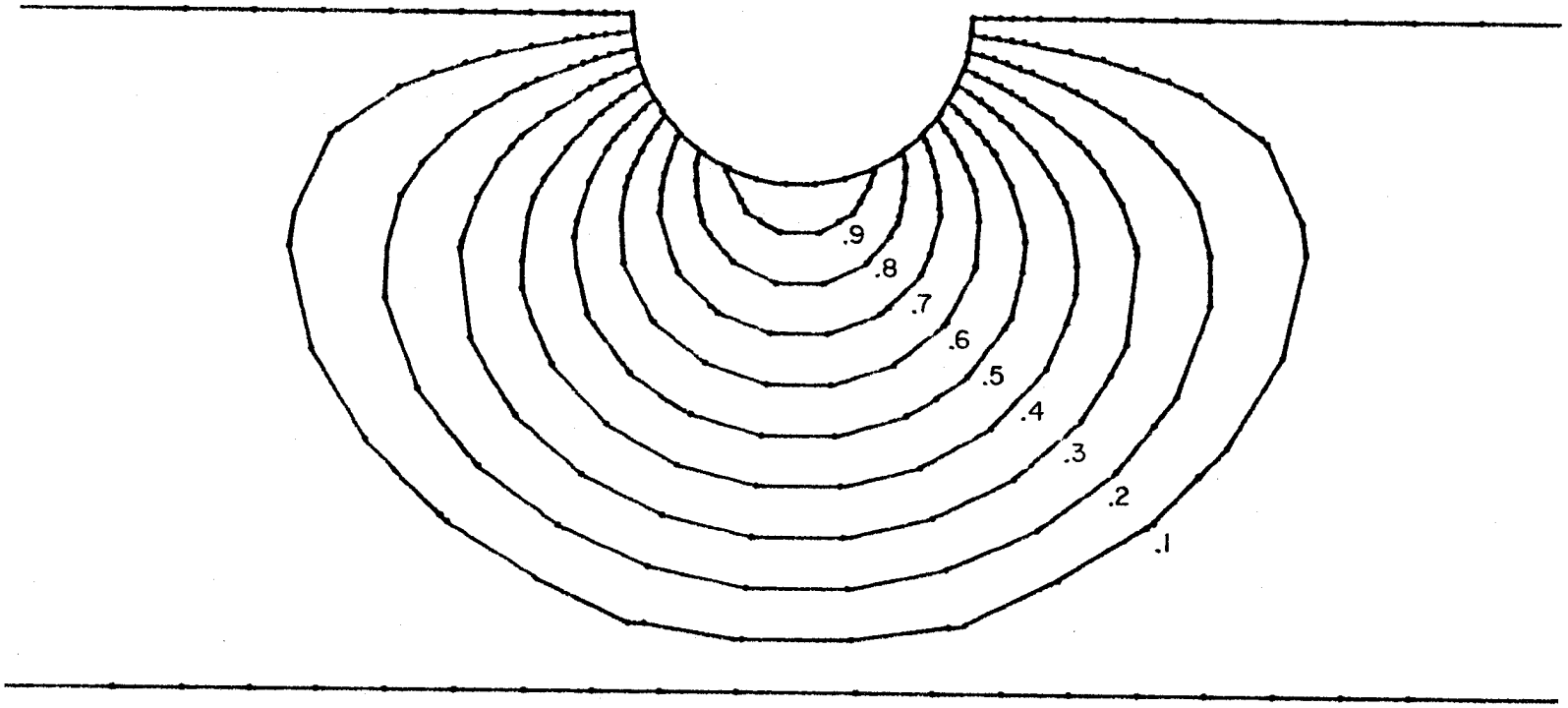

FIG. 2.10 CONTOURS OF CONSTANT f : CASE 6

the radial component. This exponential relationship has the general form:

$$f(r,\alpha) = Ae^{-Br}\sin\alpha \tag{12}$$

where A and B are constants. This expression is then subjected to the boundary conditions:

$$f(0.25, -90°) = 1.0 \tag{13}$$

and:

$$f(1.0, \alpha) = .001 \simeq 0.0 \tag{14}$$

which state that f=1.0 at the hole edge when the sine function is unity, and f≃0.0 at a distance of three radii from the hole edge regardless of the angle. From (13) and (14):

$$\begin{aligned} A &= -10.0 \\ B &= 9.21 \end{aligned} \tag{15}$$

Hence:

$$f(r,\alpha) = -10e^{-9.21r} \sin \alpha \qquad 0.25 \leq r \leq 1.0 \qquad (16)$$
$$-180° \leq \alpha \leq 0.0°$$

By using this function the value of f drops off to at most f=0.1 within one radius of the hole edge. A contour plot for constant values of f is shown in Figure 2.11.

CASE 8:

When a real fluid flows past a cylinder a small boundary layer can form near the cylinder wall. This boundary layer can have the effect of causing a larger area to be affected by shearing forces downstream of the cylinder than the area affected upstream. Thus, there will be a tendency for fibers downstream to retain a degree of columnation within a larger region than the region containing similar columnation upstream.

In the cases studied thus far the Hermans Orientation Factor had a symmetrical distribution about $\alpha = -90°$. However, if the boundary layer effect is taken into account, a particular point downstream may have a higher f value, i.e., have a higher degree of columnation, than its symmetrical counterpart upstream. In an attempt to model this phenomenon two different expressions are used. For the part of the structure lying upstream, i.e., to the left of the hole center, the expression derived for Case 7

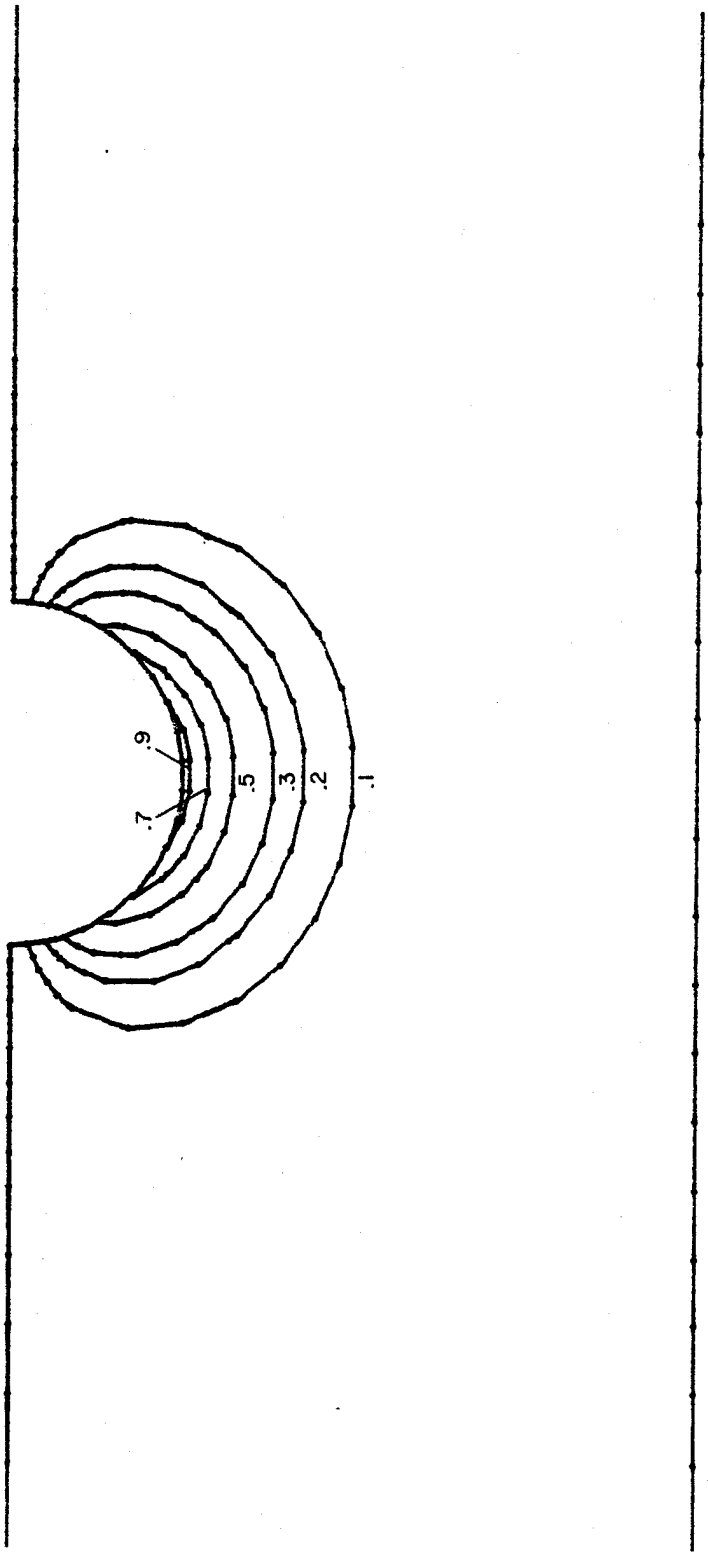

FIG. 2.11 CONTOURS OF CONSTANT f : CASE 7

(equation (16)) is used. For the part lying downstream of the hole a combination of the functions used in Cases 6 and 7 is used to model the fiber behavior there. Both of these expressions are shown and explained below.

$$f(r,\alpha) = -10e^{-9.21r}\sin\alpha \qquad 0.25\leq r\leq 1.0 \qquad (17)$$
$$-180°\leq\alpha\leq -90°$$
$$\text{Upstream}$$

$$f(r,\alpha) = -[10e^{-9.21r}u + (\tfrac{4}{3})(1-r)(1-u)]\sin\alpha \qquad (18)$$
$$0.25\leq r\leq 1.0$$
$$-90°\leq\alpha\leq 0.0°$$
$$\text{Downstream}$$

where:

$$u(\alpha) = (\frac{-\alpha}{90°})^{1/2} \qquad -90°\leq\alpha\leq 0.0° \qquad (19)$$

Thus for small values of α the slower decaying linear term dominates equation (18) representing a slower transition of the fibers back to the random orientation state. As α gets larger the exponential term begins to dominate the expression representing a departure from the region affected by the boundary layer and a return to a quick drop in the degree of columnation. The controlling function $U(\alpha)$ was chosen on the basis of simplicity and

because it produced a reasonable contour plot. This contour plot of constant f values is shown in Figure 2.12.

D. MATERIAL PROPERTY ASSIGNMENT

Once the orientation state of the fibrous phase has been uniquely defined, i.e., a value of f and β has been specified at numerous points throughout the structure, elements in the finite element grid can then be assigned unique material properties. For each of the cases considered, values for the coordinates Y and Z, and values for f and β were specified at 1261 points throughout the structure. A computer code was written to generate this information. The computer-aided design program written by Quigley [4] makes use of this data deck to assign effective material properties to the elements. Incorporated in Quigley's program is a program written by Jarzebski et al. [1] which, given the fiber orientation state and material composition, provides reasonable engineering estimates for the corresponding material properties. Quigley's code takes the information generated by this subprogram and through a local averaging process uses the material properties defined for the various fiber orientations within an element to generate effective material properties for the element as a whole. This process is done for each element resulting in a structure whose material properties

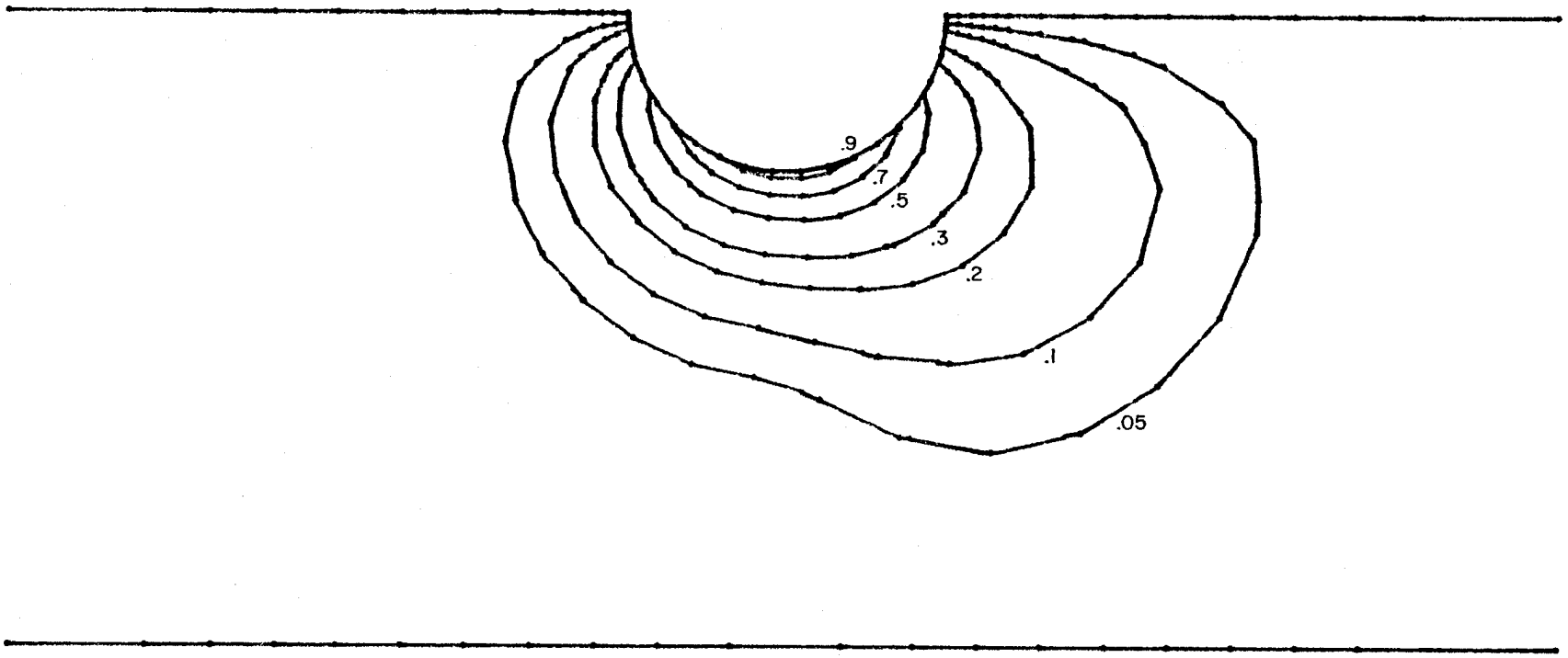

FIG. 2.12 CONTOURS OF CONSTANT f : CASE 8

are allowed to vary from element to element.

E. FINITE ELEMENT ANALYSIS

With the material property assignment complete for a particular case the problem is then ready to be prepared for a finite element analysis. Quigley's program will take all the information generated for the finite element grid, such as nodal point coordinates, boundary conditions, applied loads, element material information, etc., and organize an input data file compatible with that required for the SAPV finite element analysis code. The code is then executed. The program output contains the stress and displacement information to be used in the performance analysis.

III. RESULTS

The results for each case will be presented in two parts. The first part will contain information pertaining to the finite element analysis. This will include a typical deformed mesh, normal stress contours, loading direction deflection contours, and Young's moduli, shear moduli, and Poisson's ratio contour plots. The second part will present a failure model for the cases studied which also extends the results to predict failure in similar structures with hole sizes other than 0.25 inch (6.35 mm).

All of the information presented in the first section was created with the aid of Quigley's [4] computer-aided design program. This program has the capability of reading in solution output data created by the SAPV program and use the information to plot contours of stress and deflection. The material property contour plots are constructed using the information contained in the element material property data file. The variation of these parameters with the fiber orientation state is then discussed.

In section 2 the reduction in strength of the part due to the presence of the hole or notch is compared with the unnotched strength. To accomplish this, models proposed by Whitney [5,6] and Karlak [2] are used as a guideline. Whitney has proposed a failure criterion based on the stress distribution adjacent to the notch. The criterion assumes that failure occurs when the stress at some characteristic length, d_o, from the edge of the hole reaches the unnotched ultimate strength of the material. That is, when:

$$\sigma Y\Big|_{x=R+d_o} = \sigma_o \tag{20}$$

where σ_o is the unnotched strength. Figure 3.1 shows the variables used in the model.

For an infinite orthotropic plate containing a circular hole a simplified expression for the stress distribution along the x-axis has been calculated using the exact elasticity solution to be [8]:

$$\sigma Y/\bar{\sigma} = (\tfrac{1}{2})\,[2+(R/X)^2+3(R/X)^4-(K_T^{\infty}-3)\,[5(R/X)^6-7(R/X)^8]] \tag{21}$$

where:

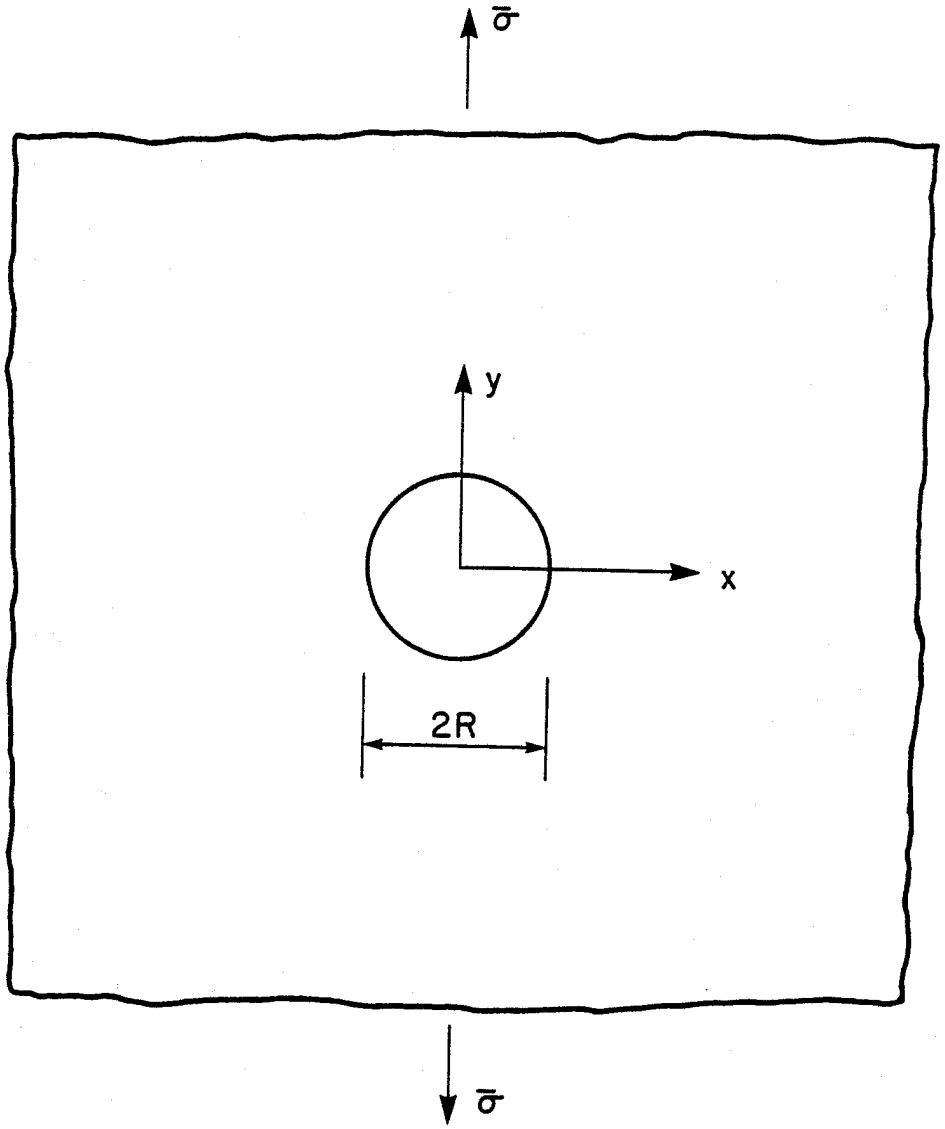

FIG. 3.1 GEOMETRY FOR FAILURE ANALYSIS

$$K_T^{\infty} = 1+[2[(E_Y/E_X)^{1/2}-\nu_{YX}]+E_Y/G_{YX}]^{1/2} \qquad (22)$$

K_T^{∞} is the stress concentration factor, E_X, E_Y, ν_{YX}, and G_{YX} are the effective orthotropic elastic material constants, and $\bar{\sigma}$ is the nominal stress in the part.

Whitney [5,6] suggested that the dimension d_o be a material constant. However, Karlak has proposed a modification in which d_o is a function of the notch radius. Pipes [3,7] suggested that the relationship have the form:

$$d_o = R^m/C \qquad (23)$$

where m and C are material dependent parameters.

By combining equations (21), (22), and (23) an equation is established which predicts the notched tensile strength as a function of the notch radius and the parameters m, C, and σ_o.

$$\sigma_N/\sigma_o = 2\{2+\lambda^2+3\lambda^4-(K_T^{\infty}-3)[5\lambda^6-7\lambda^8]\}^{-1} \qquad (24)$$

where:

$$\lambda = (1+R^{m-1}C^{-1})^{-1} \qquad (25)$$

σ_N is the notched strength of the material. It should be noted that as R approaches infinity λ approaches 1.0 and consequently σ_N/σ_o approaches $1/K_T^{\infty}$. This model has been shown to be in good agreement with experimental data [3].

Using this model as a guideline a failure model was developed for each of the cases studied. In these models the parameters m, and C are assumed to have the constant values given below. In reality these parameters

$$\begin{aligned} m &= 0.5 \\ C &= 10.0 \end{aligned} \tag{26}$$

may vary with fiber orientation, but this variation is neglected here. In each of the cases a polynomial, similar in form to equation (21), was fit to the stress distribution near the notch as predicted by the finite element analysis. This polynomial has the form:

$$\sigma_Y/\bar{\sigma} = 1 + B(R/X)^2+C(R/X)^4+D(R/X)^6+E(R/X)^8 \tag{27}$$

where B, C, D, and E are constants for a particular case and $\bar{\sigma}$ = 1000 PSI for all cases. Using the failure criterion established above in combination with equation (27) it is possible to express the notched strength of the structure in a form similar to equation (24).

$$\sigma_N/\sigma_o = [1+B\lambda^2+C\lambda^4+D\lambda^6+E\lambda^8]^{-1} \qquad (28)$$

where:

$$\lambda = [1 + R^{m-1}C^{-1}]^{-1} \qquad (29)$$

and σ_N is the notched strength.

In summary, for a particular case the polynomial of equation (27) is fit to the stress distribution near the notch predicted by the finite element analysis. This is done to establish the constants B, C, D, and E. Once established they are then used in equation (28) to express the notched strength of the structure as a function of the notch radius. Thus, this establishes a failure criterion for similar structures with hole sizes other than the one examined in this study. This was all accomplished with the aid of short computer programs and plotting routines and the results are presented, along with the finite element results, in the following section.

RESULTS

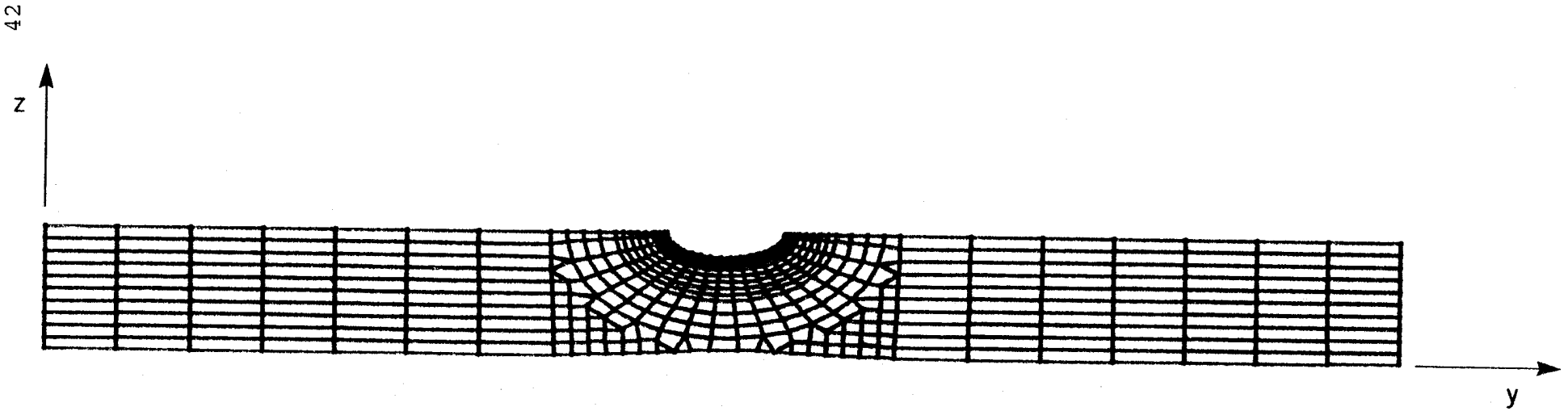

FIG. 3.2 TYPICAL DEFORMED MESH
DISPLACEMENT MAGNIFICATION: 500X

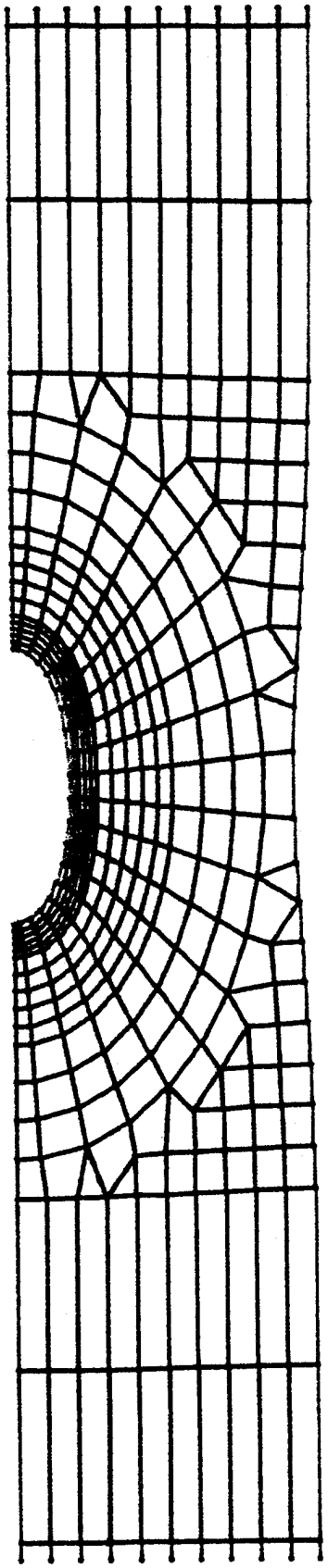

FIG. 3.3 ENLARGED DEFORMED MESH NEAR THE HOLE
Displacement Magnification : 500X

A. CASE 1

$f = 0.0$; $\beta = 0.0$ (Planar Isotropic)

1. Finite Element Results

Fig. 3.4	Y-Deflection Contours
Fig. 3.5	σ_Y-Stress Contours

2. Failure Model

Fig. 3.6	Strength Ratio vs. Notch Radius
Fig. 3.7	Strength Ratio vs. Log Radius

Note: $E_Y = 0.201 \times 10^7$ PSI

$E_Z = 0.201 \times 10^7$ PSI

$G_{YZ} = 0.779 \times 10^6$ PSI

$\nu_{YZ} = 0.291$

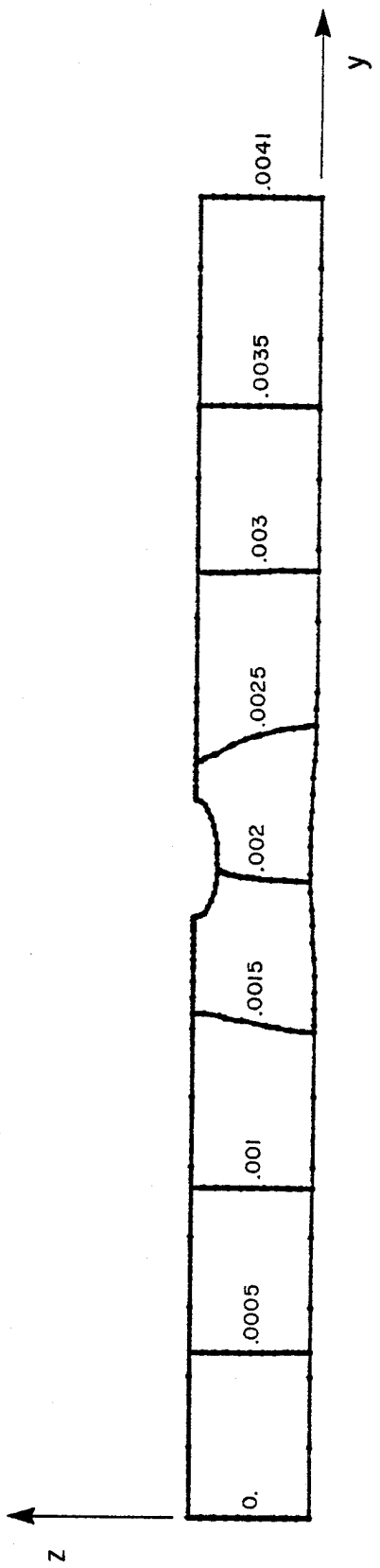

FIG. 3.4 Y-DEFLECTION CONTOURS (INCHES)
OUTLINE DEFORMATION MAGNIFICATION: 500X

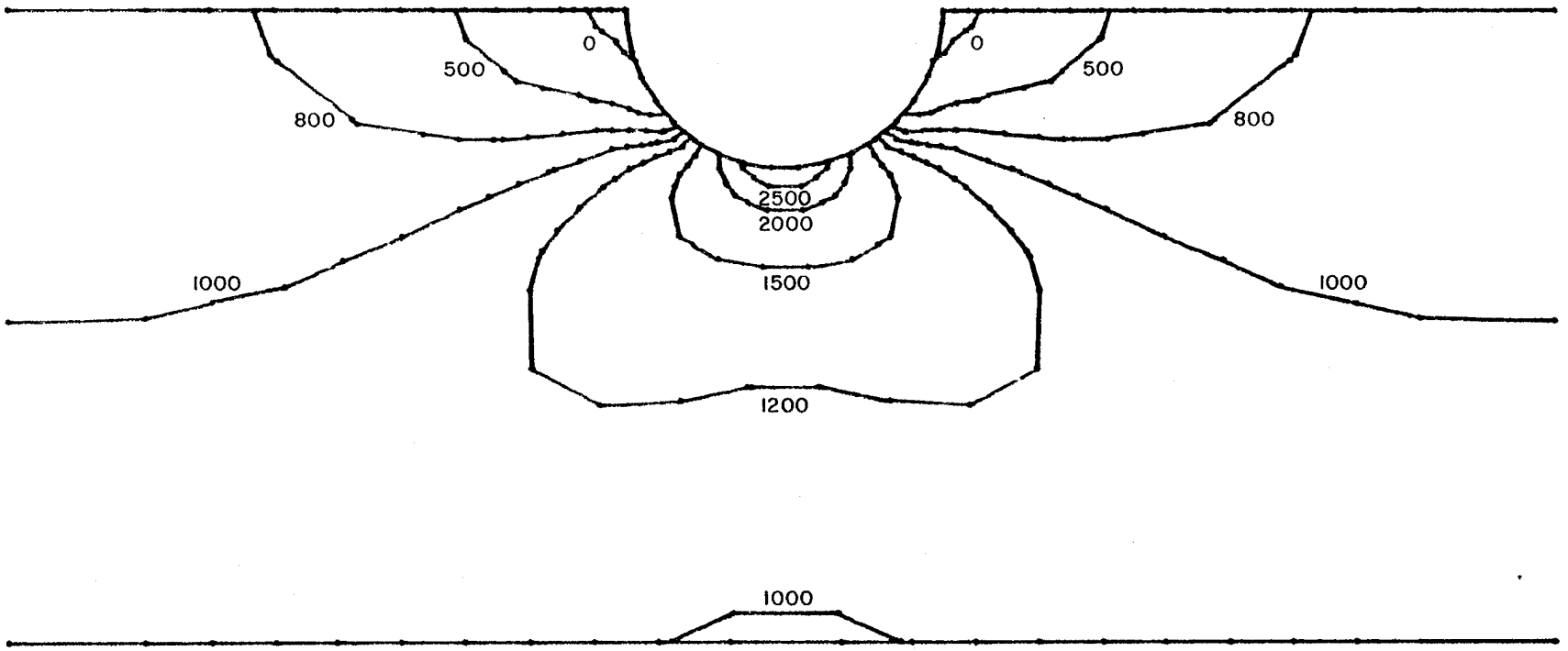

FIG. 3.5 σ_Y-STRESS CONTOURS (PSI)

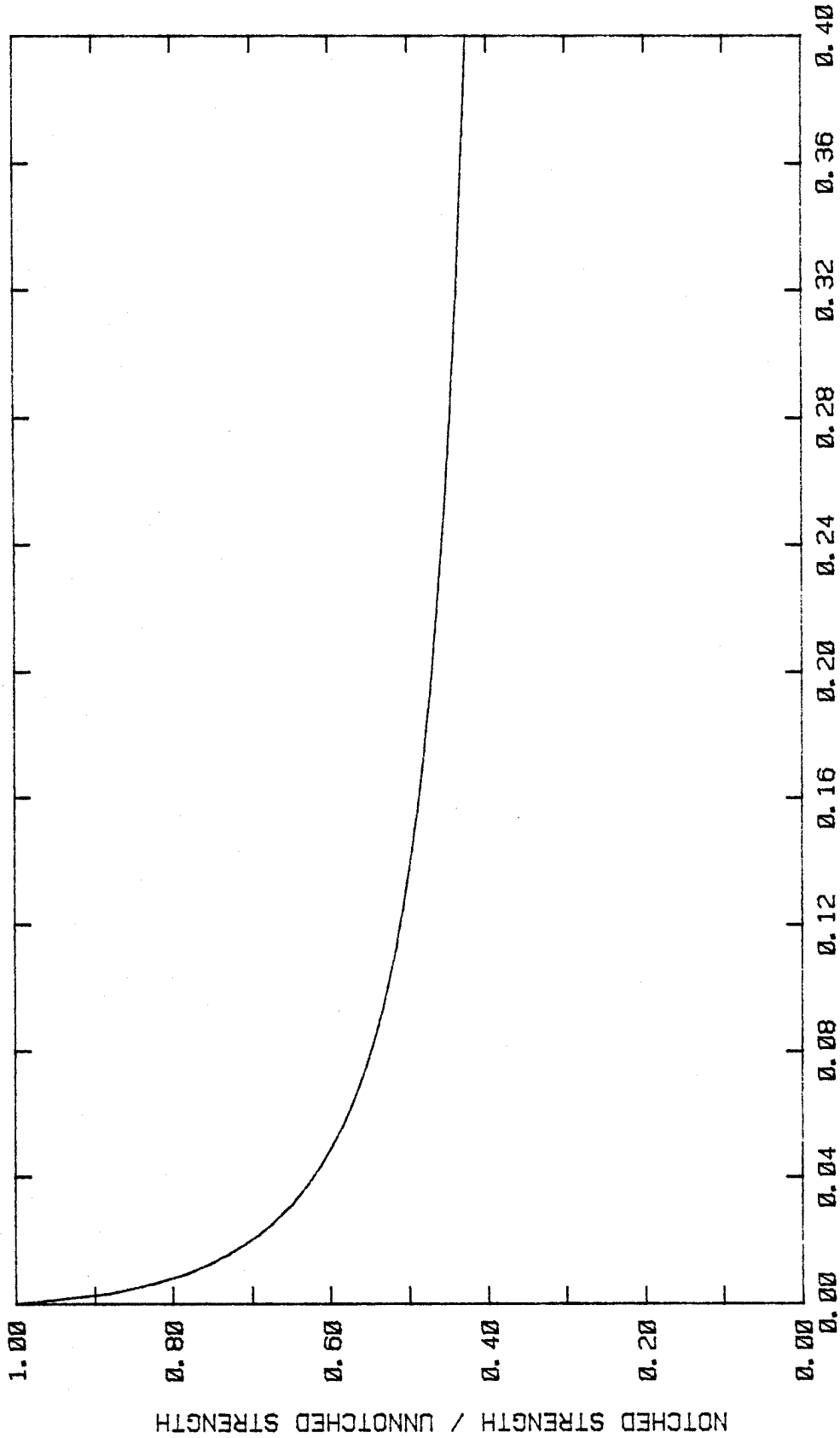

FIG. 3.6 STRENGTH RATIO VS. NOTCH RADIUS

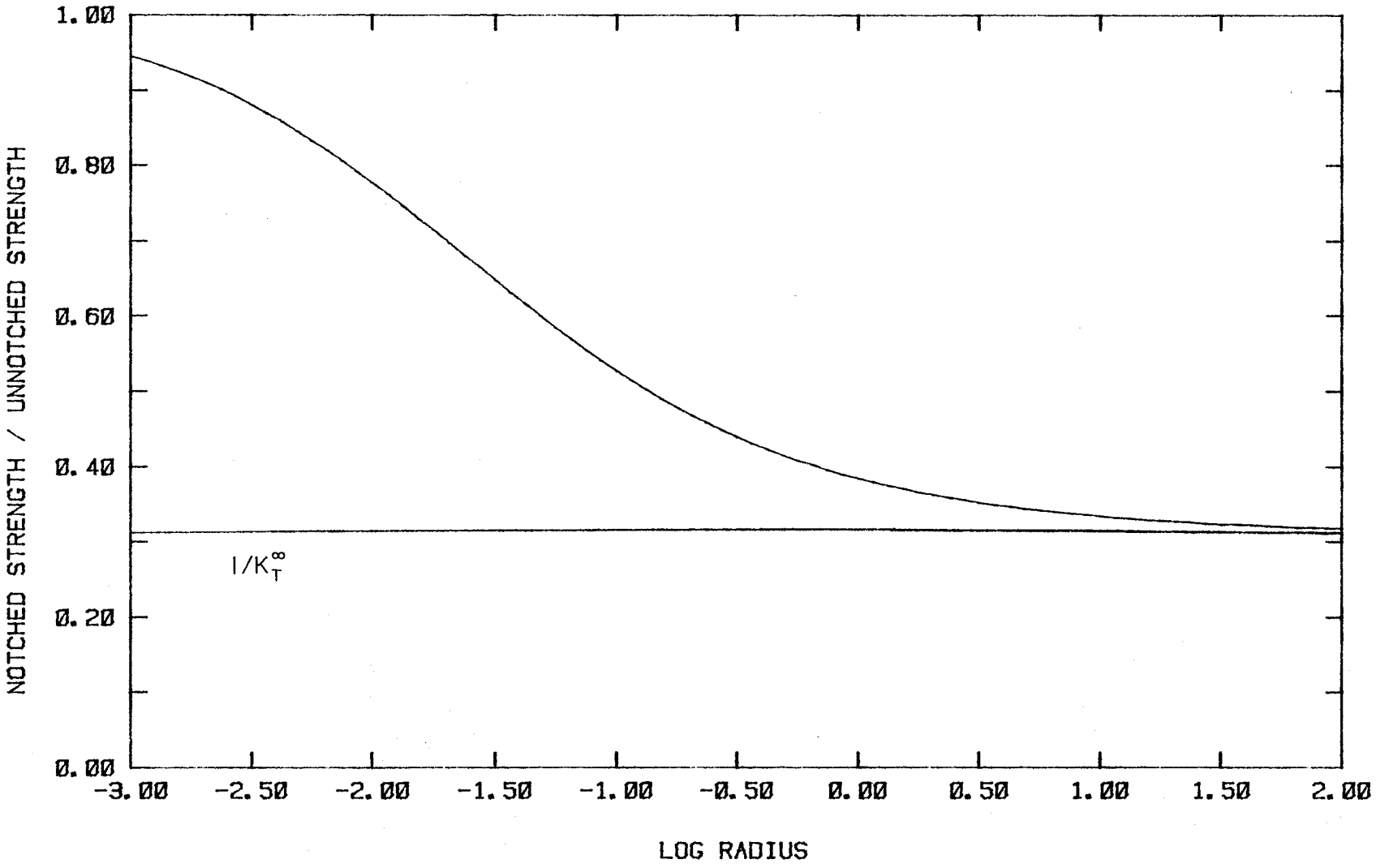

FIG. 3.7 STRENGTH RATIO VS. LOG RADIUS

B. CASE 2

$f = 1.0$; $\beta = 0.0$ (Planar Orthotropic)

1. Finite Element Results

Fig. 3.8 Y-Deflection Contours

Fib. 3.9 σ_Y-Stress Contours

2. Failure Model

Fig. 3.10 Strength Ratio vs. Notch Radius

Fig. 3.11 Strength Ratio vs. Log Radius

Note: $E_Y = 0.286 \times 10^7$ PSI

$E_Z = 0.159 \times 10^7$ PSI

$G_{YZ} = 0.637 \times 10^6$ PSI

$\nu_{YZ} = 0.296$

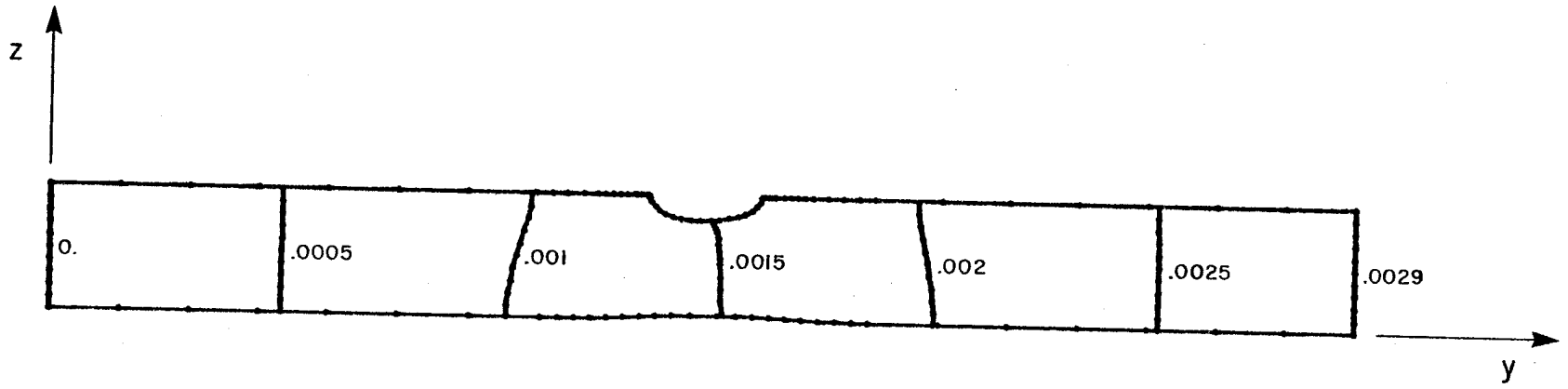

FIG. 3.8 Y-DEFLECTION CONTOURS (INCHES)
OUTLINE DEFORMATION MAGNIFICATION: 500X

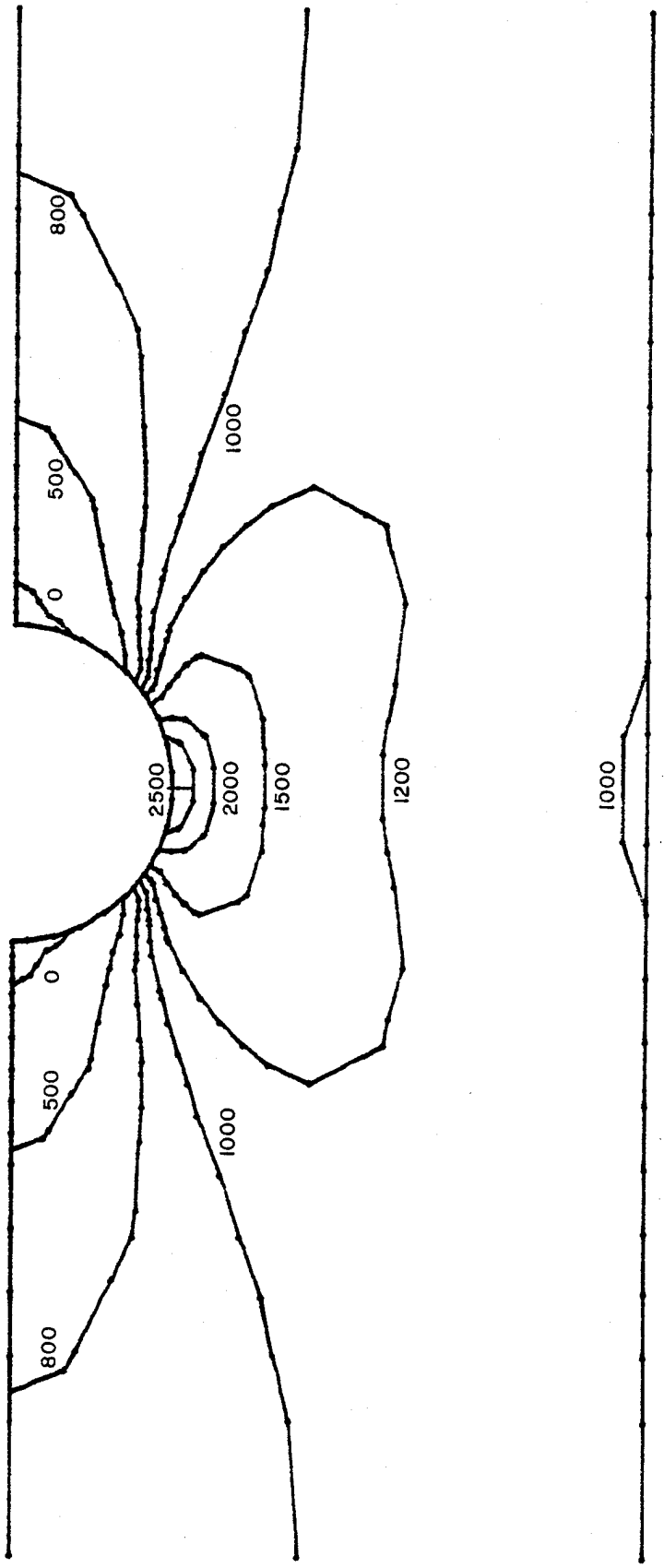

FIG. 3.9 σ_Y-STRESS CONTOURS (PSI)

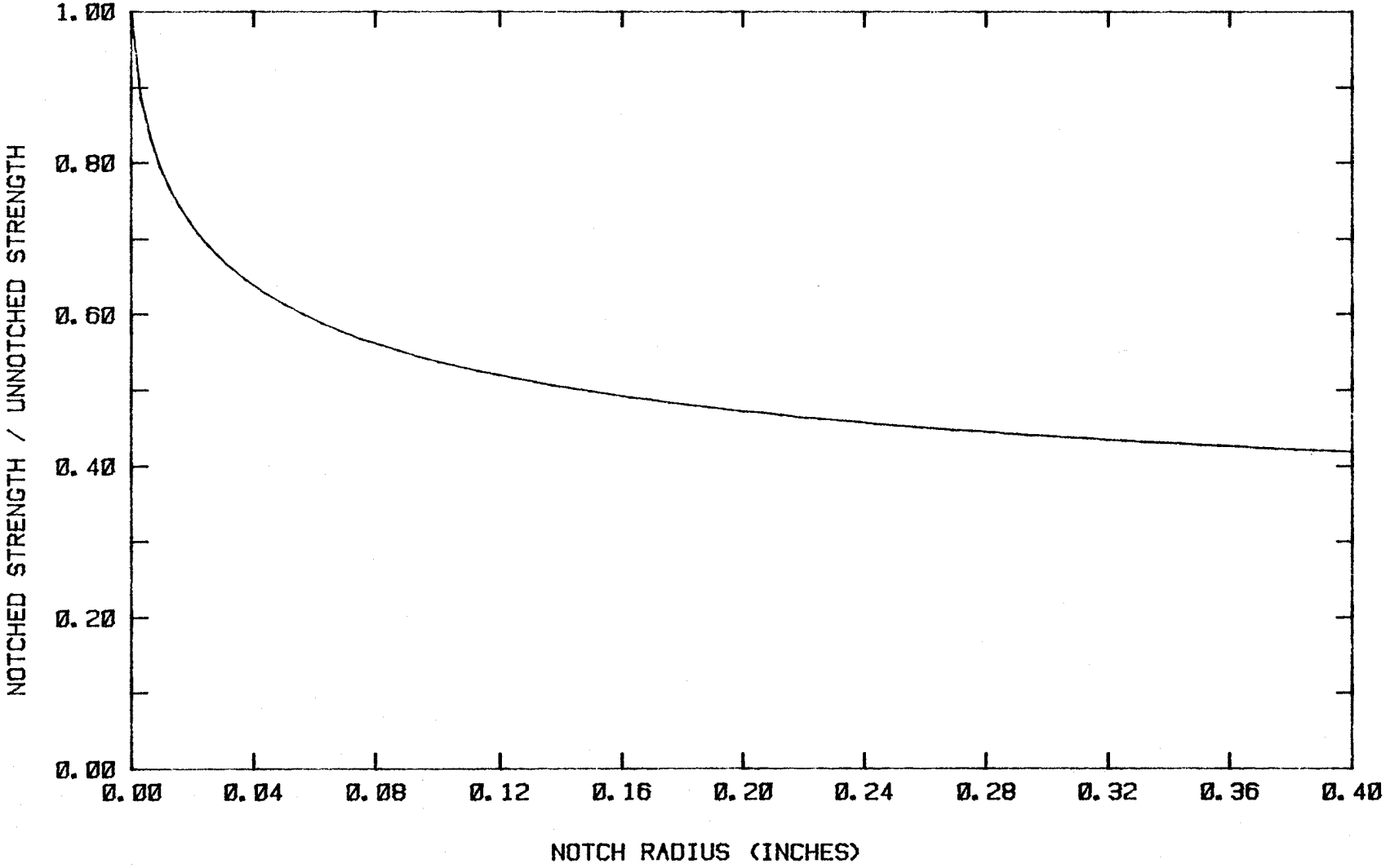

FIG. 3.10 STRENGTH RATIO VS. NOTCH RADIUS

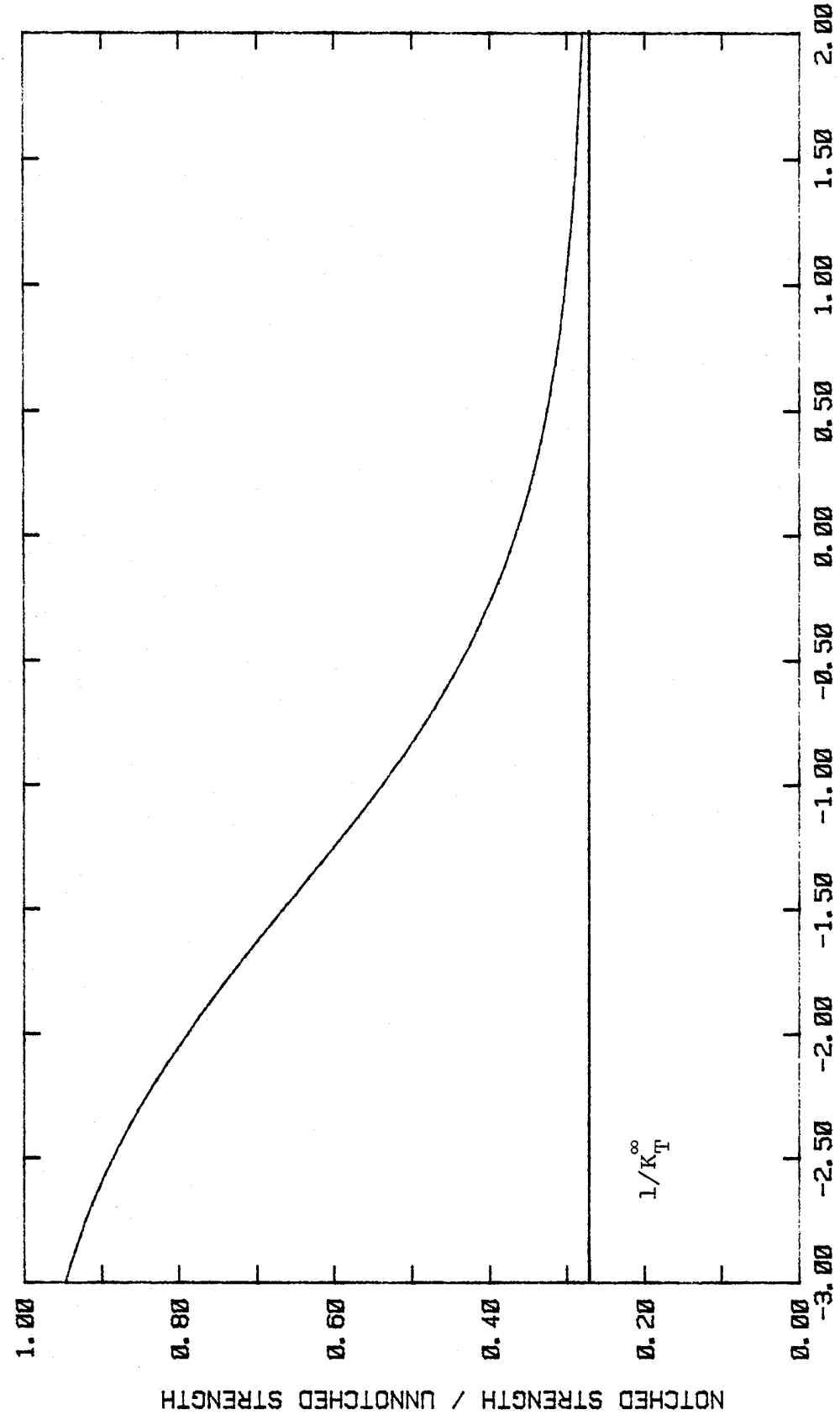

FIG. 3.11 STRENGTH RATIO VS. LOG RADIUS

C. CASE 3

$f = 0.5$; $\beta = 0.0$ (Planar Orthotropic)

1. Finite Element Results

Fig. 3.12 Y-Deflection Contours

Fib. 3.13 σ_Y-Stress Contours

2. Failure Model

Fig. 3.14 Strength Ratio vs. Notch Radius

Fig. 3.15 Strength Ratio vs. Log Radius

Note: $E_Y = 0.231 \times 10^7$ PSI

$E_Z = 0.170 \times 10^7$ PSI

$G_{YZ} = 0.779 \times 10^6$ PSI

$\nu_{YZ} = 0.342$

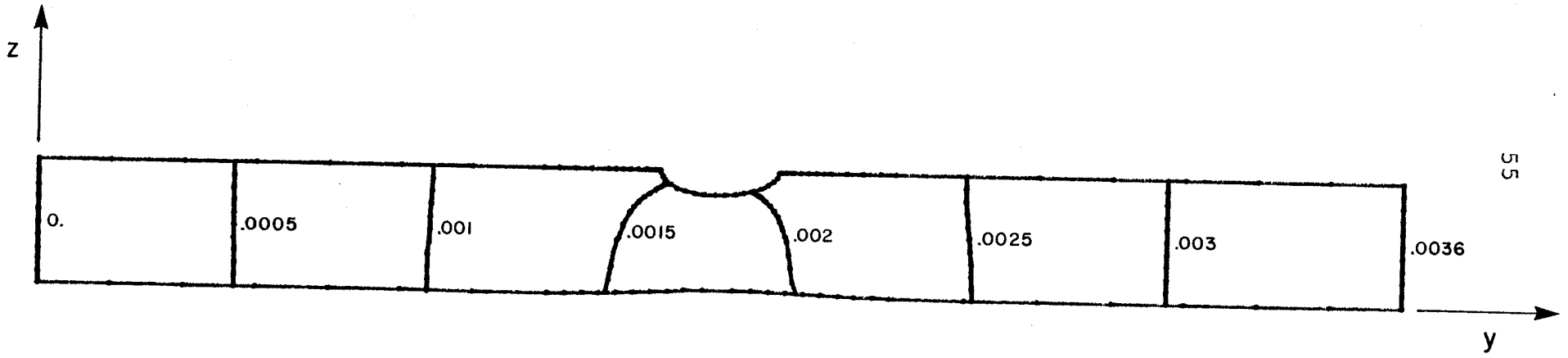

FIG. 3.12 Y-DEFLECTION CONTOURS (INCHES)
OUTLINE DEFORMATION MAGNIFICATION: 500X

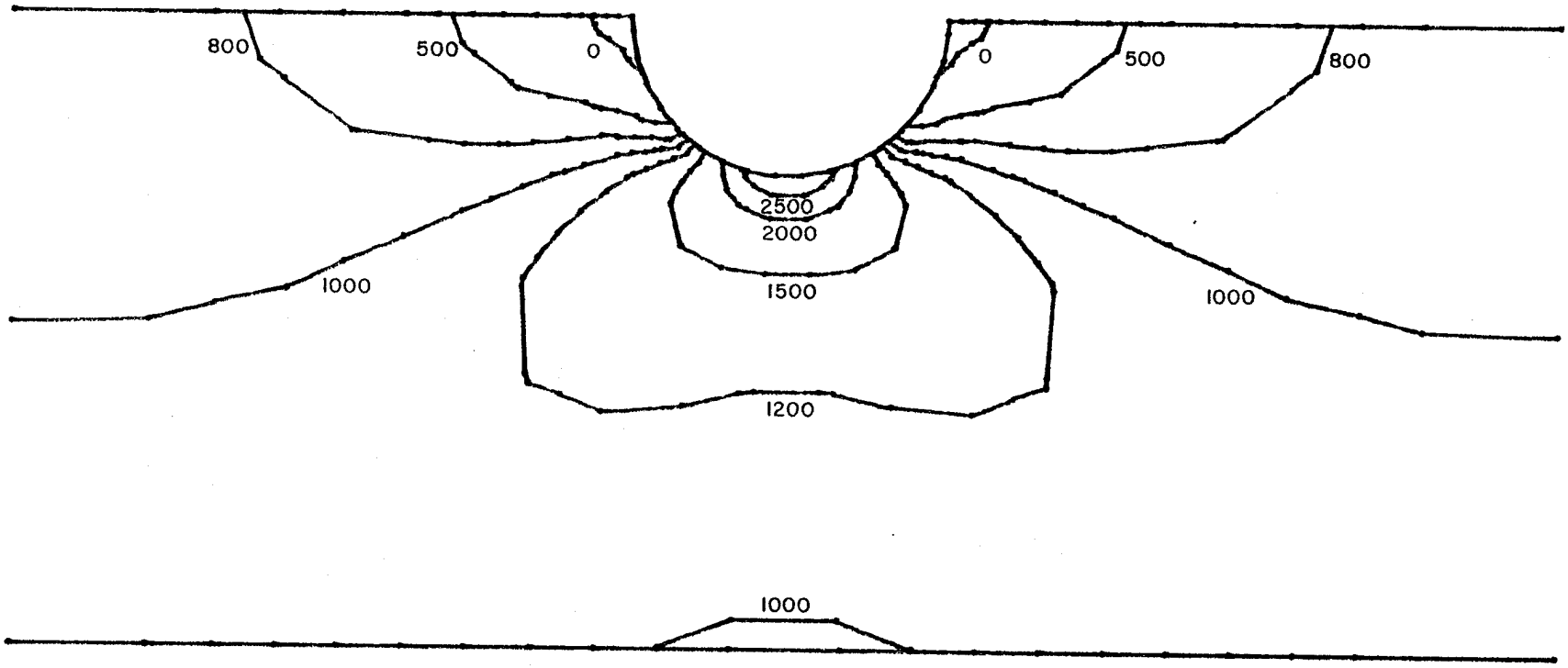

FIG. 3.13 σ_Y-STRESS CONTOURS (PSI)

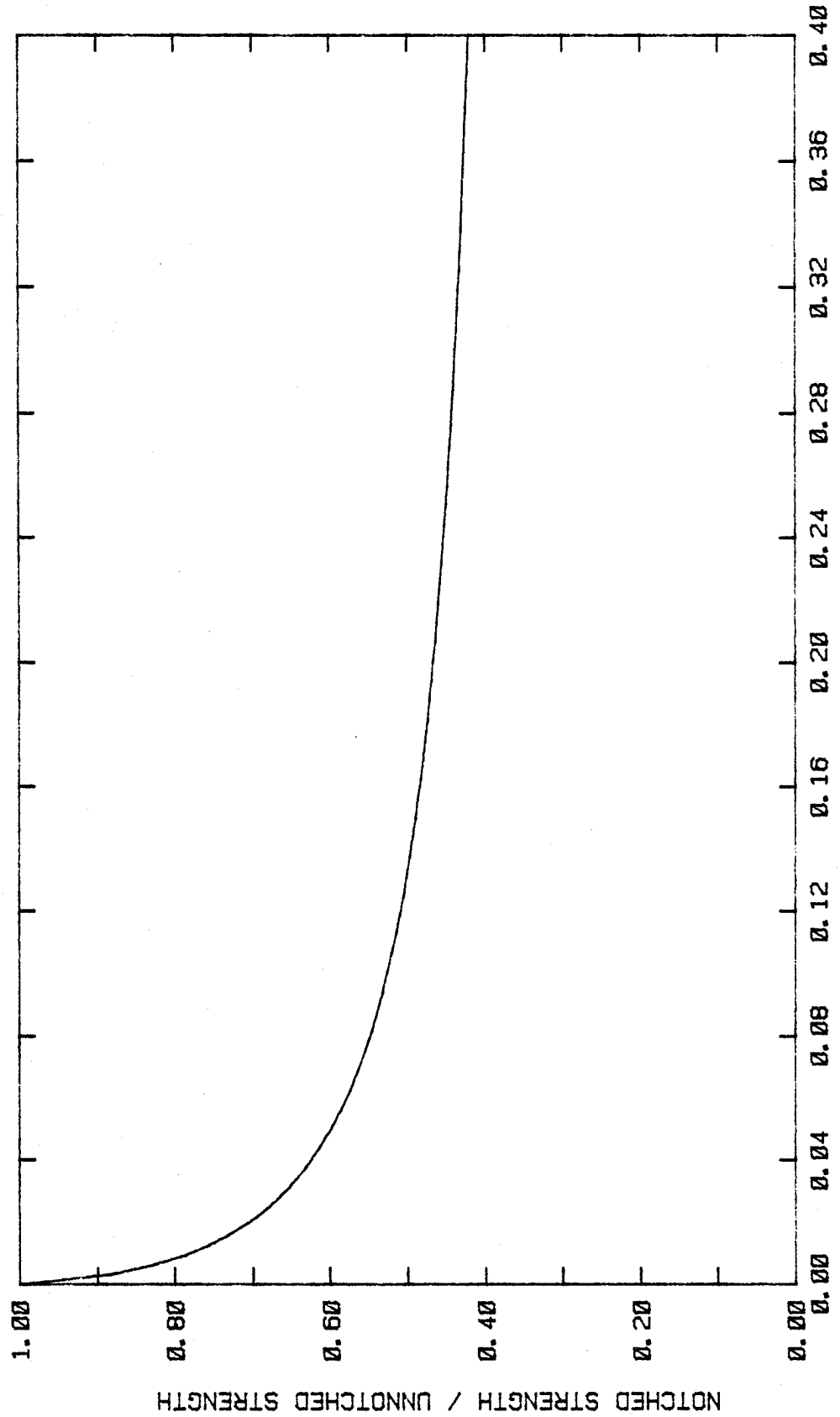

FIG. 3.14 STRENGTH RATIO VS. NOTCH RADIUS

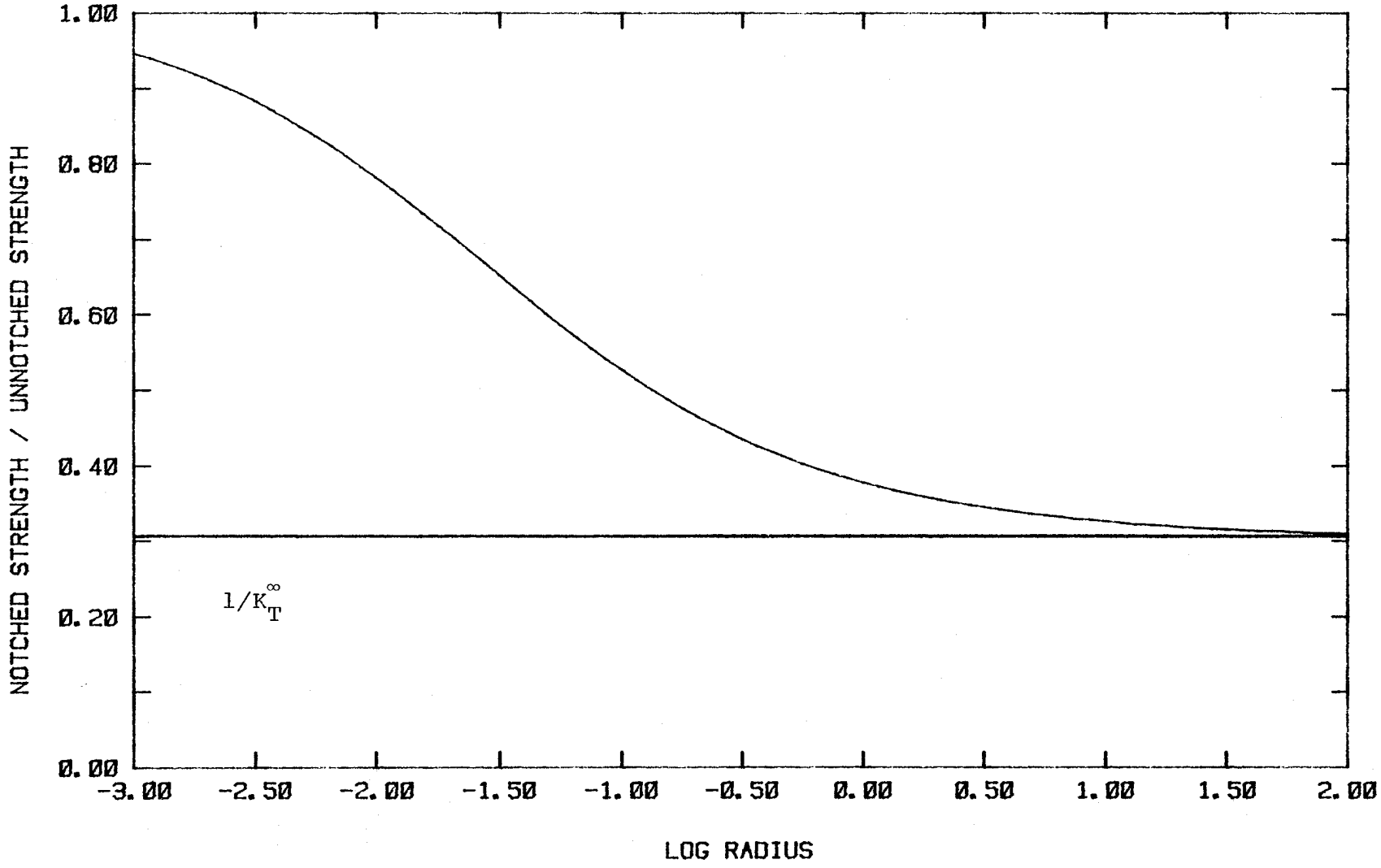

FIG. 3.15 STRENGTH RATIO VS. LOG RADIUS

D. CASE 4

$f = 1.0$

$\beta = \beta$ (Streamlines)

1. Finite Element Results

Fig. 3.16 Y-Deflection Contours

Fig. 3.17 σ_Y-Stress Contours

Fig. 3.18 Longitudinal Young's Modulus Contours

Fig. 3.19 Transverse Young's Modulus Contours

Fig. 3.20 In-Plaine Shear Modulus Contours

Fig. 3.21 In-Plane Poisson's Ratio Contours

2. Failure Model

Fig. 3.22 Strength Ratio vs. Notch Radius

Fig. 3.23 Strength Ratio vs. Log Radius

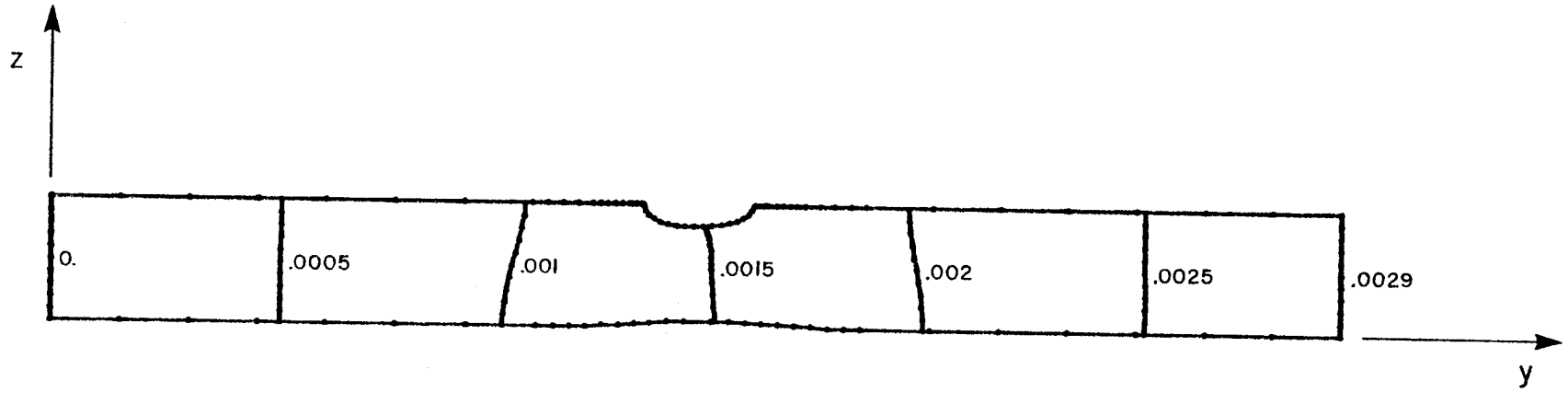

FIG. 3.16 Y-DEFLECTION CONTOURS (INCHES)
OUTLINE DEFORMATION MAGNIFICATION: 500X

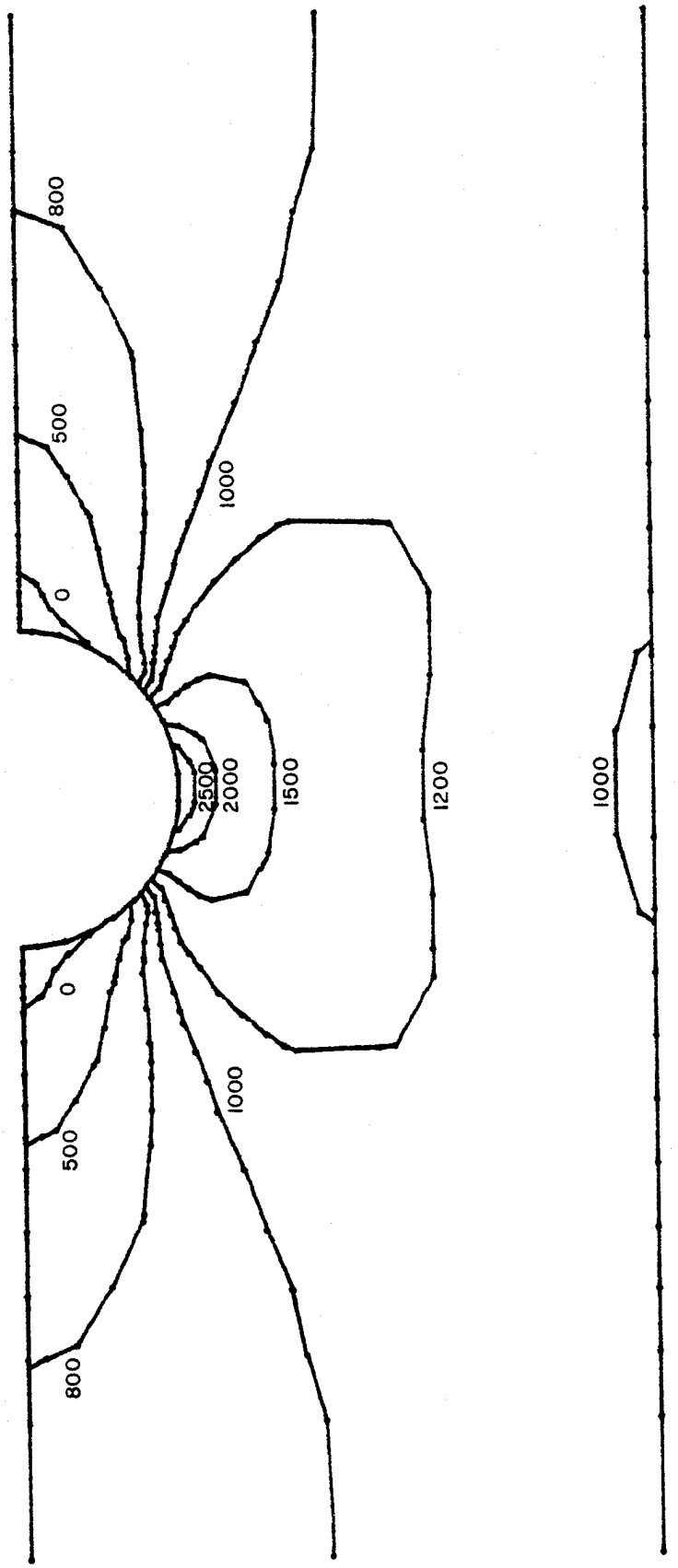

FIG. 3.17 σ_Y-STRESS CONTOURS (PSI)

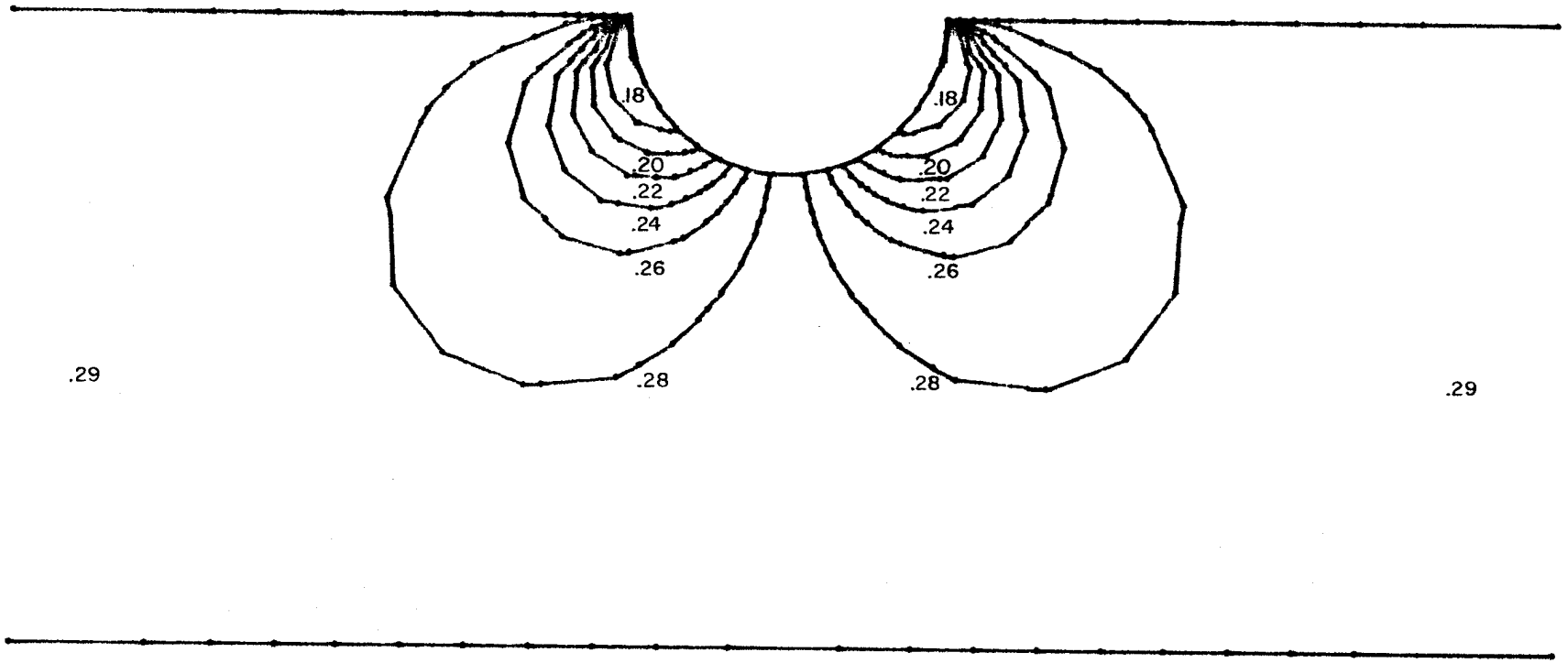

FIG. 3.18 LONGITUDINAL YOUNG'S MODULUS CONTOURS, E_y (X 10^7 PSI)

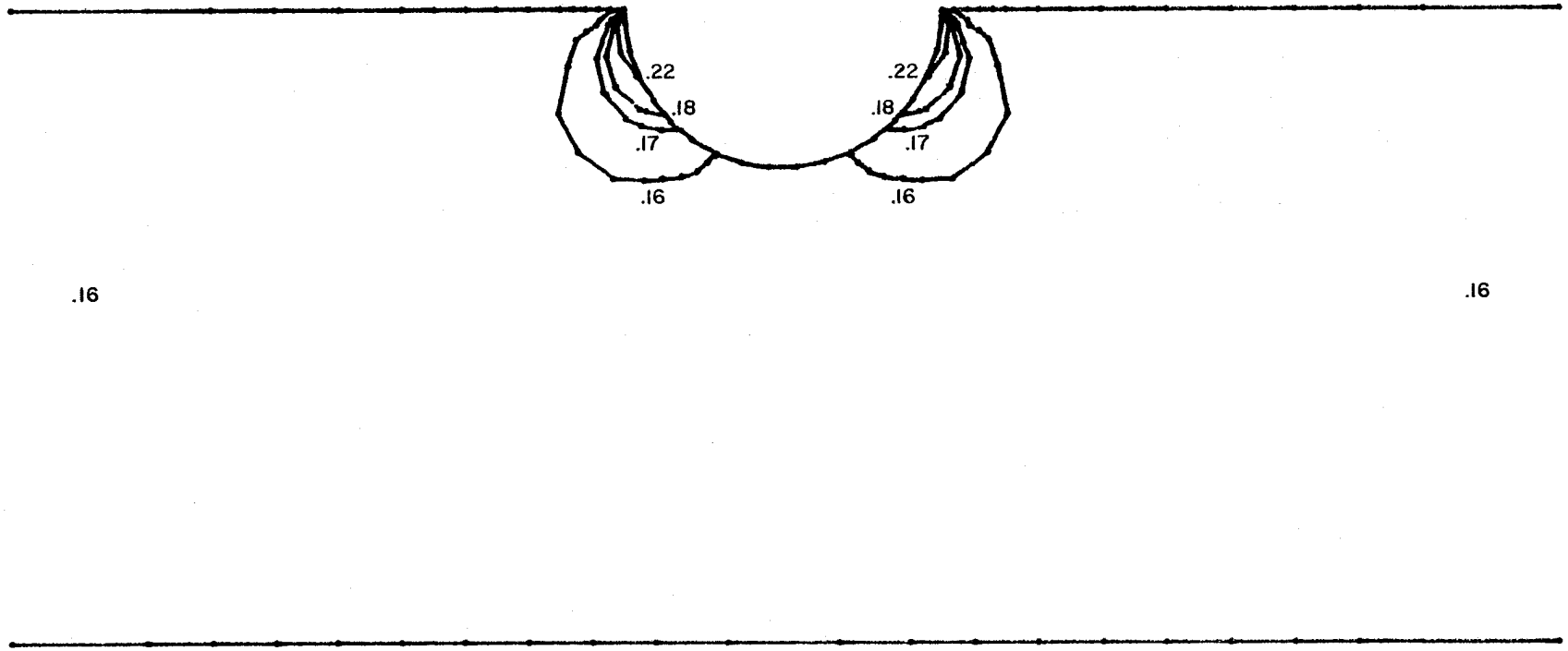

FIG. 3.19 TRANSVERSE YOUNG'S MODULUS CONTOURS, E_z (X 10^7 PSI)

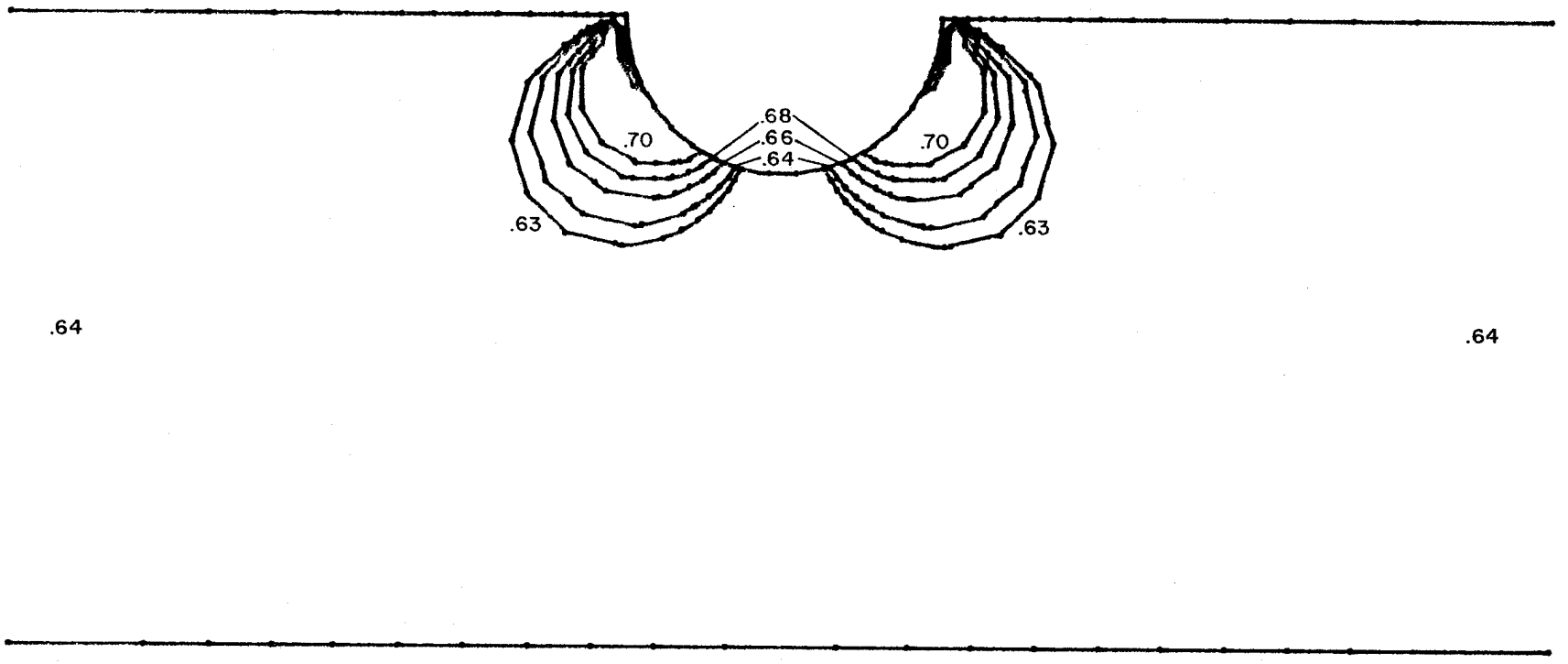

FIG. 3.20 IN-PLANE SHEAR MODULUS CONTOURS, G_{yz} (X 10^6 PSI)

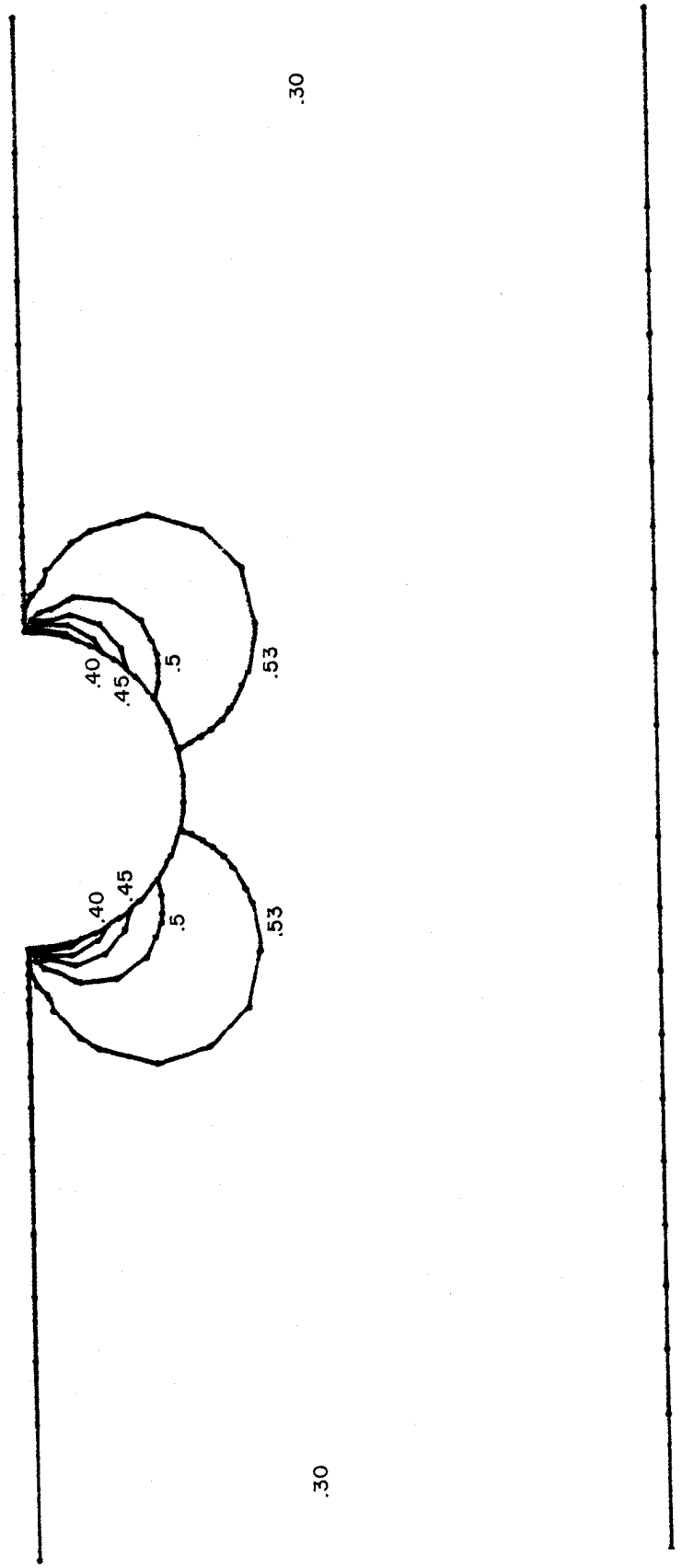

FIG. 3.21 IN-PLANE POISSON'S RATIO CONTOURS, ν_{yz}

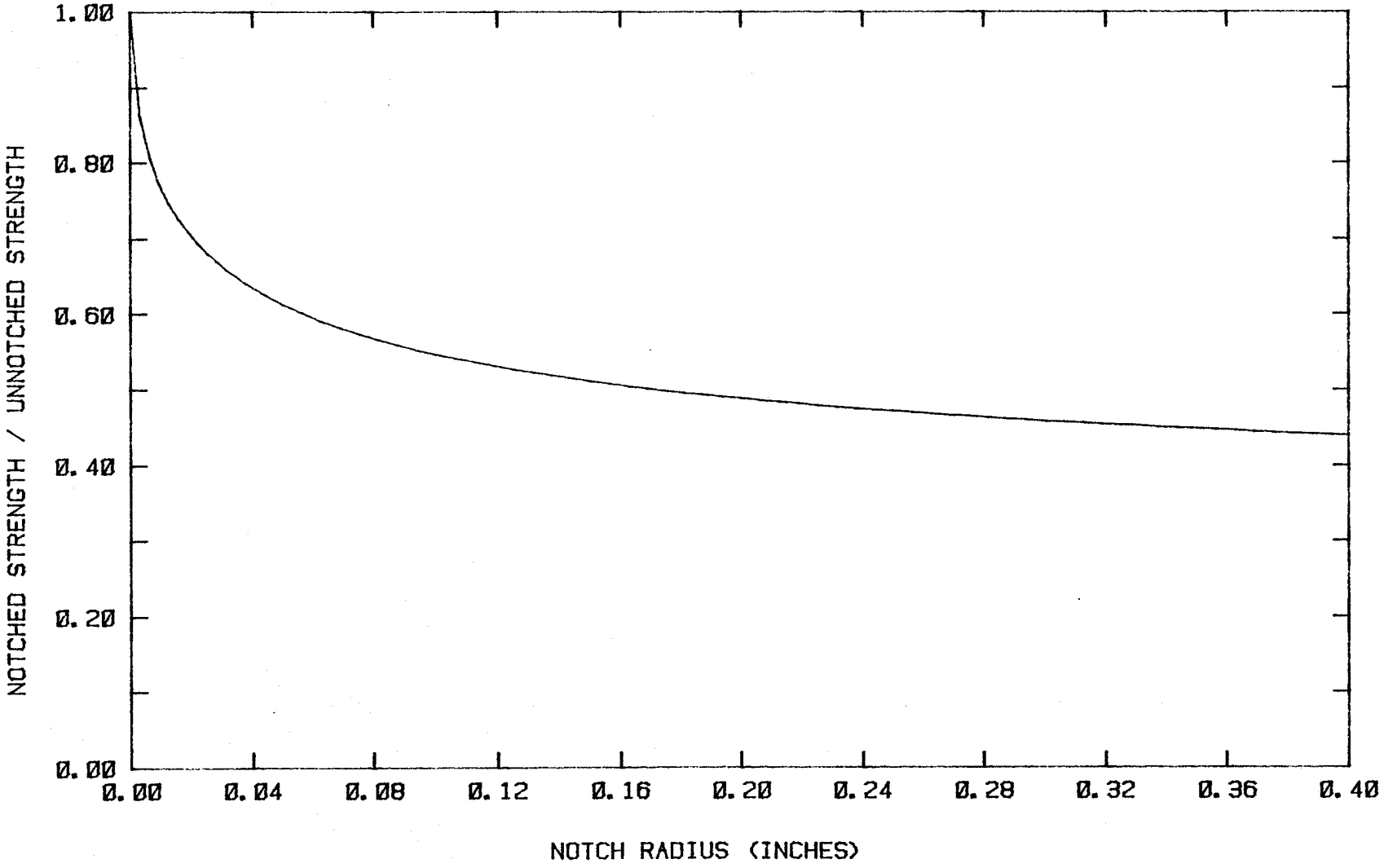

FIG. 3.22 STRENGTH RATIO VS. NOTCH RADIUS

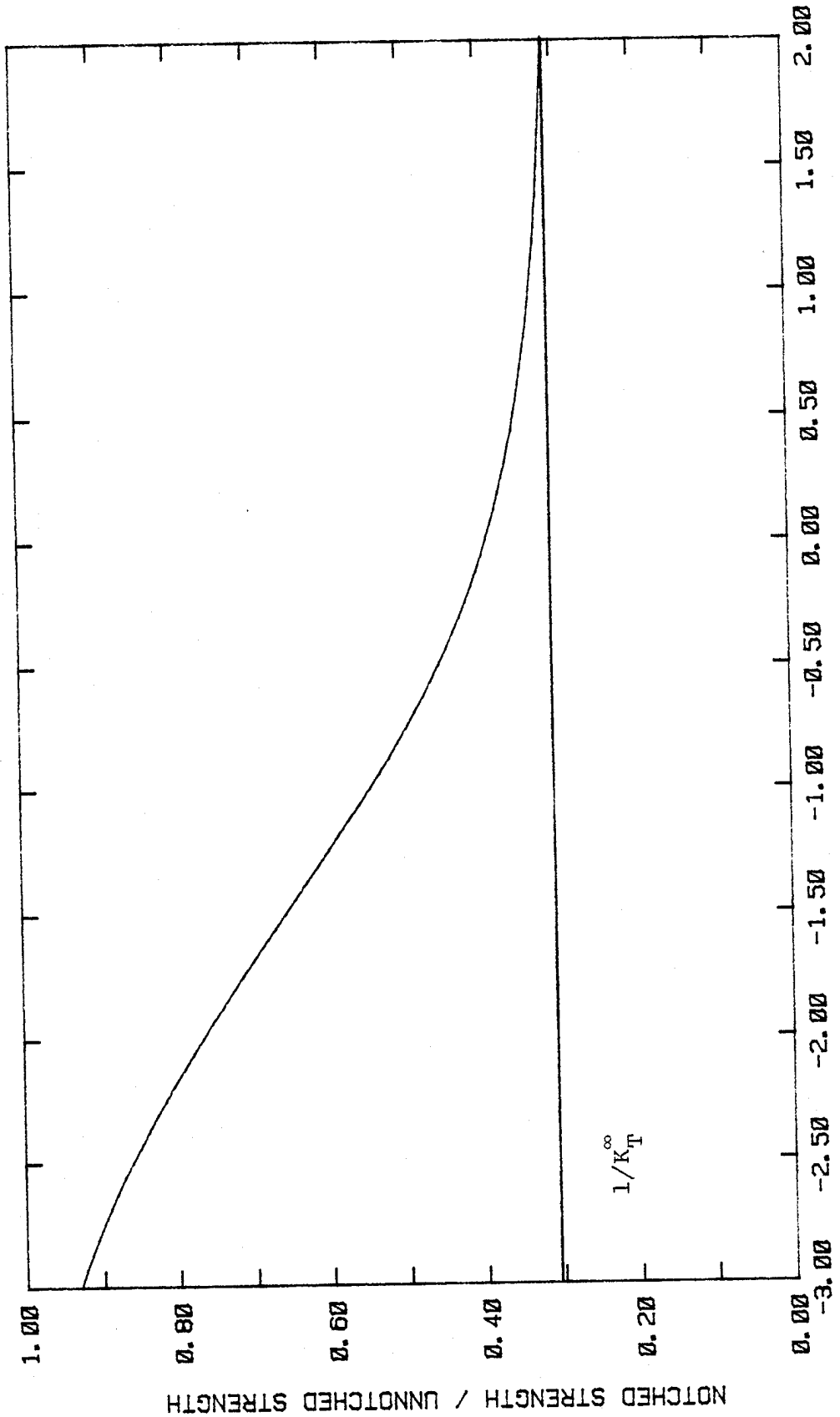

FIG. 3.23 STRENGTH RATIO VS. LOG RADIUS

E. CASE 5

$f(r) = (4/3)(1-r)$ (Linear)

$\beta = \beta$ (Streamlines)

1. Finite Element Results

2. Failure Model

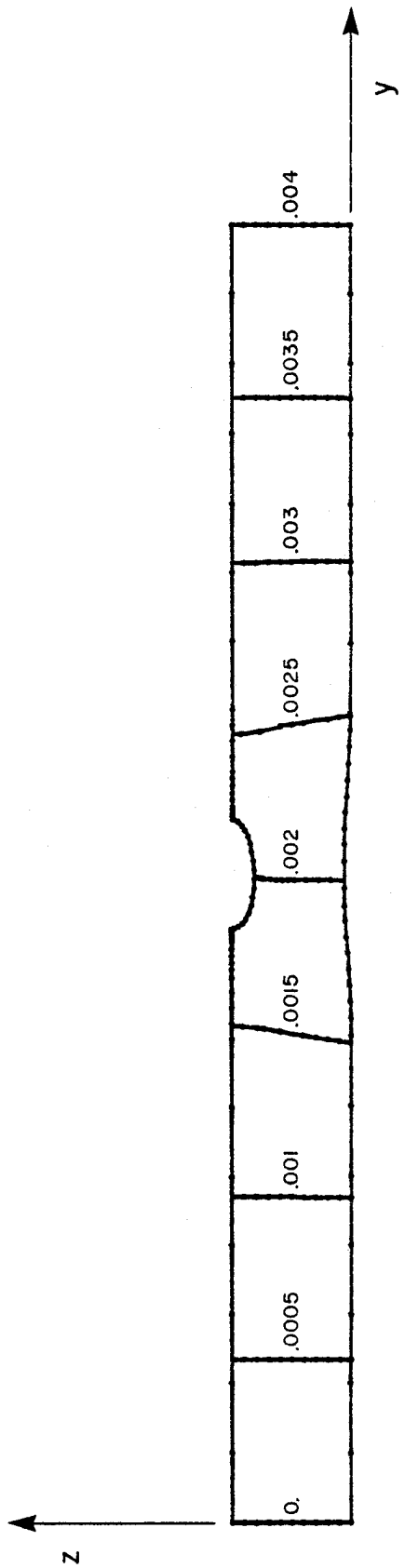

FIG. 3.24 OUTLINE DEFORMATION MAGNIFICATION: 500X

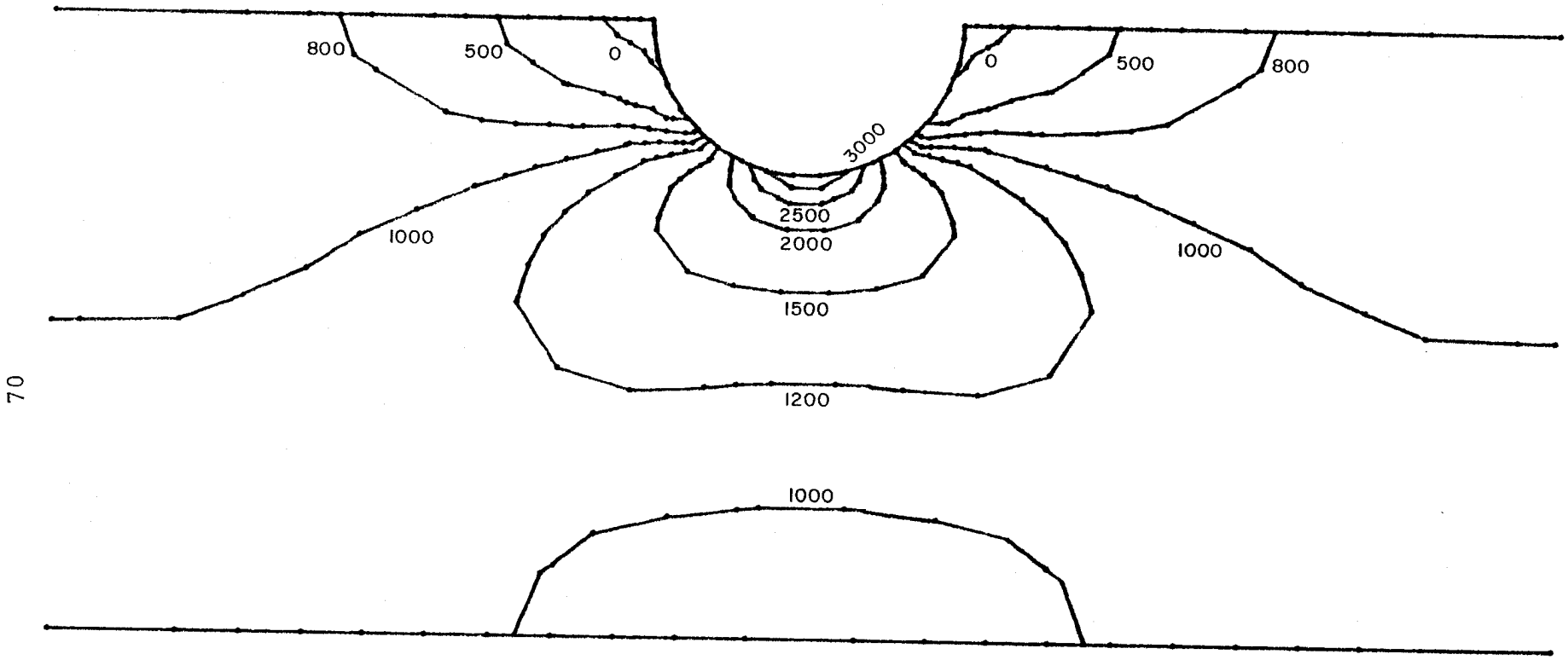

FIG. 3.25 σ_Y-STRESS CONTOURS (PSI)

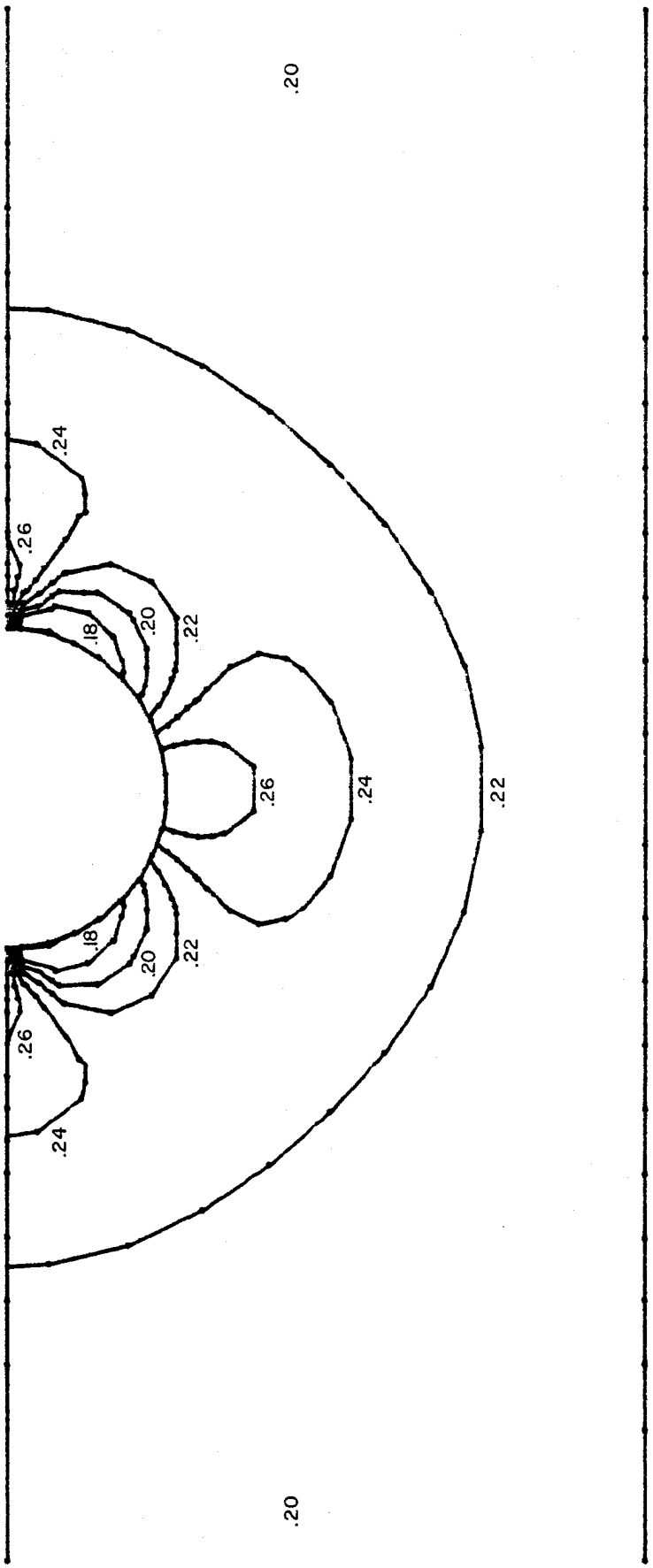

FIG. 3.26 LONGITUDINAL YOUNG'S MODULUS CONTOURS, E_y (X 10^7 PSI)

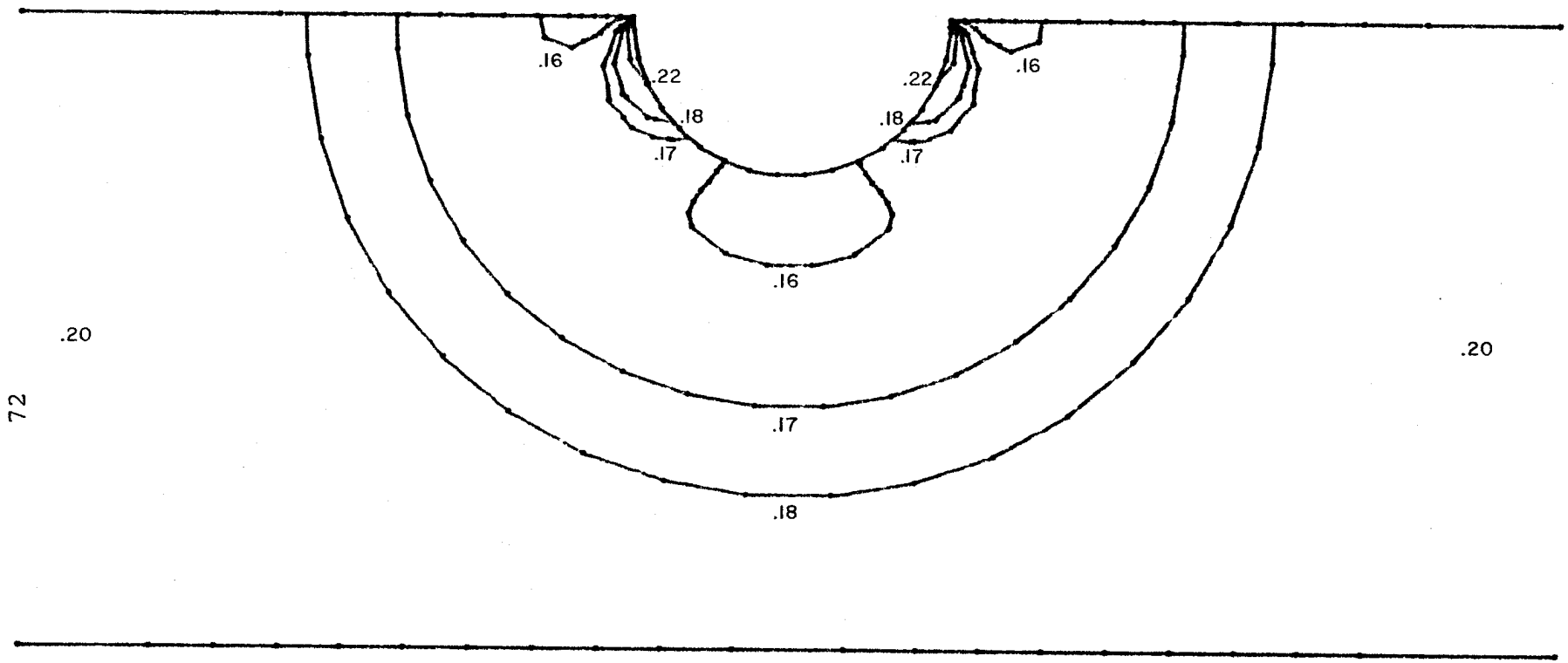

FIG. 3.27 TRANSVERSE YOUNG'S MODULUS CONTOURS, E_z (X 10^7 PSI)

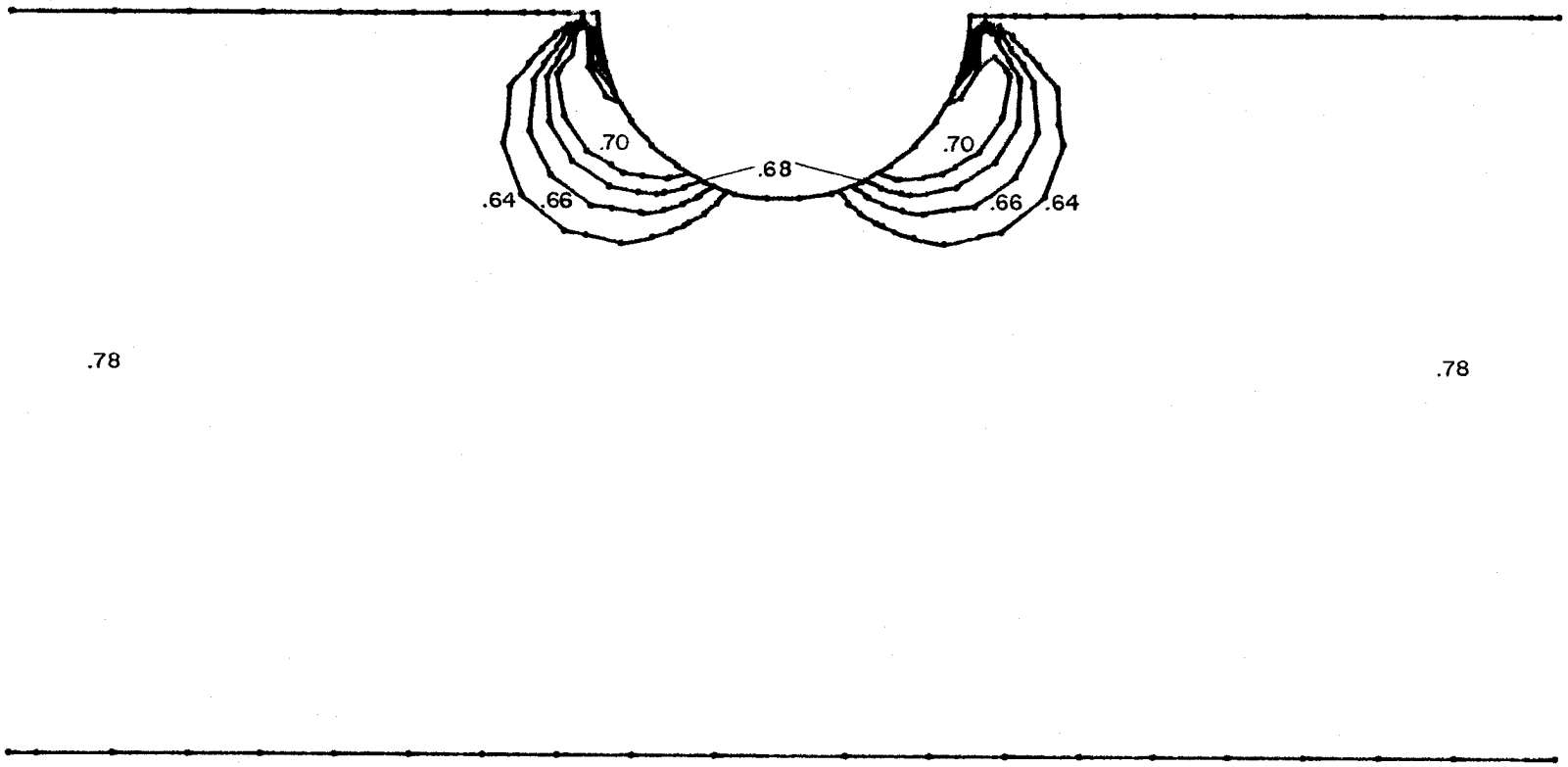

FIG. 3.28 IN-PLANE SHEAR MODULUS CONTOURS, G_{yz} (X 10^6 PSI)

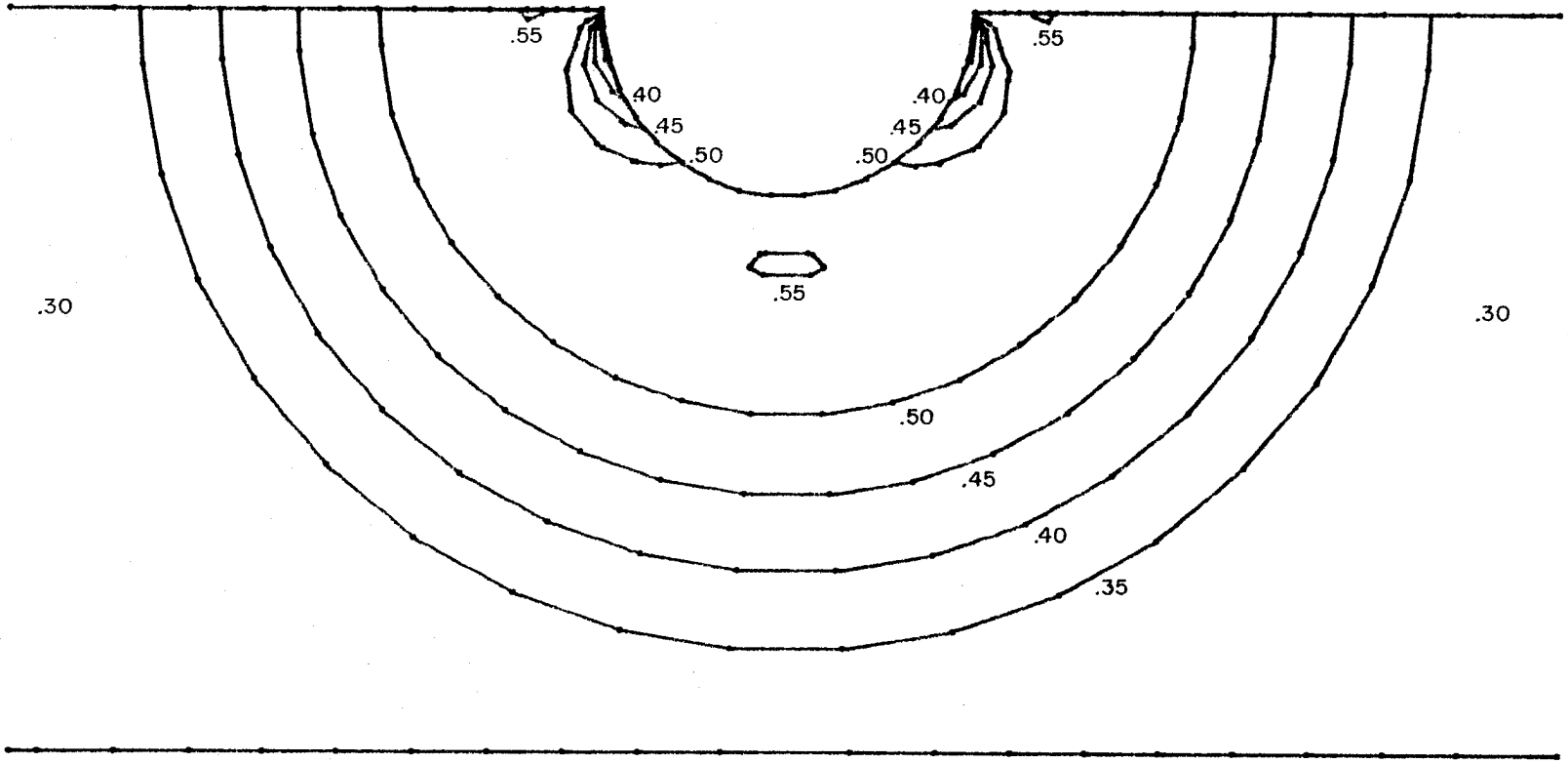

FIG. 3.29 IN-PLANE POISSON'S RATIO CONTOURS, ν_{yz}

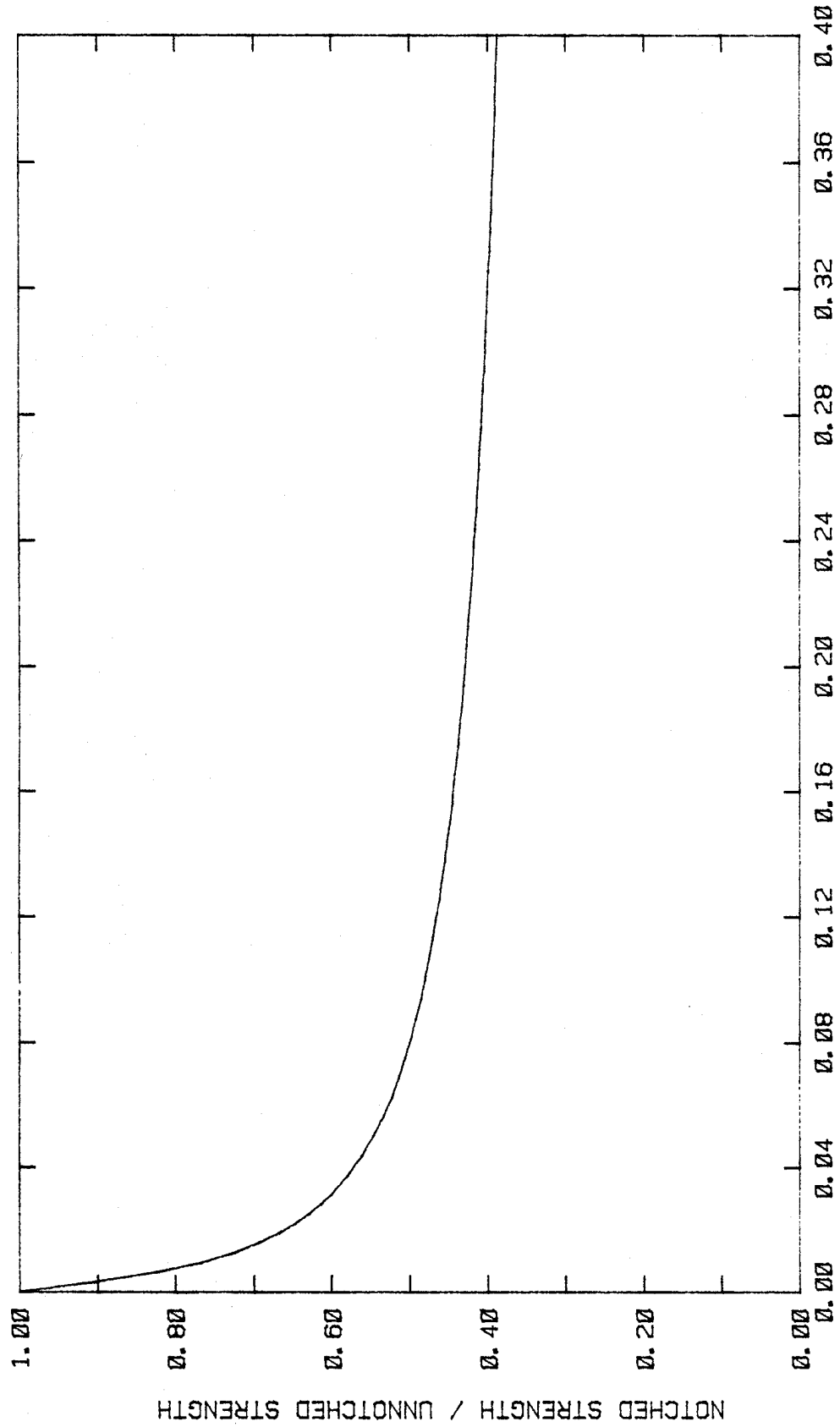

FIG. 3.30 STRENGTH RATIO VS. NOTCH RADIUS

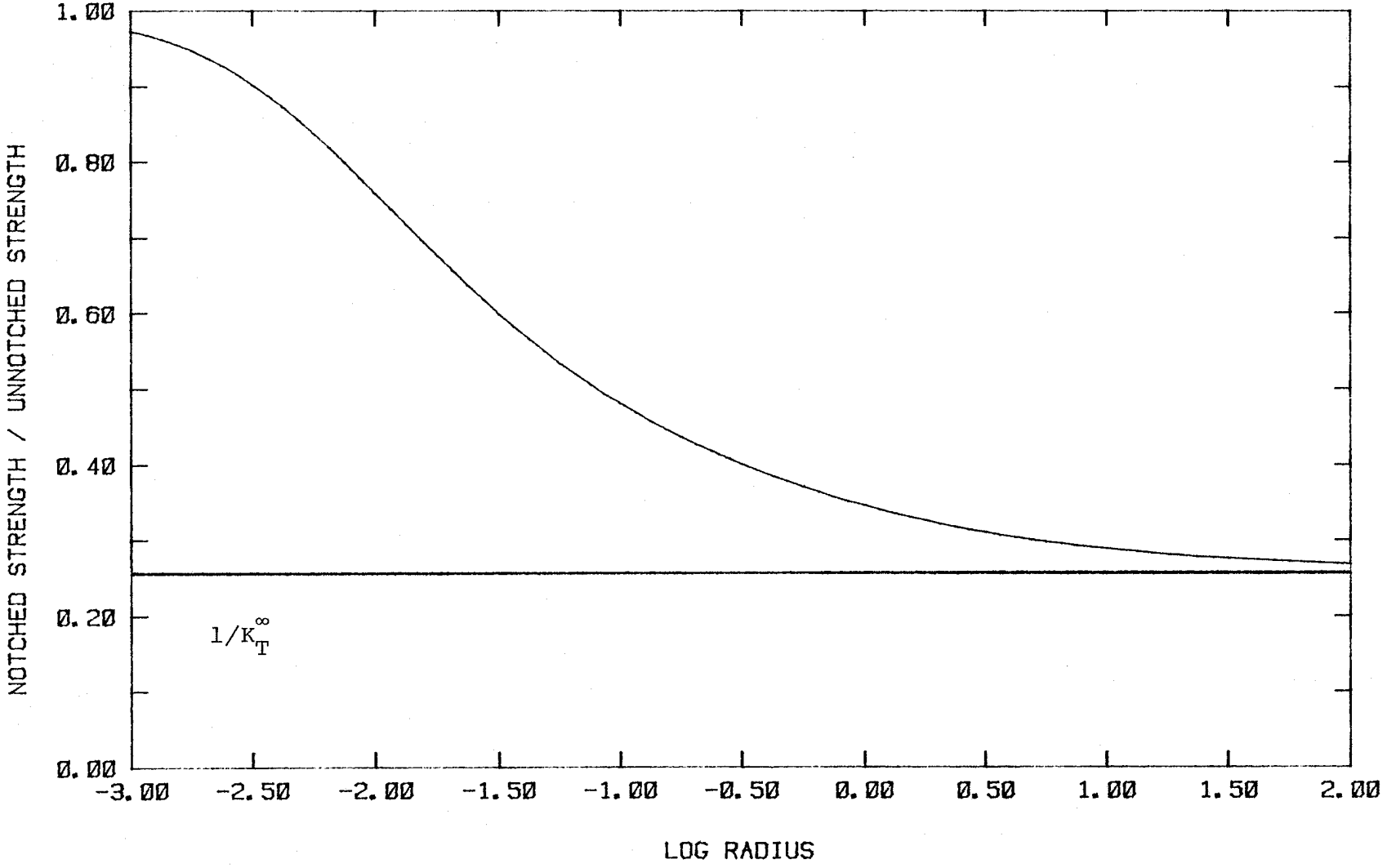

FIG. 3.31 STRENGTH RATIO VS. LOG RADIUS

F. CASE 6

$f(r,\alpha) = -(4/3)(1-r)\sin\alpha$ (Angular Dependent Linear)

$\beta = \beta$ (Streamlines)

1. Finite Element Results

2. Failure Model

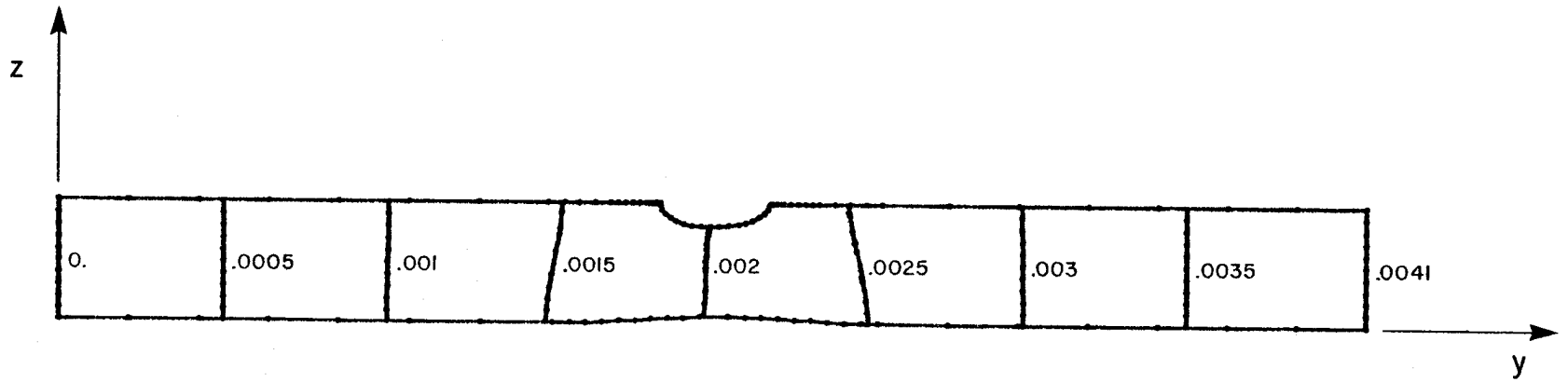

FIG. 3.32 Y-DEFLECTION CONTOURS (INCHES)
OUTLINE DEFORMATION MAGNIFICATION: 500X

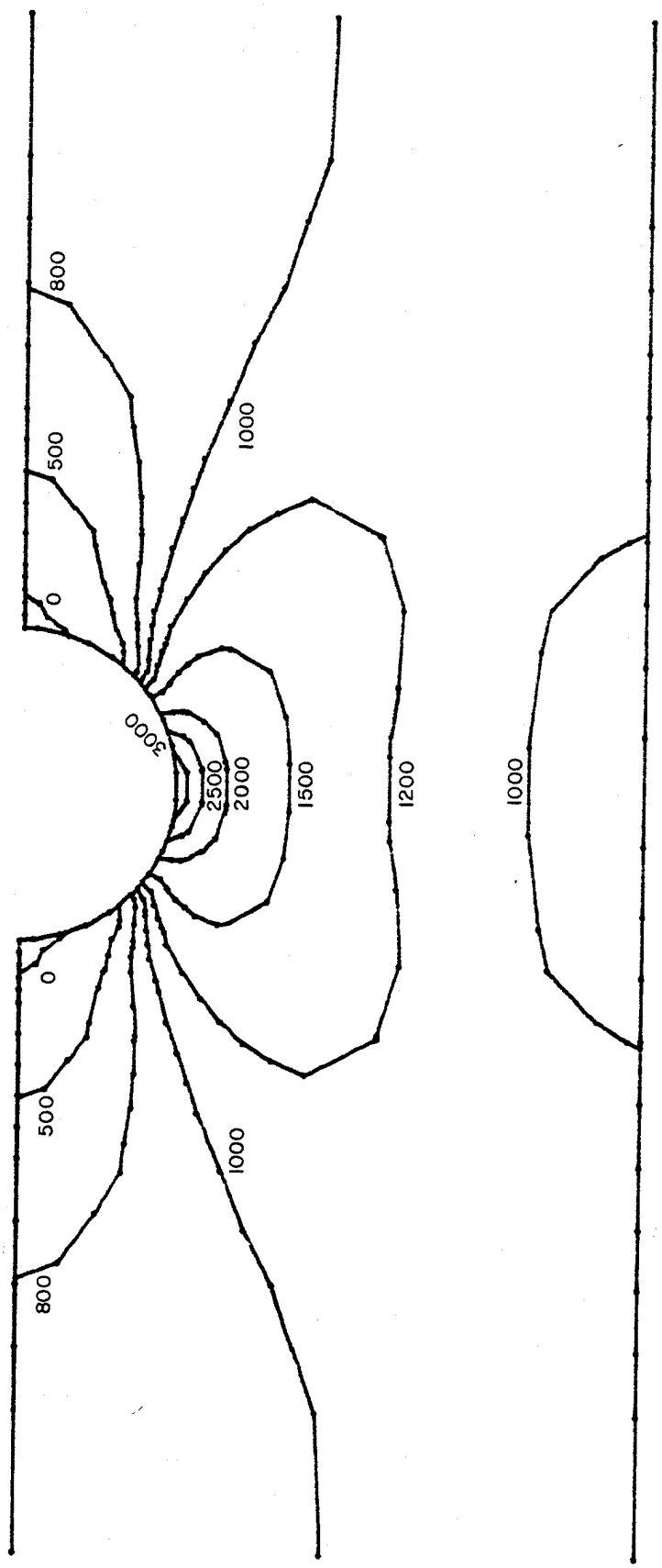

FIG. 3.33 σ_Y-STRESS CONTOURS (PSI)

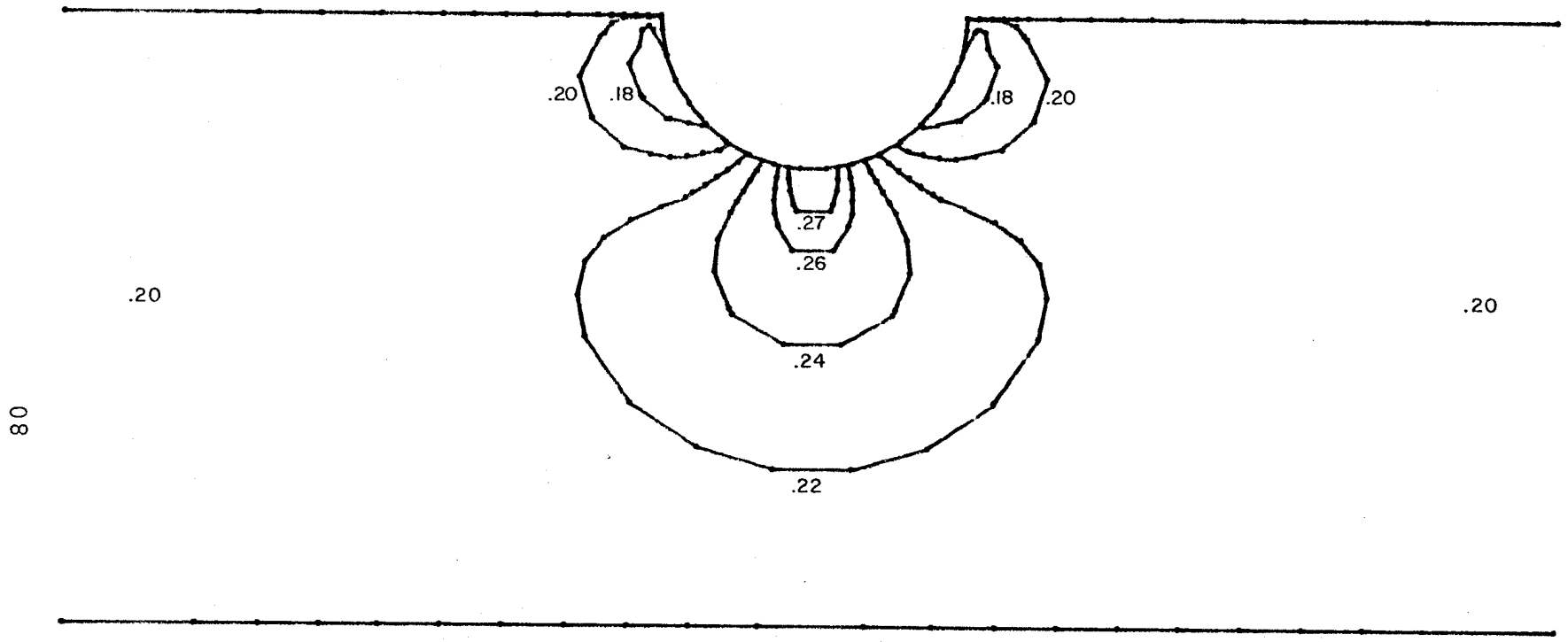

FIG. 3.34 LONGITUDINAL YOUNG'S MODULUS CONTOURS, E_y (X 10^7 PSI)

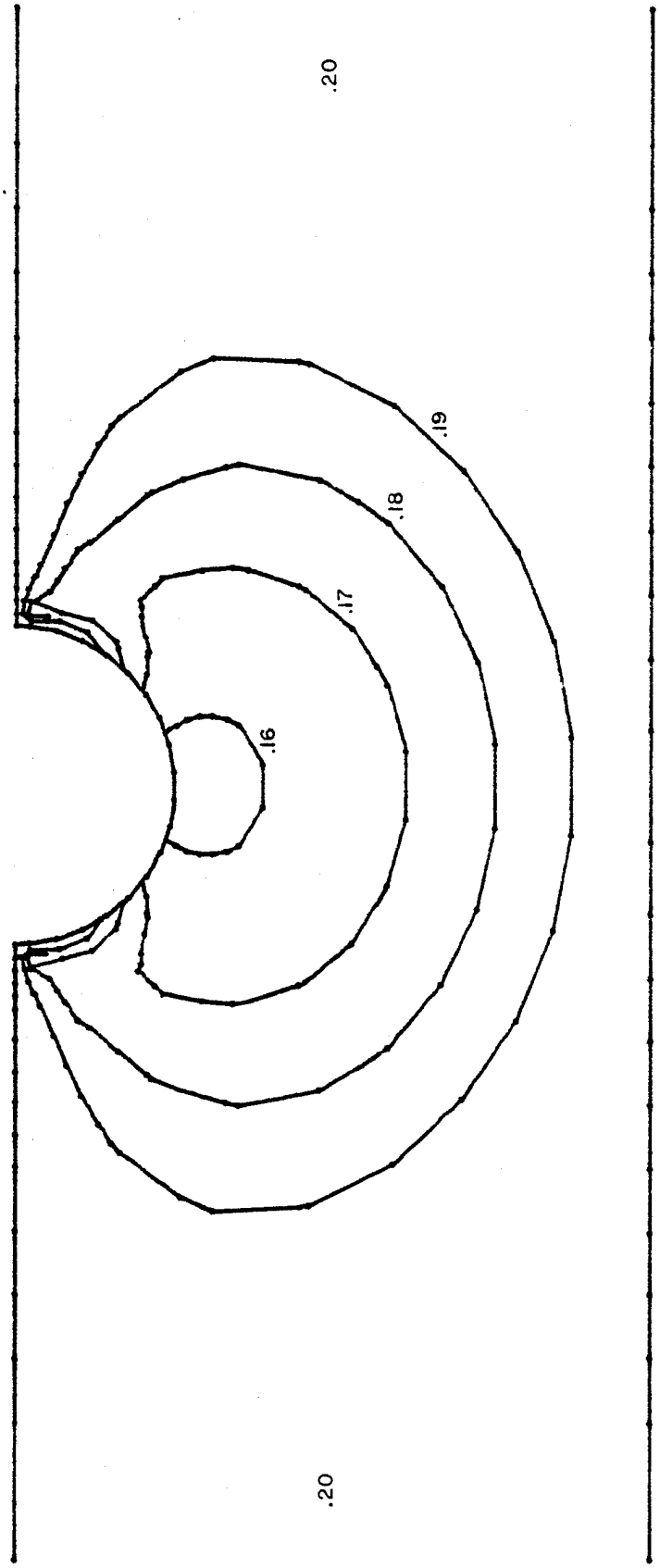

FIG. 3.35 TRANSVERSE YOUNG'S MODULUS CONTOURS, E_z (X 10^7 PSI)

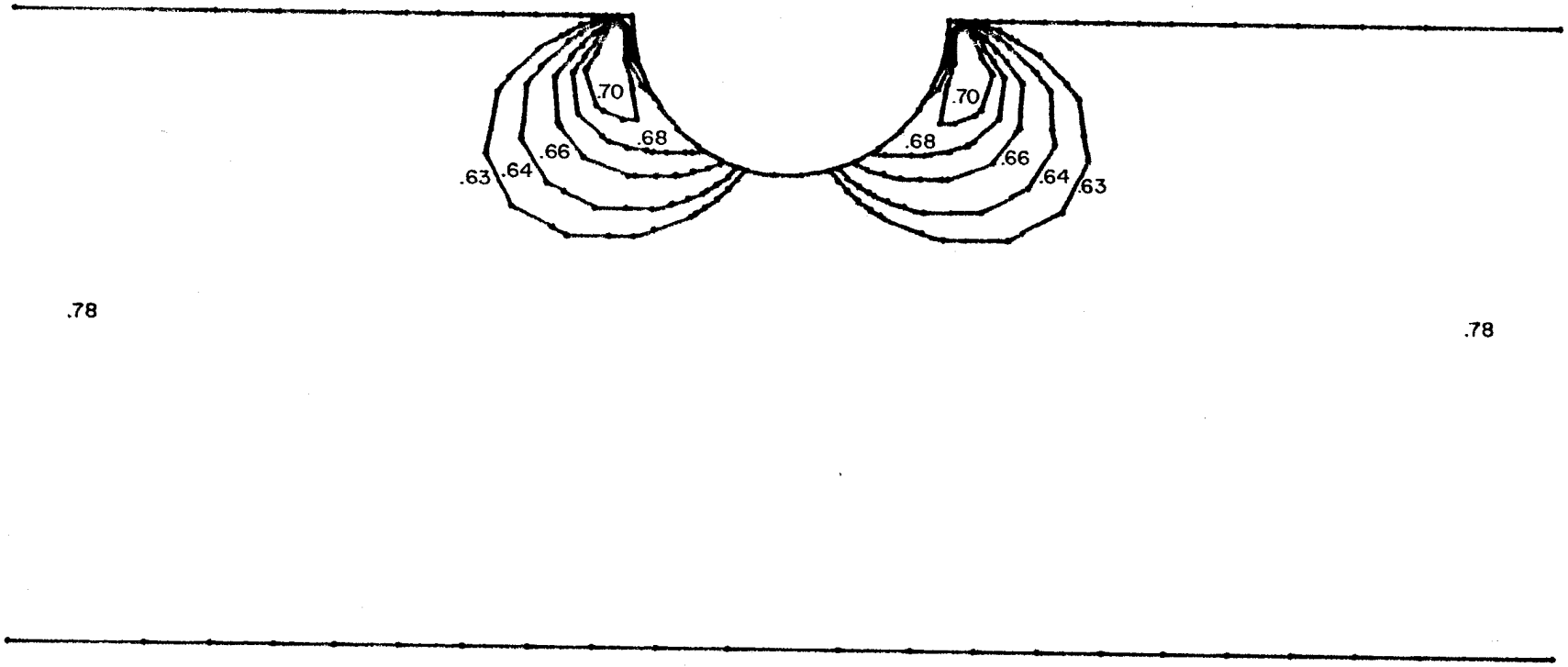

FIG. 3.36 IN-PLANE SHEAR MODULUS CONTOURS, G_{yz} (X 10^6 PSI)

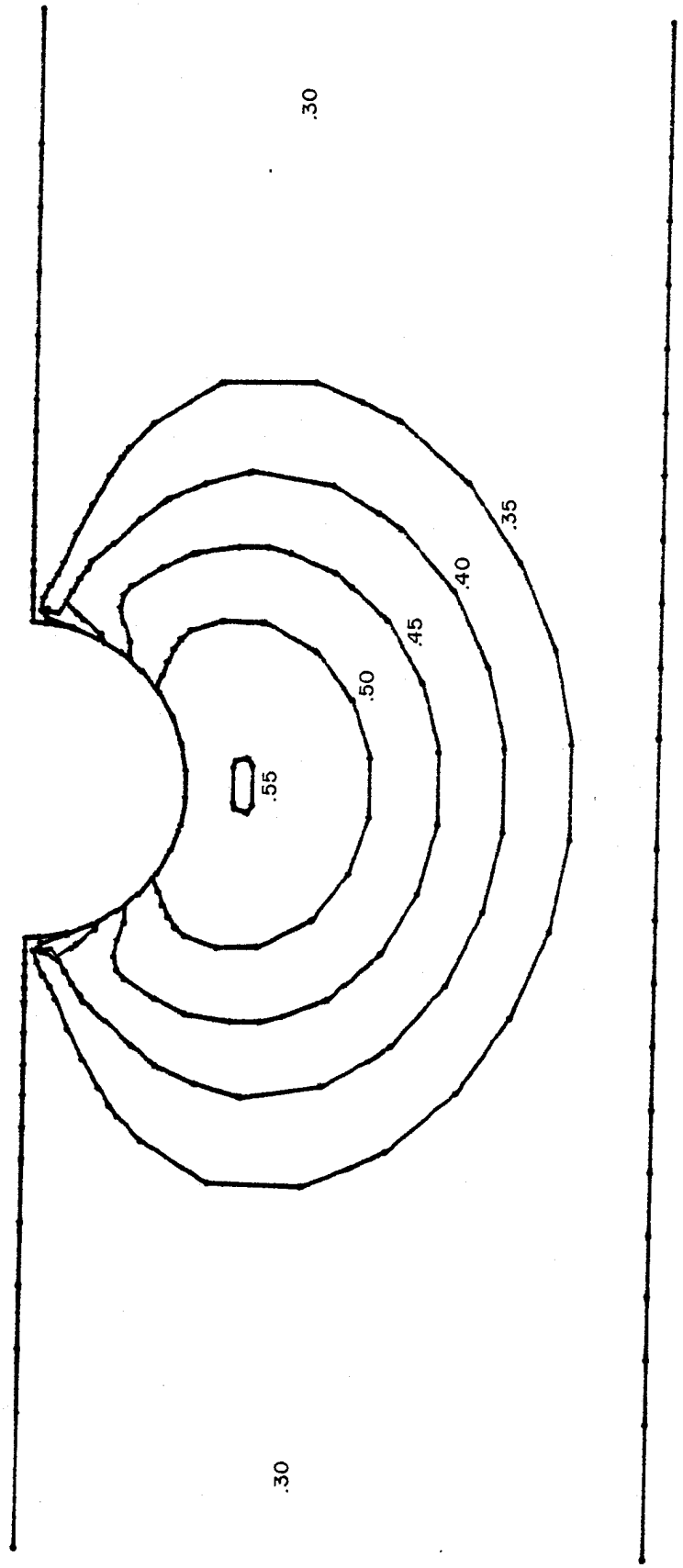

FIG. 3.37 IN-PLANE POISSON'S RATIO CONTOURS, ν_{yz}

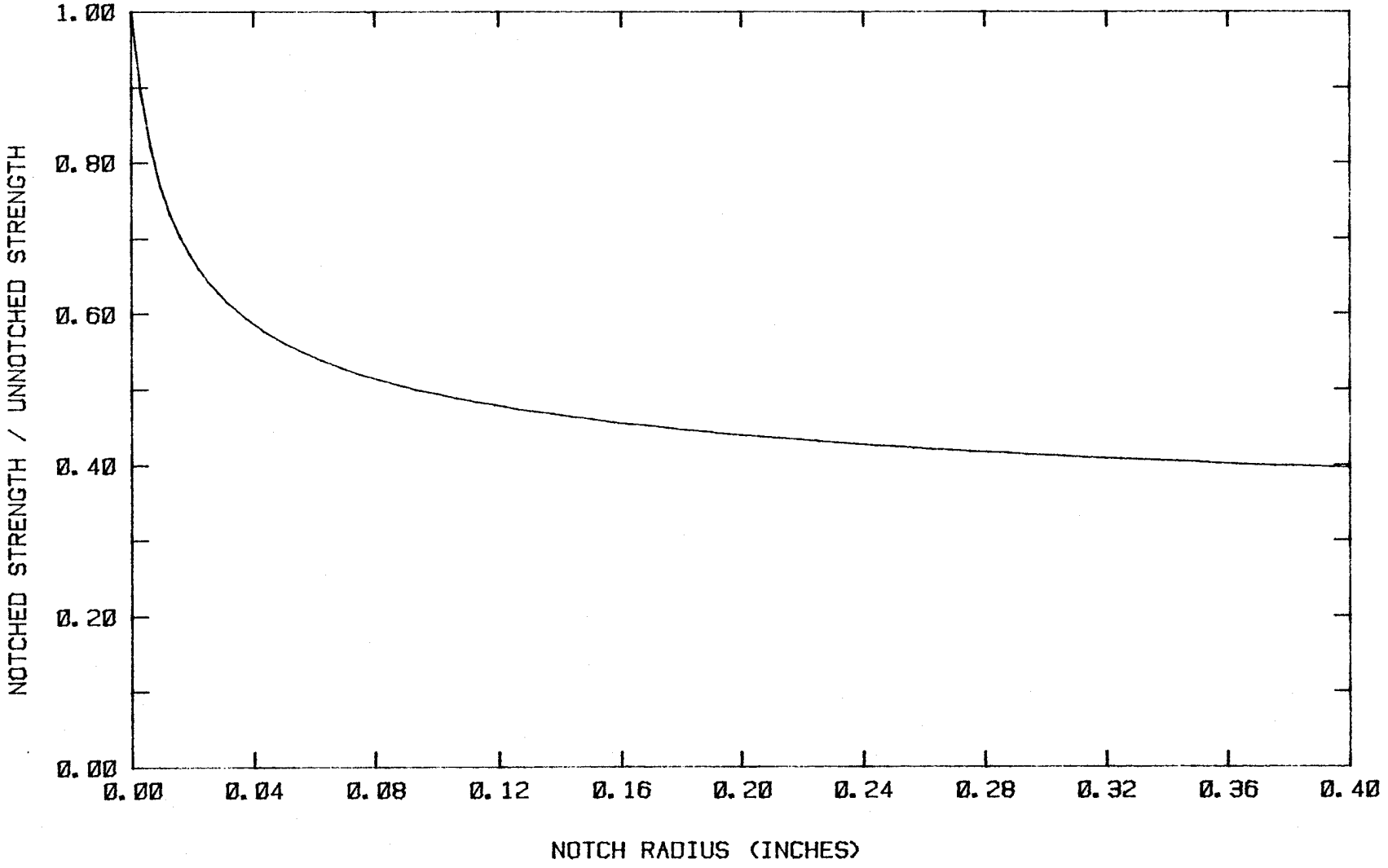

FIG. 3.38 STRENGTH RATIO VS. NOTCH RADIUS

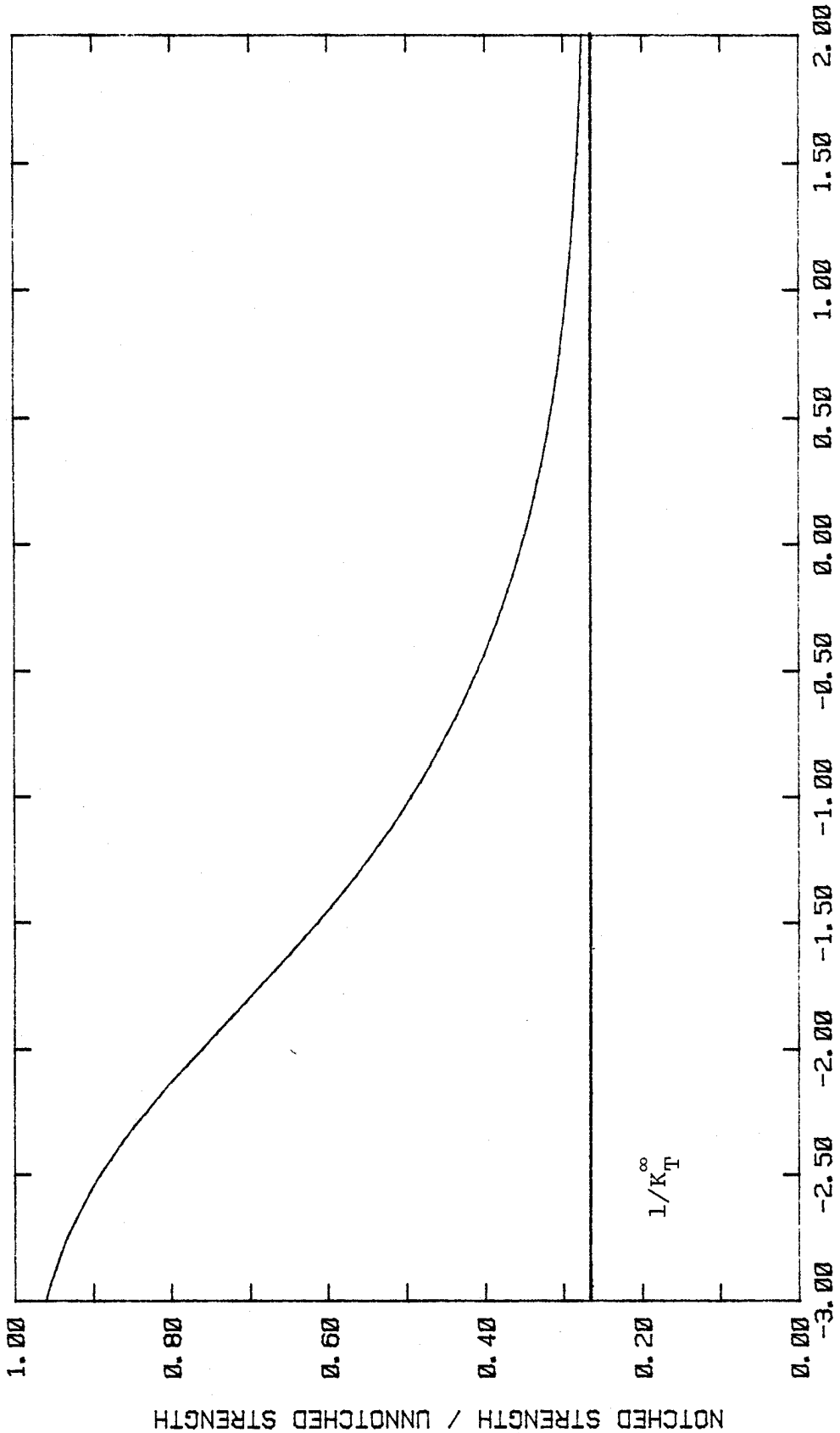

FIG. 3.39 STRENGTH RATIO VS. LOG RADIUS

G. CASE 7

$$f(r,\alpha) = -10e^{-9.21r}\sin\alpha \quad \text{(Angular Dependent Exponential)}$$

$$\beta = \beta \quad \text{(Streamlines)}$$

1. Finite Element Results

Fig. 3.40 Y-Deflection Contours

Fig. 3.41 σ_Y-Stress Contours

Fig. 3.42 Longitudinal Young's Modulus Contours

Fig. 3.43 Transverse Young's Modulus Contours

Fig. 3.44 In-Plane Shear Modulus Contours

Fig. 3.45 In-Plane Poisson's Ratio Contours

2. Failure Model

Fig. 3.46 Strength Ratio vs. Notch Radius

Fig. 3.47 Strength Ratio vs. Log Radius

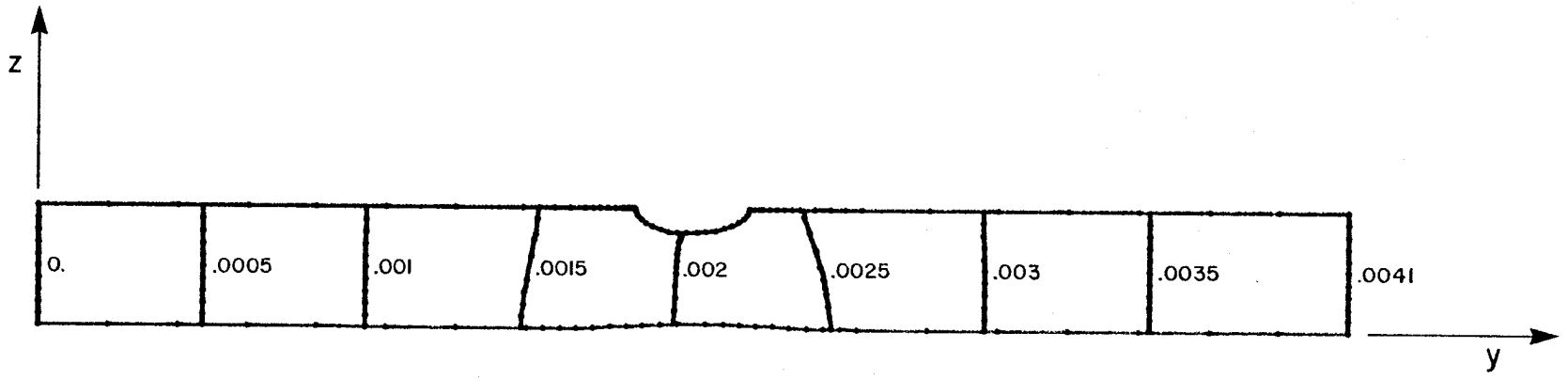

FIG. 3.40 Y-DEFLECTION CONTOURS (INCHES)
OUTLINE DEFORMATION MAGNIFICATION: 500X

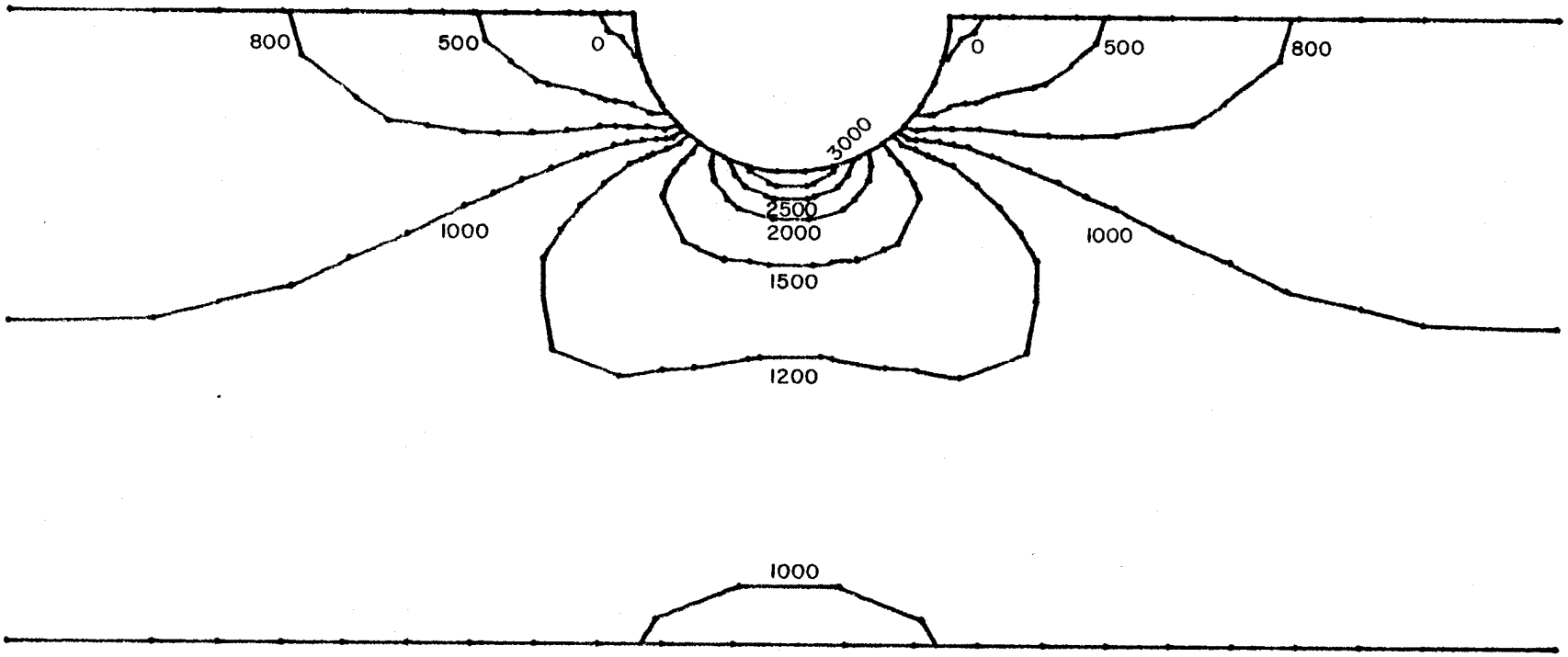

FIG. 3.41 σ_Y-STRESS CONTOURS (PSI)

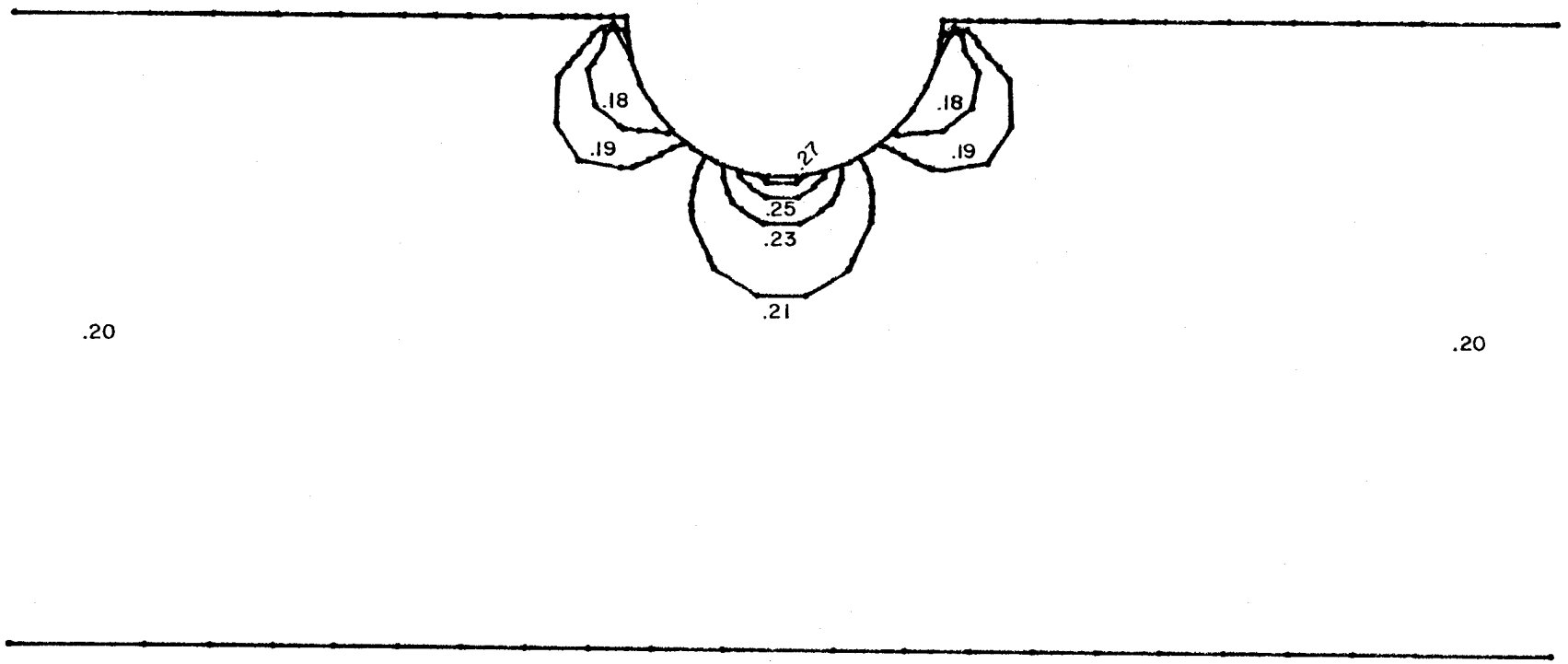

FIG. 3.42 LONGITUDINAL YOUNG'S MODULUS CONTOURS, E_y (X 10^7 PSI)

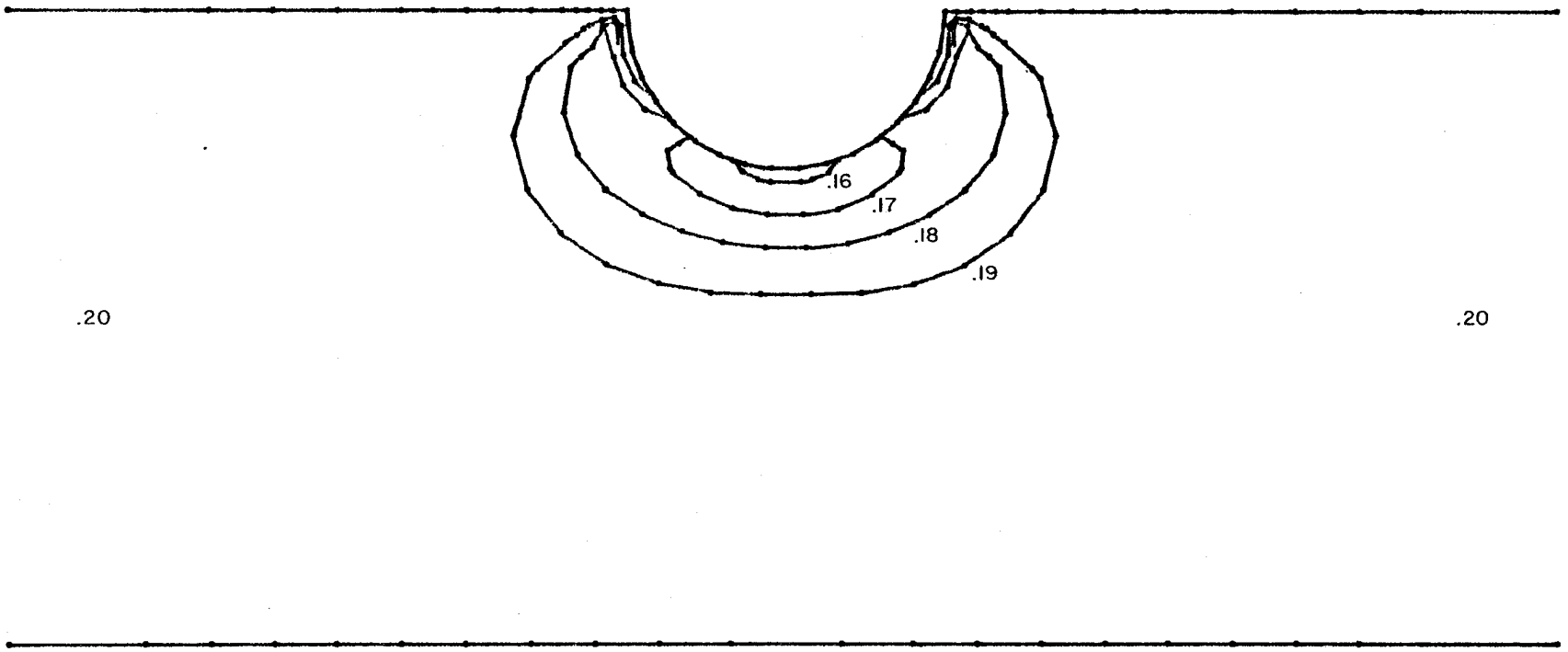

FIG. 3.43 TRANSVERSE YOUNG'S MODULUS CONTOURS, E_z (X 10^7)

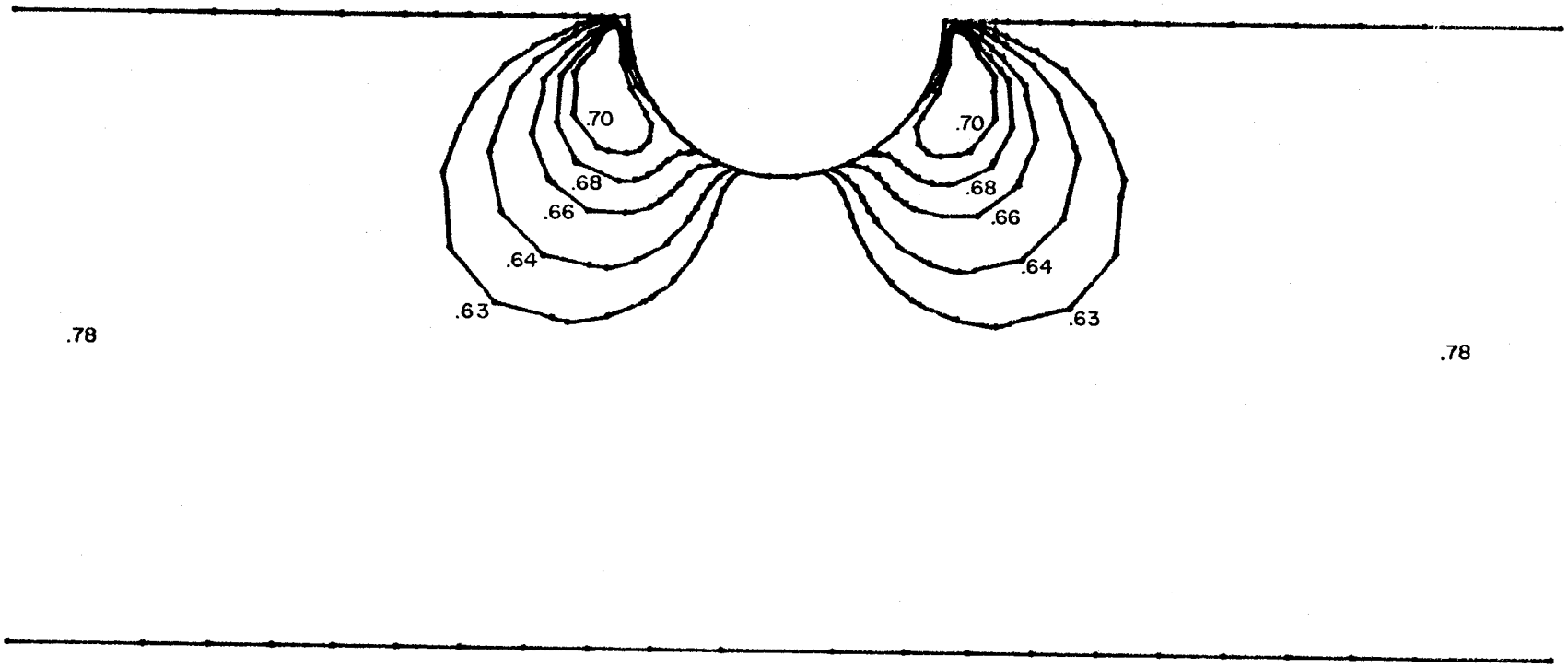

FIG. 3.44 IN-PLANE SHEAR MODULUS CONTOURS, G_{yz} (X 10^6 PSI)

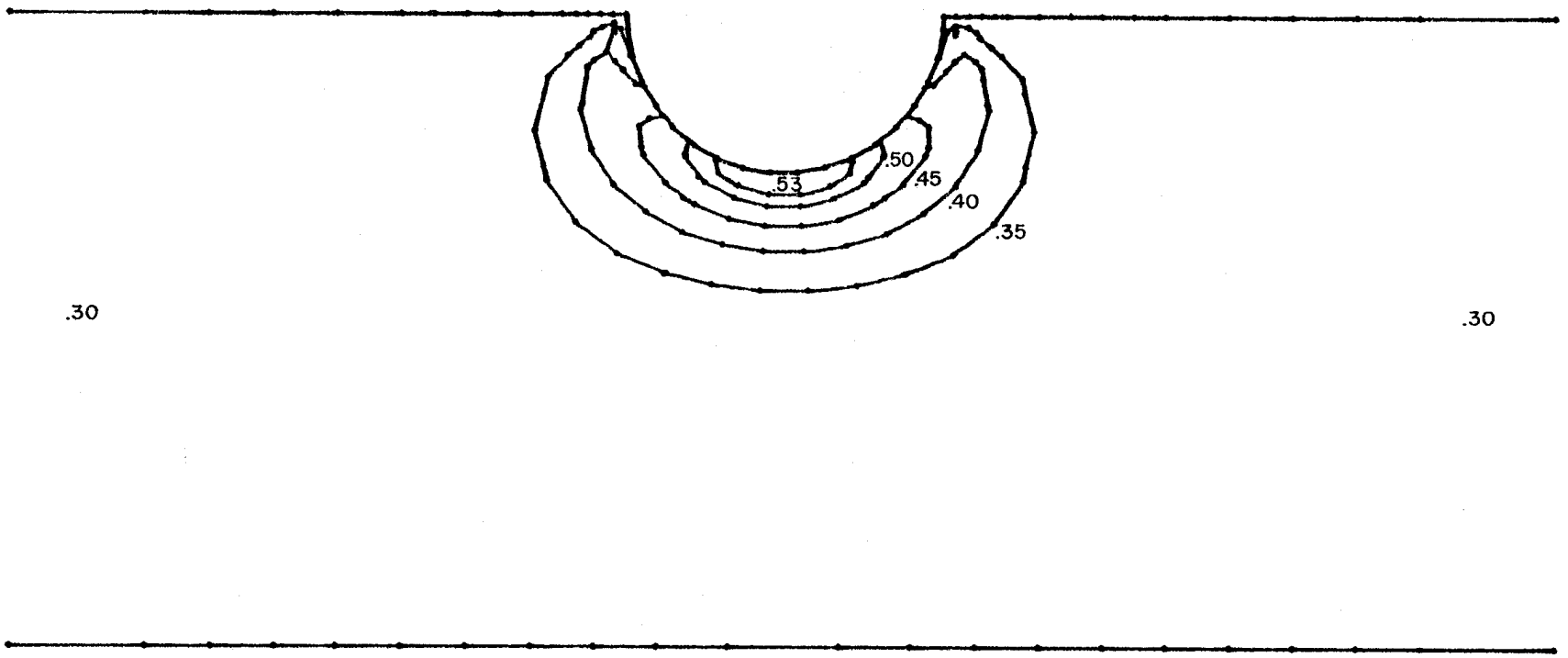

FIG. 3.45 IN-PLANE POISSON'S RATIO CONTOURS, ν_{yz}

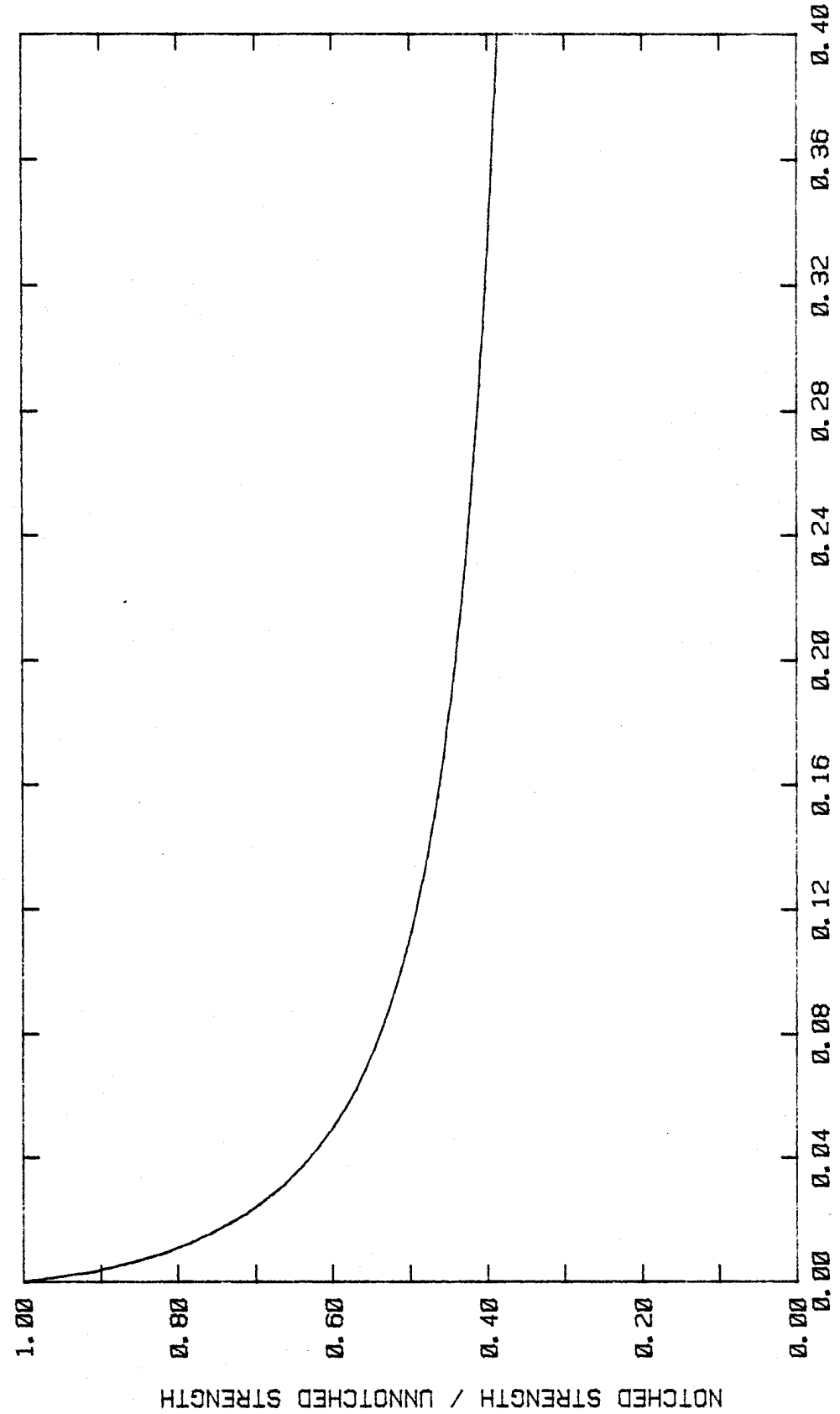

FIG. 3.46 STRENGTH RATIO VS. NOTCH RADIUS

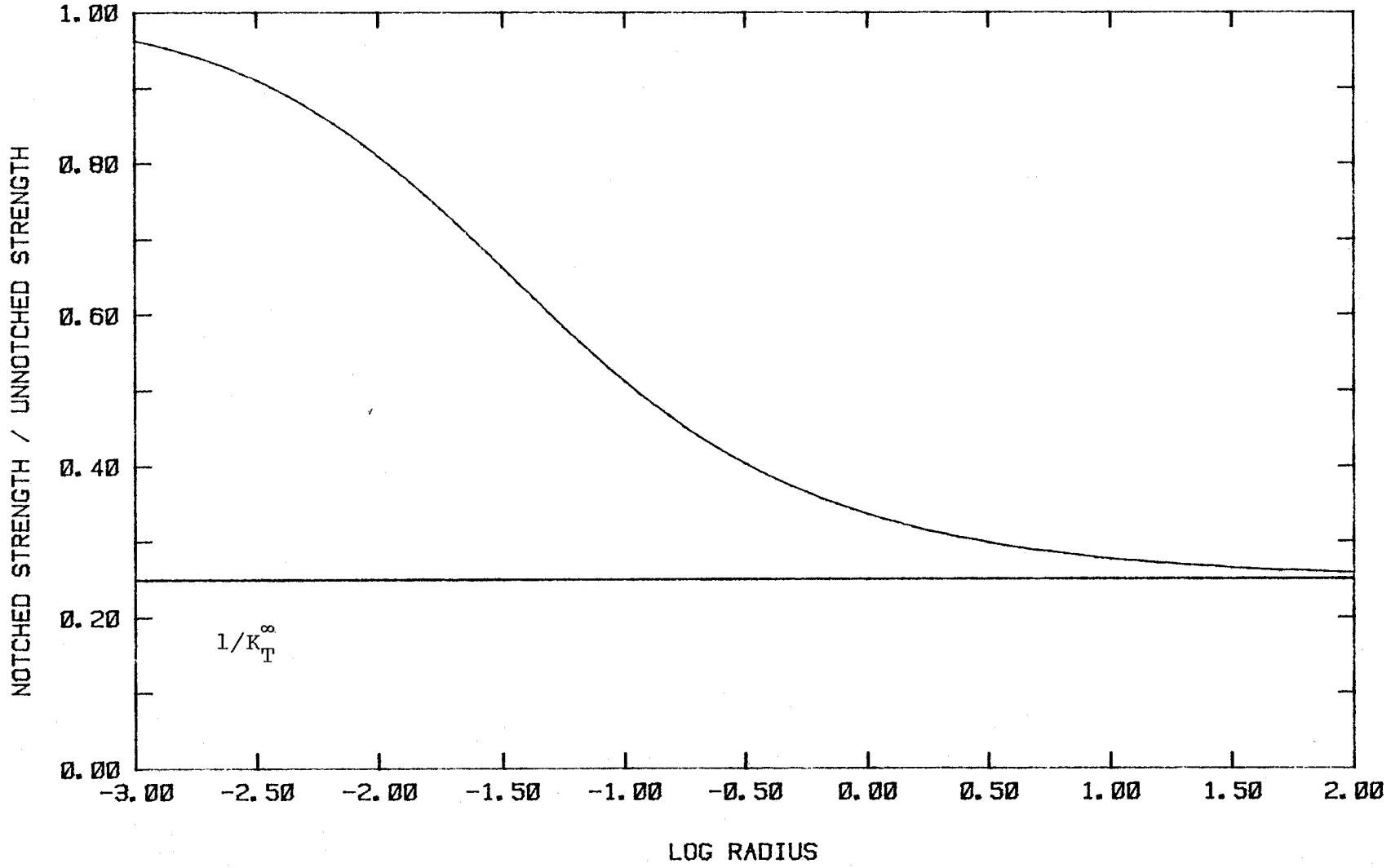

FIG. 3.47 STRENGTH RATIO VS. LOG RADIUS

H. CASE 8

$$f(r,\alpha) = -[10e^{-9.21r}u + (4/3)(1-r)(1-u)]\sin\alpha$$

$$u(\alpha) = (-\alpha/90°)^{\frac{1}{2}} \quad -90° \leq \alpha \leq 0°$$

(Angular Dependent Linear-Exponential Mix)

$$f(r,\alpha) = -10e^{-9.21r}\sin\alpha \quad -180° \leq \alpha \leq -90°$$

(Angular Dependent Exponential)

$$\beta = \beta \quad \text{(Streamlines)}$$

1. Finite Element Results

Fig. 3.48 Y-Deflection Contours

Fig. 3.49 σ_Y-Stress Contours

Fig. 3.50 Longitudinal Young's Modulus Contours

Fig. 3.51 Transverse Young's Modulus Contours

Fig. 3.52 In-Plane Shear Modulus Contours

Fig. 3.53 In-Plane Poisson's Ratio Contours

2. Failure Model

Fig. 3.54 Strength Ratio vs. Notch Radius

Fig. 3.55 Strength Ratio vs. Log Radius

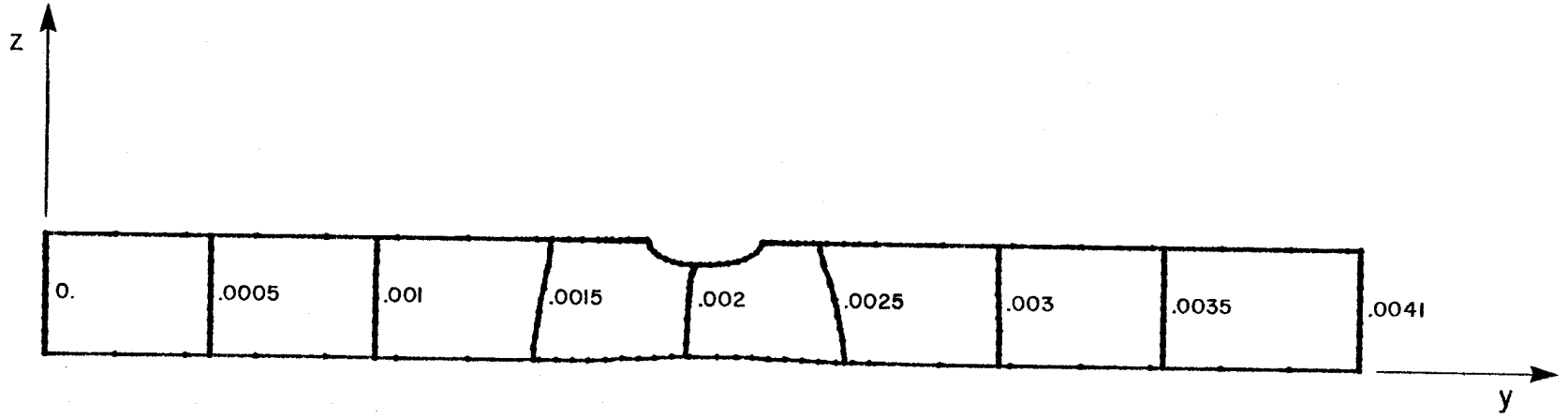

FIG. 3.48 Y-DEFLECTION CONTOURS (INCHES)
OUTLINE DEFORMATION MAGNIFICATION: 500X

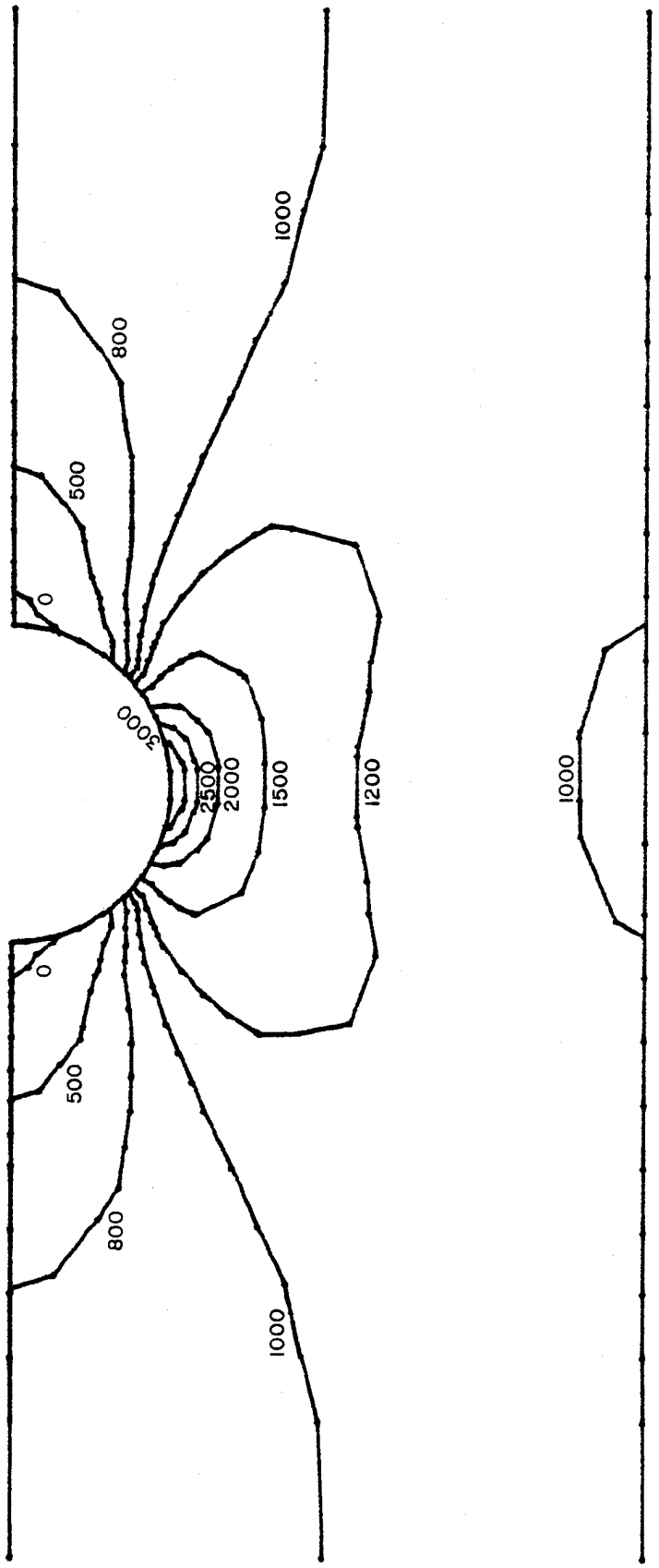

FIG. 3.49 σ_Y-STRESS CONTOURS (PSI)

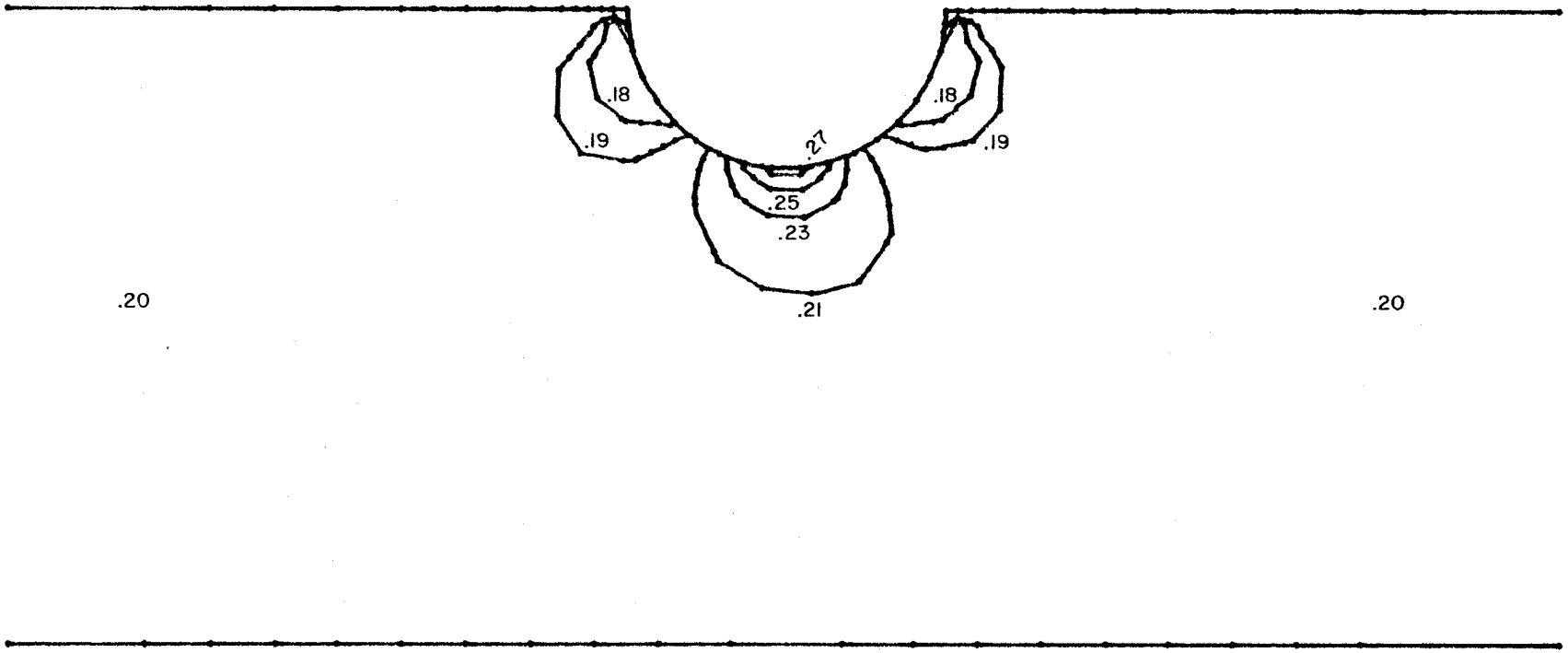

FIG. 3.50 LONGITUDINAL YOUNG'S MODULUS CONTOURS, E_y (x 10^7 PSI)

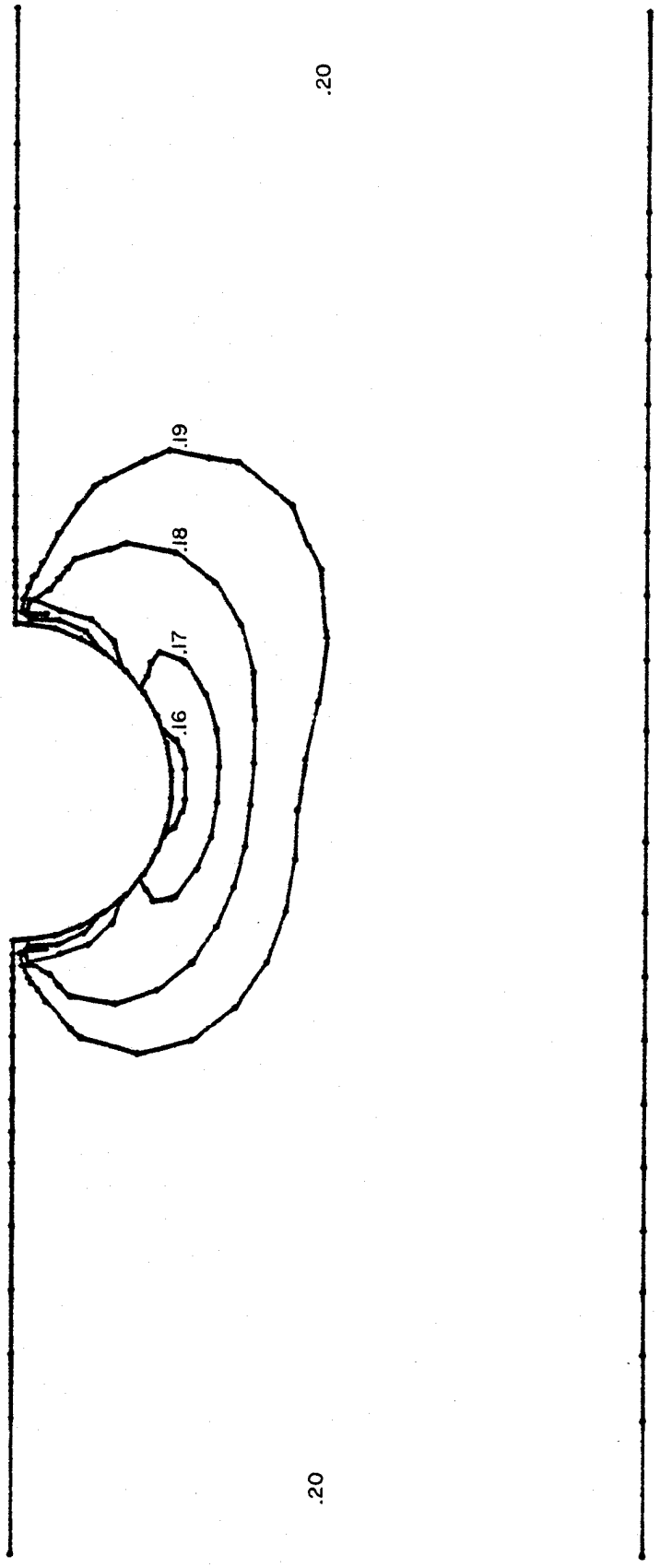

FIG. 3.51 TRANSVERSE YOUNG'S MODULUS CONTOURS, E_z (X 10^7 PSI)

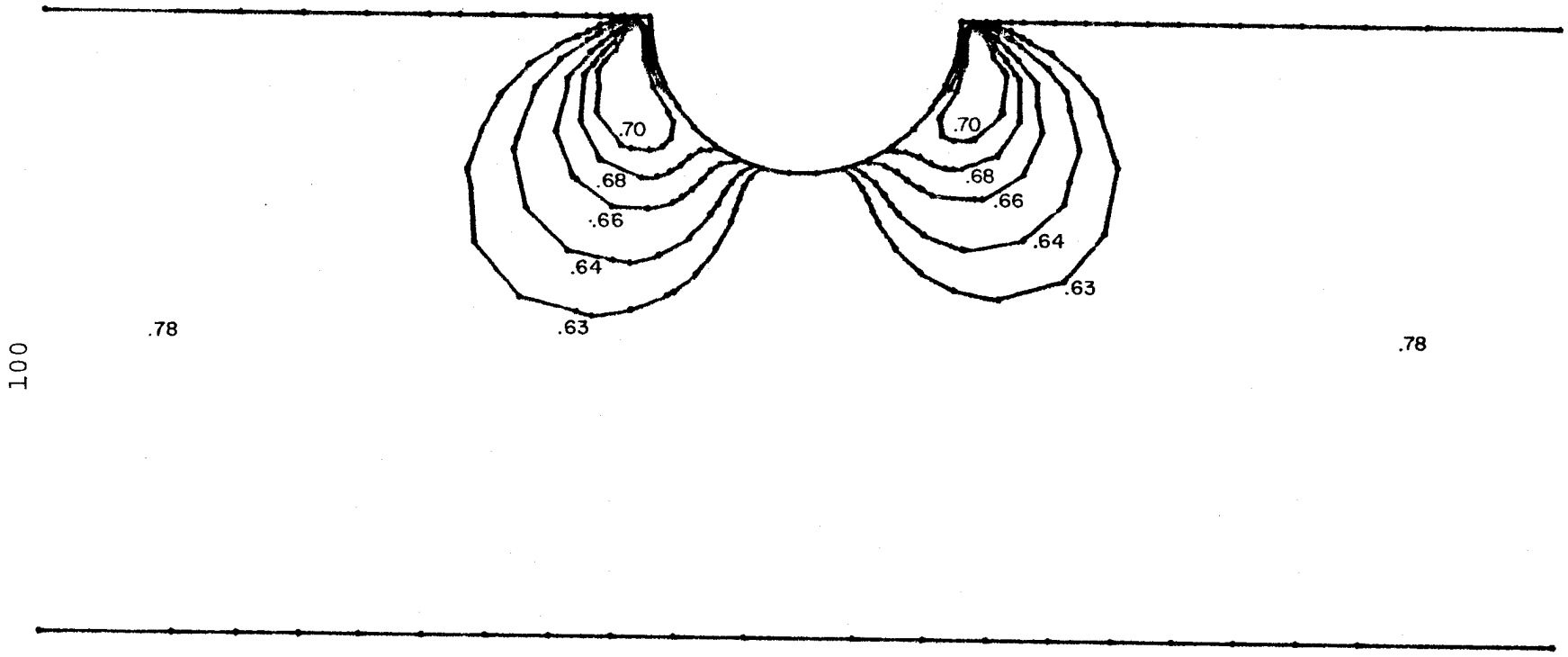

FIG. 3.52 IN-PLANE SHEAR MODULUS CONTOURS, G_{yz} (x 10^6 PSI)

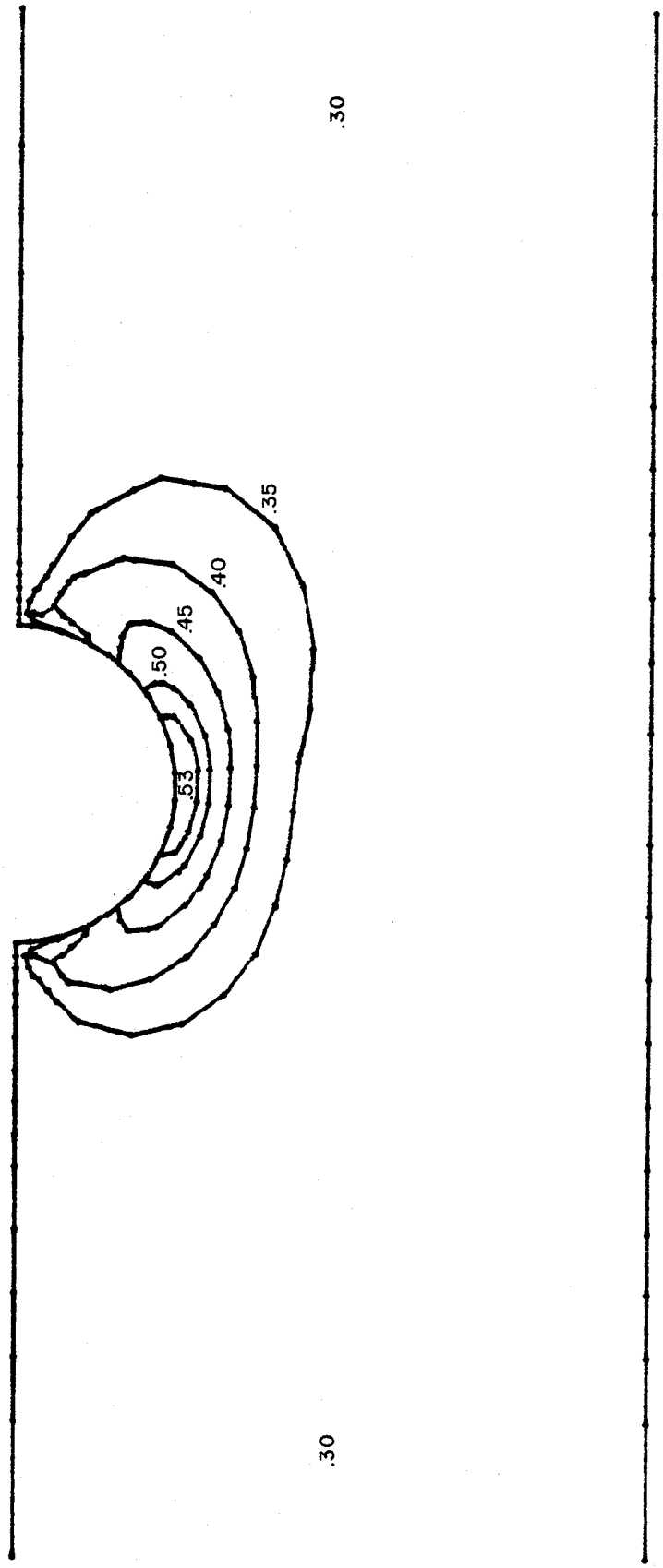

FIG. 3.53 IN-PLANE POISSON'S RATIO CONTOURS, ν_{yz}

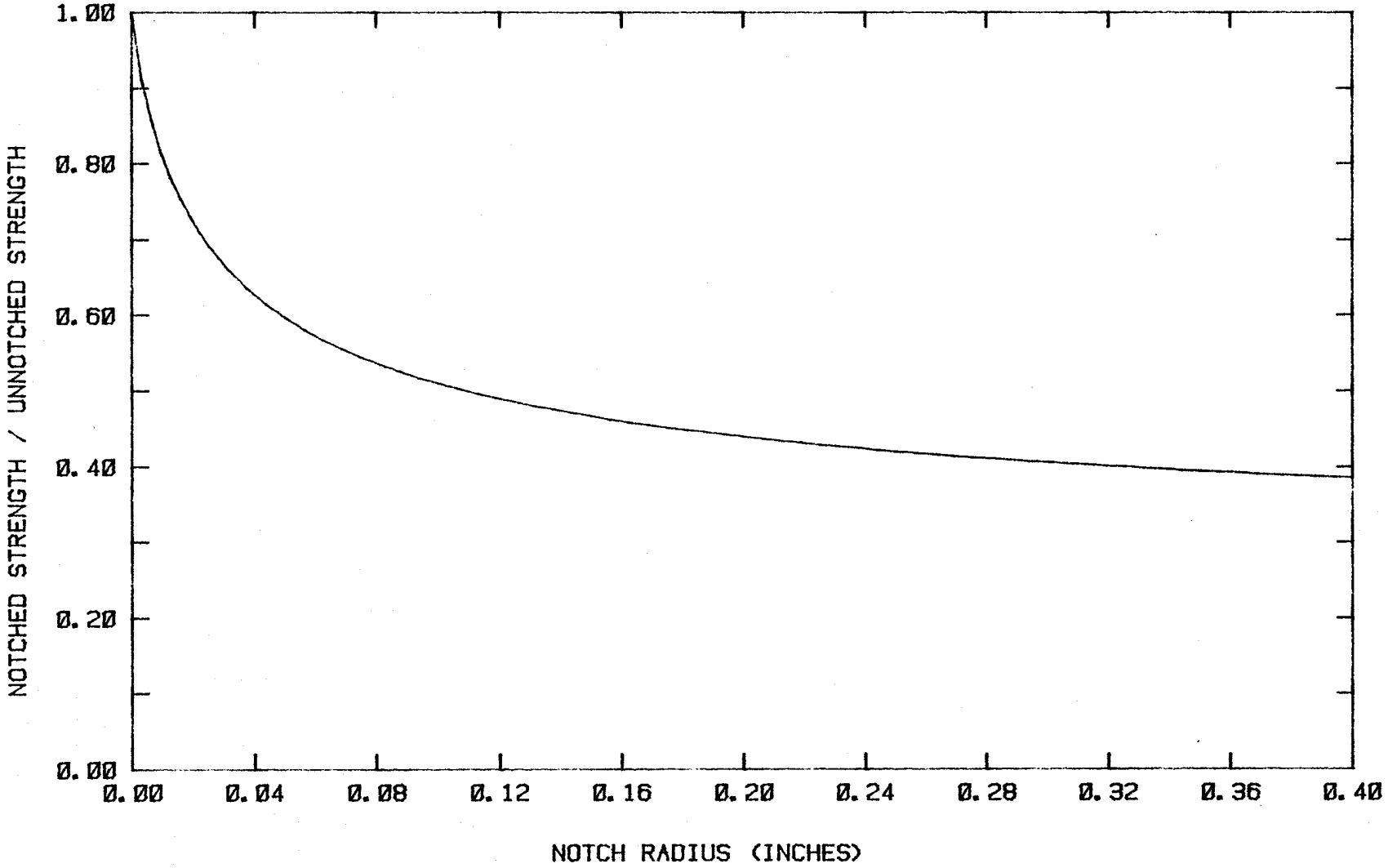

FIG. 3.54 STRENGTH RATIO VS. NOTCH RADIUS

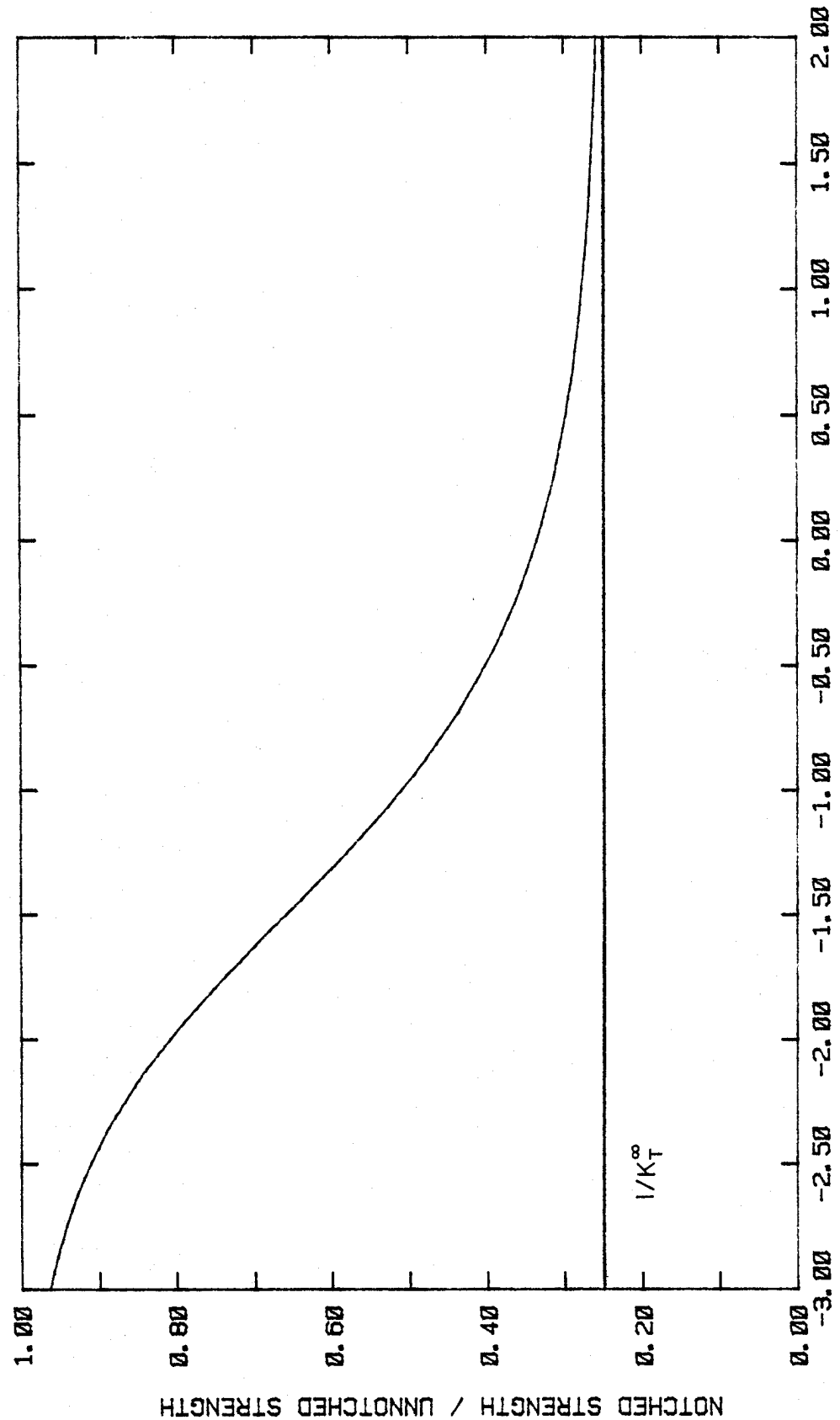

FIG. 3.55 STRENGTH RATIO VS. LOG RADIUS

IV. SUMMARY AND DISCUSSION OF RESULTS

The most important factor determining the strength of discontinuous short fiber composites is the state of orientation of the fibrous phase. The effect of this orientation is particularly important in structures containing notches of some sort since the stress concentration near the notch plays an important role in determining the part's strength. It has been the objective of this paper to present several models of fiber orientation within a notched composite and graphically show how various material and strength characteristics are affected by the orientation state. The primary tools used were a finite element code and the failure model suggested by Whitney [5,6], Karlak [2], and Pipes [3,7].

Quigley's computer-aided design program [4] played a major role in developing the finite element model and in translating the results into the numerous contour plots presented. It is with these contour plots that material characteristics can be compared. Using the developed failure model as a guideline, failure curves were presented for each case which predict failure strength as a function of

absolute hole size. The major results of this study are summarized and interpreted below.

A. EFFECT OF FIBER ORIENTATION ON MATERIAL PROPERTIES

In cases 1 through 3, material properties were constant everywhere since homogeneous materials were being analyzed. In cases 4 through 8, however, material properties varied throughout the structure depending upon the Hermans Orientation Factor and the local fiber bundle rotation.

In Case 4, where the fibers were completely columnated but followed the streamlines, all of the material property contours are quite similar in shape to the streamline contours. This stands to reason since, due to the fact that $f = 1.0$ everywhere, the only factor affecting the material properties is the streamline slope. Thus for this type of situation the material property contours could be assumed to have patterns identical to any streamline distribution that may be imposed.

For the remaining cases the material property contours were more complex since they also depend on the Hermans Orientation Factor. In general, the longitudinal and transverse Young's Modulus contours in the vicinity of

the hole near $\alpha = -90°$ had shapes somewhat similar to the Hermans Orientation contours in that region. Their sharpness in variation depended upon the sharpness in variation of f. Maximum values of the longitudinal moduli occurred near the hole edge near $\alpha = -90°$, while the smallest values occurred near the hole edge near $\alpha = 0°$ and $\alpha = -180°$. This follows from the fact that the fibers are generally aligned in the loading direction in the former instance and are aligned transverse to the loading direction in the latter. The transverse moduli values exhibit just the opposite pattern.

The in-plane shear modulus contours for all cases appeared to have a pattern very similar to the streamline contours with maximum values occurring near the hole edge near $\alpha = 0°$ and $\alpha = -180°$. Their variation with radial position is dependent upon the degree of variation in f.

In contrast, the in-plane Poisson's ratio contours assumed shapes extremely similar to the particular Hermans Orientation Factor contours. Maximum values typically occur near the hole edge near $\alpha = -90°$ and decrease in the same manner the f contours decrease.

B. EFFECT OF FIBER ORIENTATION ON STRENGTH CHARACTERISTICS

More important than the particular material property distribution was the effect of that distribution on the state of stress and corresponding strength in a structure. A summary of some stress and strength characteristics for the cases examined is provided in Table 2. As it turns out, for the hole size used in this study, the isotropic model had the lowest stress concentration factor, one of the lowest stiffnesses, and an intermediate strength value when compared to the other cases. The highest stress concentration factor occurred in Case 8, the model attempting to best represent actual orientation conditions. This case had the same stiffness as the isotropic case but yielded a 7 percent lower strength. The strongest model was Case 4, where completely columnated fibers followed ideal streamlines. This case also had a high stiffness and a low stress concentration factor. Case 5 was the weakest model, where the Hermans Orientation Factor varied linearly with radial distance independent of the angular position. This model had low stiffness and a high stress concentration factor.

In order to contrast strength characteristics of the various cases with those of the isotropic orientation state, Table 3 is provided. This table shows the percent change in stress and strength characteristics from those

CASE	MAXIMUM AVERAGE ENGINEERING STRAIN, $\Delta L/L$ ($\times 10^{-4}$)	MAXIMUM STRESS AT HOLE EDGE σ_y (PSI)	STRESS CONCENTRATION FACTOR K_T^∞	$\frac{\text{NOTCHED STRENGTH}}{\text{UNNOTCHED STRENGTH}}$ FOR R = .25 in σ_N/σ_O	HOLE RADIUS FOR N PERCENT STRENGTH REDUCTION (INCHES)		
					10 PERCENT	20 PERCENT	30 PERCENT
1	5.1	2950	2.95	.45	.0024	.0080	.0200
2	3.6	3260	3.26	.45	.0025	.0089	.0232
3	4.5	3030	3.03	.45	.0024	.0083	.0208
4	3.6	2970	2.97	.47	.0018	.0068	.0205
5	5.0	3400	3.40	.41	.0032	.0074	.0149
6	5.1	3320	3.32	.42	.0028	.0074	.0160
7	5.1	3530	3.53	.42	.0037	.0108	.0238
8	5.1	3540	3.54	.42	.0037	.0107	.0235

TABLE 2. SUMMARY OF STRESS AND STRENGTH CHARACTERISTICS

CASE	% CHANGE IN MAXIMUM AVERAGE ENGINEERING STRAIN %	% CHANGE IN MAXIMUM STRESS AT HOLE EDGE %	% CHANGE IN STRESS CONCENTRATION FACTOR %	% CHANGE IN STRENGTH FOR R = .25 in %	% CHANGE IN HOLE RADIUS NEEDED TO CAUSE N% STRENGTH REDUCTION %		
					10%	20%	30%
2	-30	11	11	0	4	11	16
3	-12	3	3	0	0	4	4
4	-30	0	0	4	-25	-15	3
5	-2	15	15	-9	33	-8	-26
6	0	13	13	-7	17	-8	-20
7	0	20	20	-7	54	35	19
8	0	20	20	-7	54	34	18

TABLE 3. PERCENT CHANGE IN STRENGTH CHARACTERISTICS FROM THOSE IN THE ISOTROPIC CASE (CASE 1)

in the isotropic case. It is seen that for the hole size studied, strength varied by no more than 10 percent, while stiffness may vary by as much as 30 percent and stress concentration may vary by 20 percent.

Similarly, Table 4 is provided in order to show the percent change in stress and strength characteristics from those occurring in the completely columnated, orthotropic case. In this instance, strength and stress concentration change by no more than 10 percent, while stiffness can vary by as much as 41 percent. Thus, it is evident that for the models presented and the hole size used, strength values vary by no more than 10 percent from the values occurring in the isotropic or orthotropic orientation conditions.

In order to judge how much the strength varies for hole sizes other than 0.25 inches a plot is provided comparing strength curves for the isotropic case and the two cases whose strength curves deviate most from the isotropic plot. This is shown in figure 4.1. It can be seen from this plot that over a wide range of hole radii the strength varies by no more than 10-11 percent from the isotropic predictions. The same holds true for comparisons with the completely columnated, orthotropic case since figure 4.2 shows that the strength curves for this case and the isotropic case are almost coincident.

CASE	% CHANGE IN MAXIMUM AVERAGE ENGINEERING STRAIN %	% CHANGE IN MAXIMUM STRESS AT HOLE EDGE %	% CHANGE IN STRESS CONCENTRATION FACTOR %	% CHANGE IN STRENGTH FOR R = .25 in %	% CHANGE IN HOLE RADIUS NEEDED TO CAUSE N% STRENGTH REDUCTION %		
					10%	20%	30%
1	41	-10	-10	0	-4	-10	-14
3	24	-7	-7	0	-4	-7	-10
4	0	-9	-9	4	-28	-24	-12
5	38	4	4	-9	28	-17	-36
6	41	2	2	-7	12	-17	-31
7	41	8	8	-7	48	21	3
8	41	9	9	-7	48	20	1

TABLE 4. PERCENT CHANGE IN STRENGTH CHARACTERISTICS FROM THOSE IN THE ORTHOTROPIC, COMPLETELY COLUMNATED CASE (CASE 2)

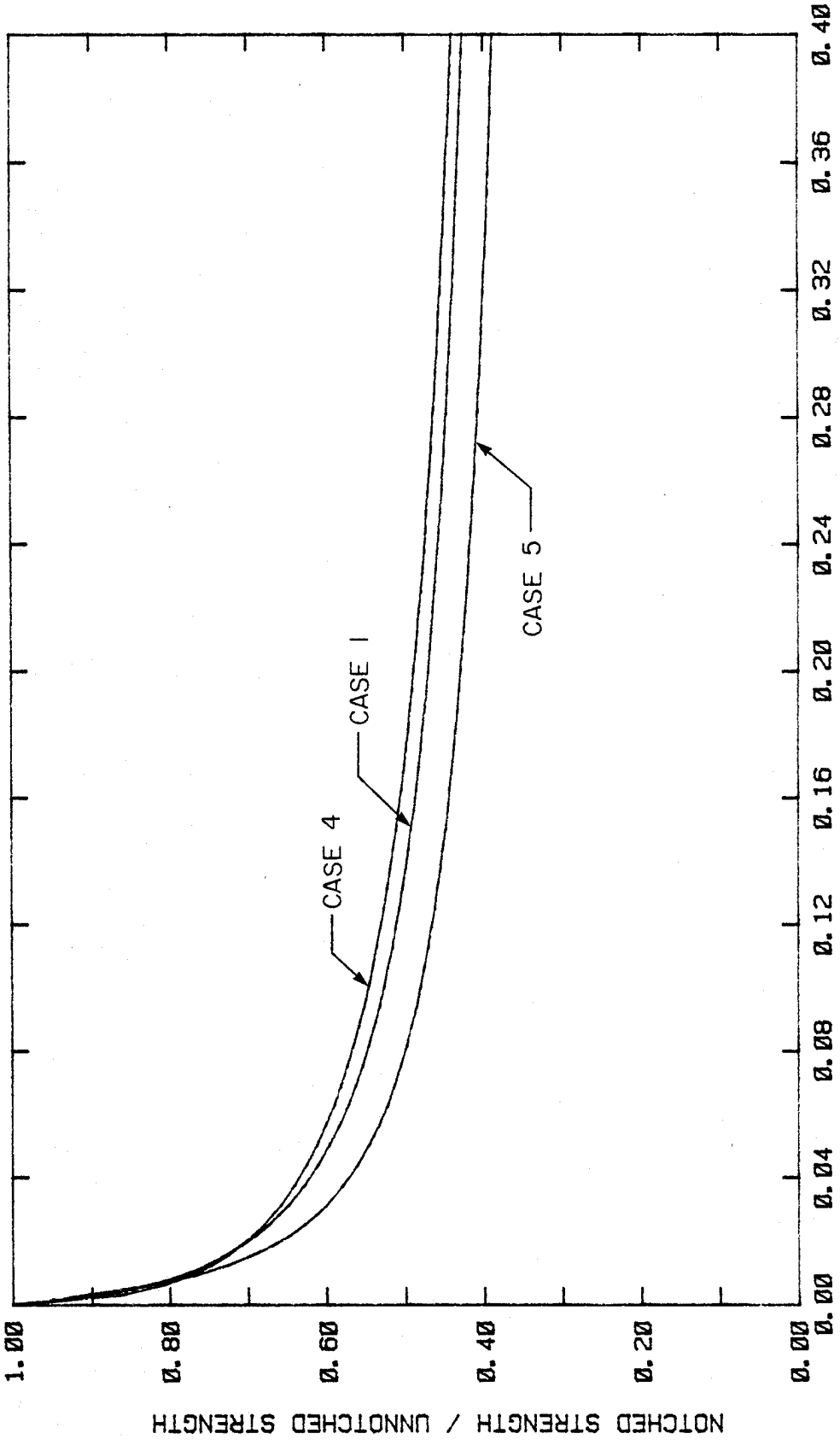

FIG. 4.1 STRENGTH RATIO VS. NOTCH RADIUS
STRENGTH DEVIATION COMPARISON

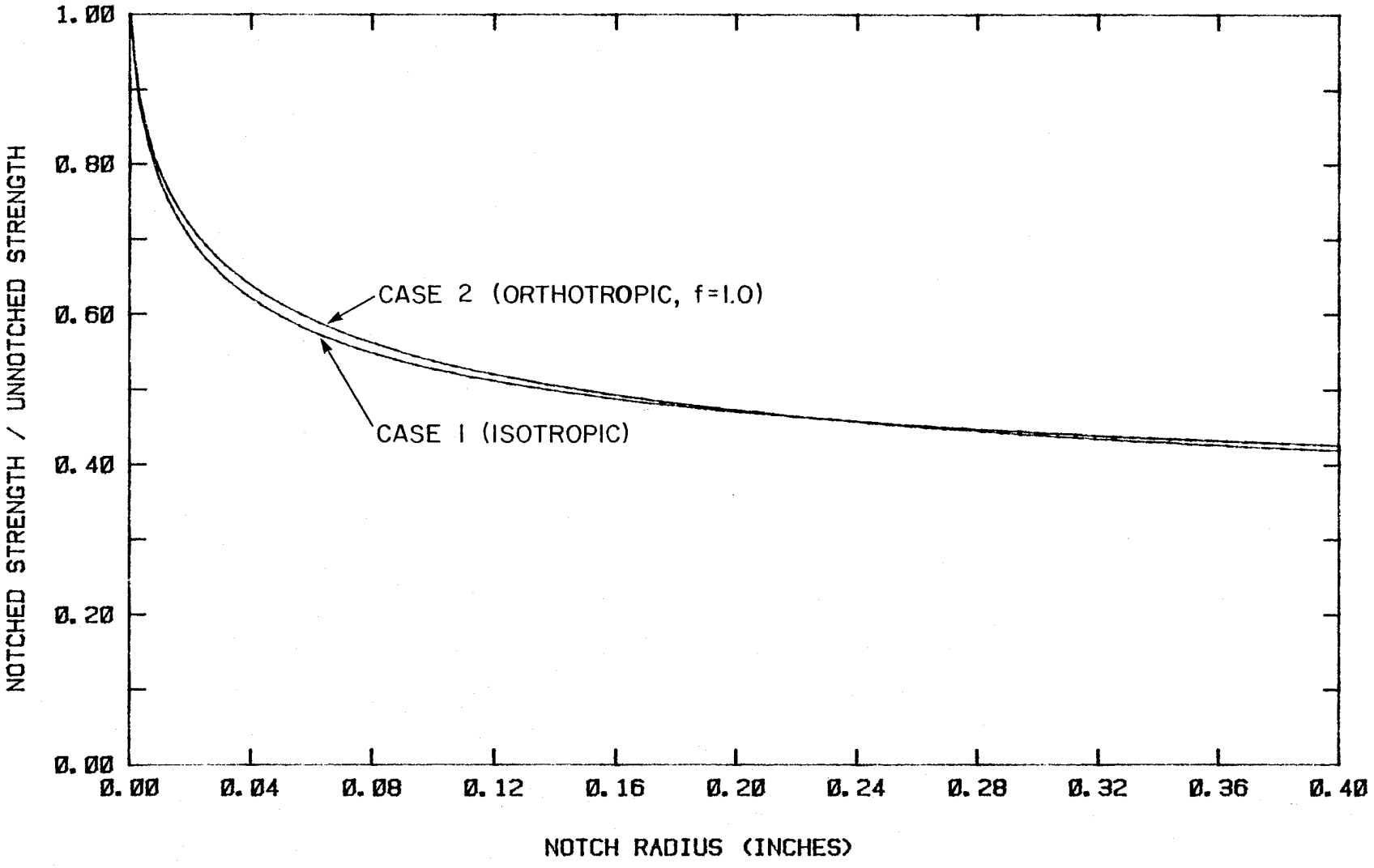

FIG. 4.2 STRENGTH RATIO VS. NOTCH RADIUS
ISOTROPIC-ORTHOTROPIC COMPARISON

Another interesting feature of Table 2 is the information showing the hole size required to cause a certain percent strength reduction. To indicate the variation in hole size for the different cases, Table 3 and Table 4 are provided to show the percent change in hole size from the isotropic and completely columnated, orthotropic cases respectively. Thus, if the strength of an isotropic or orthotropic part containing a particular hole size is known, the hole size required to cause the same strength reduction in a part with a complex orientation state can be found. It can be seen from the tables that the hole sizes can vary by as much as 50 percent. It is also evident from the tables that a particular case may be stronger than the isotropic or orthotropic case at a certain strength level, i.e. be capable of sustaining a larger hole size, and may be weaker at another. This is expressed by the intersection of the various strength curves such as that shown in figure 4.3. Thus, different orientations have different relative strengths depending upon the absolute hole size.

C. CONCLUSION

It has been shown in this investigation that fiber orientation plays a major role in determining material property distributions and corresponding strength characteristics. Material properties were seen to be distributed in

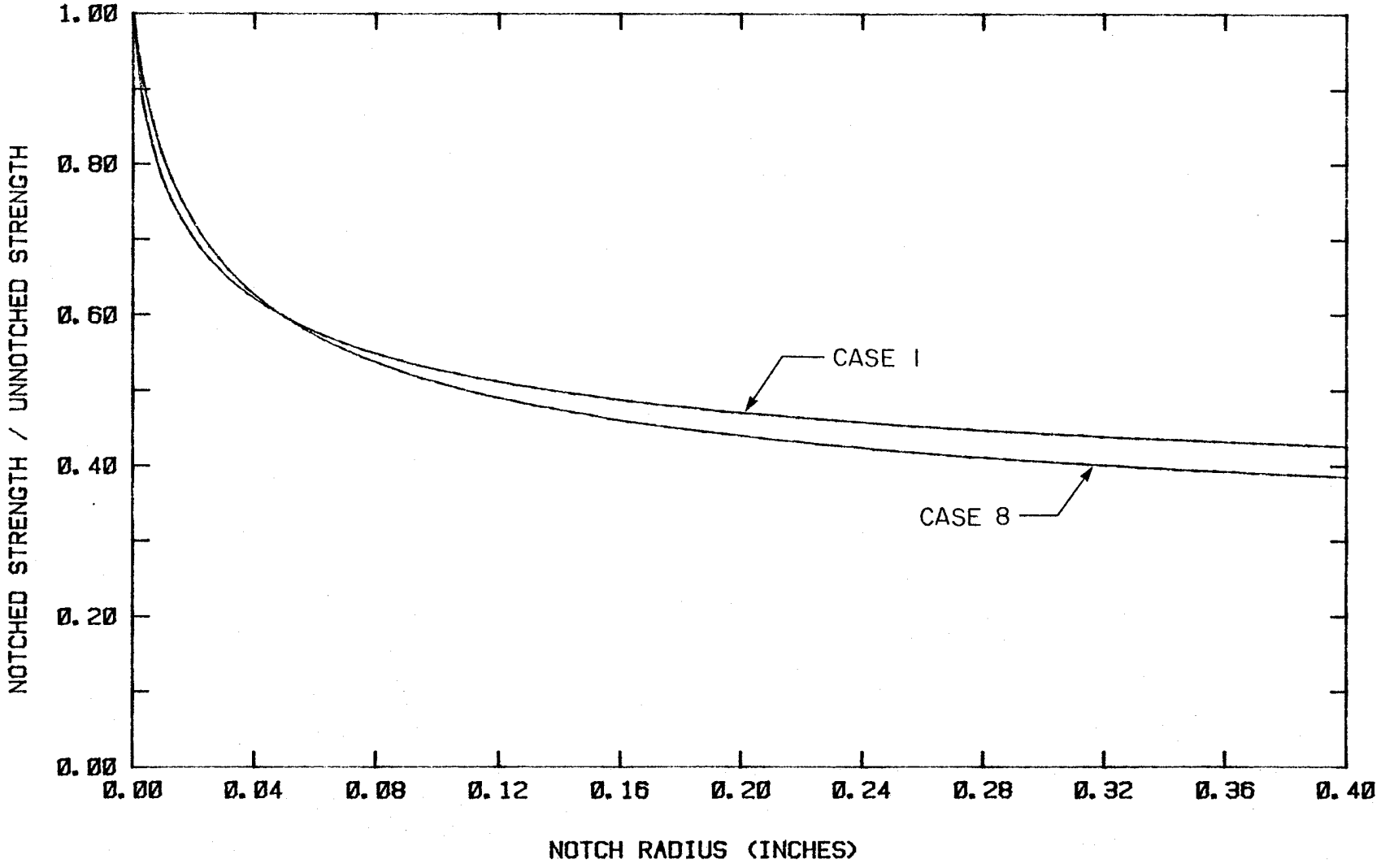

FIG. 4.3 STRENGTH RATIO VS. NOTCH RADIUS
RELATIVE STRENGTH COMPARISON

patterns very similar to the fiber orientation patterns. Their sharpness in variation depended upon the sharpness in variation of the local orientation. Since fiber patterns are determined by flow conditions during molding, pointwise material property variation should be expected in regions within a mold where uniform flow is interrupted.

When compared to the isotropic and orthotropic cases, the strength levels of the various models varied by no more than 11 percent given a particular notch size. It was seen that, given a notch size in the isotropic or orthotropic case, notch sizes up to 50 percent larger could be present in other models and yet cause no greater strength reduction. Also, it was shown that a particular model might be stronger than another for a certain notch size range and be weaker for a different range. Thus, relative strengths may vary depending upon the absolute hole size.

Future work in this area should be directed toward developing a fiber orientation model which takes into account the complexity of the flow conditions and has a greater flexibility with material specifications. It would also be interesting to test the particular structure modeled in this investigation to see whether or not any of the models reflect actual experimental data.

REFERENCES

[1] Jarzebski, G., et al., "Computational Algorithms for Predicting the Mechanical Properties of Sheet Molding Materials," CCM-79-11, Center for Composite Materials, University of Delaware, Newark, Delaware, 1979.

[2] Karlak, R. F., "Hole Effects in a Related Series of Symmetrical Laminates," Proceedings of Failure Modes in Composites III, American Society of Metals, Chicago, 1977.

[3] Pipes, R. B., and J. W. Gillespie, "Superposition of the Notched Strength of Composite Laminates," Polymer Engineering and Science, Vol. 19, No. 16, December, 1979.

[4] Quigley, J. J., IV, "Computer-Aided Design for General Composite Material Systems," CCM-80-23, Center for Composite Materials, University of Delaware, Newark, Delaware, 1980.

[5] Whitney, J. M. and R. J. Nuismer, Journal of Composite Materials, Vol. 8, p. 253, 1974.

[6] Whitney, J. M. and R. J. Nuismer, "Uniaxial Failure of Composite Laminates Continuing Stress Concentrations," in "Fracture Mechanics of Composites," ASTM STP 593, Proceedings of ASTM Symposium in High Modulus Fibers and Their Composites, Gaithersburg, Maryland, ASTM, Philadelphia, PA, 1975.

[7] Pipes, R. B., et al., "Behavior of Discontinuous Fiber Composites: Fiber Orientation," Center for Composite Materials, University of Delaware, Newark, Delaware, presented at the Japan-United States Conference on Composite Materials, Tokyo, Japan, January 1981.

[8] Lekhnitskii, S. G., "Theory of Elasticity of an Anisotropic Elastic Body," translated by P. Fern, Holden-Day Inc., San Francisco, 1968.